Diploma thesis

Superfluidity in mesoscopic systems of charged bosons

by

Jens Böning

January 2007

Institut für Theoretische Physik und Astrophysik
der Universität Kiel

Supervisor/1st examiner: Prof. Dr. Michael Bonitz

2nd examiner: _____

Contents

1. Introduction

1.1. Motivation

Back in 1937, the groups of Kapitsa and Misener demonstrated that liquid helium below 2.2 K behaves as if composed of two parts. The normalfluid component shows no peculiarities, while the *superfluid* component is characterized by the complete absence of viscosity. When set into a rotational motion, such superfluids can flow endlessly without friction. As classical explanations fail to describe this behavior, superfluidity was believed a consequence of quantum physics from the very beginning. Thus, it is one of the few quantum phenomena visible to the eyes of our macroscopic world.

The development of theoretical models showed that superfluidity is a pathology of interacting Bose systems and strongly related—yet not identical—to Bose-Einstein condensation. Up to date, superfluidity is well understood in a phenomenological sense, but analytical results derived from microscopic models are fragmentary. Superfluidity constitutes a many-body problem with inter-particle interactions and bosonic particle exchange and thus requires sophisticated numerical methods for quantitative predictions.

The first experimental realizations of Bose-Einstein condensates with dilute alkali gases in 1995 added another interesting aspect to the theory of these macroscopic phenomena. Since the experiments contain only a rather small number of atoms, the question arises, how Bose-Einstein condensation and superfluidity translate back into the world of finite systems. In particular, how far can one reduce the number of particles and still speak of superfluidity?

The methods for a definition of superfluidity in small systems are limited, as most theoretical considerations based on the relative motion of the macroscopic system are no longer applicable. The common approach uses the *Hess-Fairbank* effect denoting the inevitable deviation of the rotational moment of inertia from its classical expectation value in slowly circulation superfluids, since only the normalfluid component rotates rigidly with the container walls. The expectation value of the moment of inertia can be derived within statistical theories which makes the Hess-Fairbank effect the method-of-choice to calculate superfluid properties in small bosonic clusters.

This work considers the implications of this definition for very small Bose systems containing only a few particles. The investigation specializes to 2D systems confined in the harmonic trap with repulsive Coulomb interactions. Results are obtained from both exact analytical expressions for the ideal system and numerical simulations of the interacting system. The latter are carried out with the *path integral Monte Carlo* method based on first principles.

Superfluidity shows some peculiar properties in small systems. In particular, superfluidity is not restricted to interacting Bose systems anymore. It is intended to find methods in order to distinguish between contributions related to the finite size, inter-particle interactions, and bosonic particle exchange. Additionally, some answers to the interesting question whether a system can be simultaneously superfluid and solid are given.

1.2. Structure of this work

Chapter 1: Introduction.

Chapter 2: Quantum mechanical low temperature effects in Bose systems. This chapter reviews two aspects of macroscopic Bose systems: Bose-Einstein condensation and superfluidity. It aims to provide the reader with the necessary theoretical understanding for the further course of this work. Aside from a thoroughly analytical investigation of the established effects, an overview over the current status of research for the hotly debated topic considering potentially superfluid solids, "supersolids", is given.

Chapter 3: The path integral Monte Carlo method. The path integral Monte Carlo method combines the path integral description of quantum systems with efficient Monte-Carlo methods in order to solve the high-dimensional integrals. This second introductory chapter discusses the theoretical background and gives an overview over numerical issues. In particular, the so-called area formula devoted to the calculation of the superfluid fraction in confined Bose systems is derived.

Chapter 4: Mesoscopic Bose gases in harmonic traps. The finite system breaks with some aspects introduced in chapter 2. The question how Bose-Einstein condensation and superfluidity as effects of the macroscopic world translate to mesoscopic systems is investigated. This chapter should act as a link between the theoretical part and the following discussion.

Chapter 5: Analytical results for ideal systems. Ideal systems have the advantage to be completely accessible with analytical methods. A convenient way to calculate the exact density matrix is presented. In particular, expressions for the condensed and the superfluid fraction are derived. The results are discussed with respect to the macroscopic considerations of chapter 2 and constitute a reference case for the numerical investigations of chapter 6.

Chapter 6: Numerical results for systems with Coulomb interaction. This chapter opens with a short discussion of possible analytical approaches to strongly correlated Bose systems. The quantitative results for small interacting systems were obtained with the path integral Monte Carlo method as introduced in chapter 3. Special attention is paid to superfluidity, which shows some peculiar effects unseen in the macroscopic limit. The possibility of superfluid crystals is also considered.

Chapter 7: Conclusion.

1.3. Some remarks about the used notations

In general, derivations within this work comply to common standards. In order to avoid potential misunderstandings, this sections lists some minor particularities, which might not be throughout established.

Special notation for sums As usual, a shortcut like $\sum_{\mathbf{k}}$ denotes the summation over the whole parameter space of $\mathbf{k}$. In some cases, the element at $\mathbf{k} = 0$ must be excluded. This is indicated with a "$'$" at the symbol, i.e.,

$$\sum_{\mathbf{k}}{}' \ldots \equiv \sum_{\substack{\mathbf{k} \\ \mathbf{k}\neq 0}} \ldots \tag{1.1}$$

Averages Mathematics and physics know a great multitude of different averages, but far lesser ways to distinguish between them in the sense of notation. Due to the nature of this work, the primary used average is the *thermal average in the canonical ensemble*, which is indicated by a set of "$\langle\rangle$". In summary, this and other notations for averages read

$$\text{Thermal average (canonical ensemble)} \qquad \langle \hat{A} \rangle = \frac{1}{Z} \operatorname{Tr} \hat{\rho} \hat{A}, \tag{1.2}$$

$$\text{Arithmetic mean} \qquad \bar{a} = \frac{1}{N} \sum_{i=1}^{N} a_i, \tag{1.3}$$

$$\text{Geometric mean} \qquad \tilde{a} = \left(\prod_{i=1}^{N} a_i \right)^{1/N}. \tag{1.4}$$

(Z is the partition function of the canonical ensemble and $\hat{\rho}$ is the density operator.) At one point, namely for the Bose distribution function $\bar{n}_{\mathbf{p}}$, the thermal average of an occupied single-particle state in the grand canonical ensemble is meant.

Figures Since the bulk of the obtained results is presented in figures, some efforts with respect to consistent coloring have been made. Whenever possible, the color refers to quantities calculated for a specific number of bosons in the system.

N	2	3	4	5	more	boltzmannons[1]
color	red	green	blue	violet	others	gray

In general, boltzmannonic calculations are shown together with bosonic calculations. Boltzmannonic quantities are always indicated with gray lines since their correspondence to the number of particles is usually clear.

[1] Boltzmannons are (hypothetic) distinguishable quantum particles obeying Boltzmann statistics.

2. Quantum mechanical low temperature effects in Bose systems

2.1. Bose-Einstein condensation

The field of Bose-Einstein condensation traces its origin back to the work of Satyendra Nath Bose. He addressed himself to Albert Einstein who arranged for the publication of his paper, which laid the basis for what would become known as *Bose statistics*, in 1924 [1]. Einstein himself considered the implications for an ideal gas at low temperatures. He released a series of papers[2, 3] in which he proposed that atoms should collect predominantly in the ground state of the system. This macroscopic occupation of a single-particle state became known as *Bose-Einstein condensation (BEC)*. It is only accessible for particles of integer spin, namely *bosons*.

2.1.1. The free non-interacting Bose gas

The existence of a Bose-Einstein condensate phase follows from purely statistical arguments (see [4]). Consider a grand canonical ensemble (T, V, μ) of free, non-interacting, and spin-polarized bosons. In thermal equilibrium, the average occupation of an energy level obeys Bose statistics, i.e.,

$$\bar{n}_{\mathbf{p}} = \frac{1}{e^{\beta(\epsilon_{\mathbf{p}}-\mu)} - 1}, \tag{2.1}$$

where β is the inverse temperature and $\epsilon_{\mathbf{p}}$ denotes the energy eigenvalues of the system. Summing $\bar{n}_{\mathbf{p}}$ over momentum space yields the thermal particle number in the system and the thermal energy when weighted with the energy eigenvalues, respectively:

$$\langle N \rangle (T, V, \mu) = \sum_{\mathbf{p}} \bar{n}_{\mathbf{p}}, \qquad \langle E \rangle (T, V, \mu) = \sum_{\mathbf{p}} \epsilon_{\mathbf{p}} \bar{n}_{\mathbf{p}}. \tag{2.2}$$

Since the energy spectrum of free particles, $\epsilon_{\mathbf{p}} = p^2/2m$, is continuous, the sum can be substituted by an integral over phase space

$$\sum_{\mathbf{p}} \ldots = \frac{V}{(2\pi\hbar)^3} \int \mathrm{d}^3\mathbf{p} \ldots . \tag{2.3}$$

Taken together, the equations (2.1)–(2.3) allow for a complete statistical investigation of the non-interacting Bose gas. As usual, the first step is to derive an expression for the chemical potential μ.

It is important to note that eqs. (2.2) must be fulfilled by definition. But the integral (2.3) would diverge for $\mu = \epsilon_{\mathbf{p}}$ as (2.1) is singular at this point. Hence, the chemical potential

cannot be positive which gives $\epsilon_{\mathbf{p}} - \mu \geq 0$. One can then use the geometric series to simplify (2.1) into

$$\bar{n}_{\mathbf{p}} = \frac{e^{-\beta(\epsilon_{\mathbf{p}}-\mu)}}{1 - e^{-\beta(\epsilon_{\mathbf{p}}-\mu)}} = \sum_{l=1}^{\infty} e^{-\beta(\epsilon_{\mathbf{p}}-\mu)l}. \tag{2.4}$$

This allows for an easy evaluation of (2.3) as it now mirrors the known Gaussian integral emerging from the theory of the classical ideal gas. One obtains

$$N(T, V, \mu) = \frac{V}{\lambda^3} \sum_{l=1}^{\infty} \frac{e^{\beta\mu l}}{l^{3/2}} = \frac{V}{\lambda^3} \operatorname{Li}_{3/2}(z), \tag{2.5}$$

where $\lambda = 2\pi\hbar/\sqrt{2\pi m k_{\mathrm{B}} T}$ is the thermal De Broglie wave length and the polylogarithm,

$$\operatorname{Li}_s(z) = \sum_{l=1}^{\infty} \frac{z^l}{l^s}, \tag{2.6}$$

was introduced with the shortcut $z = \exp(\beta\mu)$. For a given temperature T and density $n = N/V$, eq. (2.5) fixes the chemical potential $\mu = \mu(T, n)$.

An investigation of the temperature dependence of $\mu(T, n)$ leads to a remarkable chain of conclusions. The thermal De Broglie wave length is proportional to $T^{-1/2}$, so in the limit of infinite temperature eq. (2.5) can only yield a finite density when the polylogarithm vanishes. This implies $z \to 0$ and $\mu \to -\infty$. As the polylogarithm is a monotonic function, its argument z must grow when the system is cooled. But the initial condition $\mu \leq 0$ implies $z \leq 1$, so there exists a critical temperature T_{c} (and a critical De Broglie wave length λ_{c}), i.e.,

$$n\lambda_{\mathrm{c}}^3 = \operatorname{Li}_{3/2}(1) = \zeta(3/2). \tag{2.7}$$

In the last step, the fact that the polylogarithm for $z = 1$ reduces to the Riemann ζ-function was used.

For $T < T_{\mathrm{c}}$, eq. (2.5) has no solution. But its origin, eq. (2.2), must have a solution on the whole temperature range. This means, something went wrong when replacing the sum with an integral. In particular, the latter is unaffected by singularities of its integrand occurring at the integration limits. For the problem in question this is exactly what happens at the critical point where μ equals zero. A correct replacement of the sum would, therefore, consider the ground state occupation N_0 separately. Instead of eq. (2.3) one has to use

$$\sum_{\mathbf{p}} \ldots = N_0 + \frac{V}{(2\pi\hbar)^3} \int \mathrm{d}^3\mathbf{p} \ldots, \tag{2.8}$$

which alters eq. (2.5) to

$$N(T, V, \mu) = \bar{n}_0 + {\sum_{\mathbf{p}}}' \bar{n}_{\mathbf{p}} = N_0 + \frac{V}{\lambda^3} \operatorname{Li}_{3/2}(z). \tag{2.9}$$

Effects related to a finite size of the system shall not be investigated at this point. The system is considered in the *thermodynamic limit*, which means

$$N \to \infty, \qquad V \to \infty, \qquad n = \frac{N}{V} = \text{const.} \tag{2.10}$$

Quantity	$T \leq T_\mathrm{c}$	$T > T_\mathrm{c}$
Condensate fraction	$1 - \left(\frac{T}{T_\mathrm{c}}\right)^{3/2}$	0
Energy per particle	$\frac{3}{2} k_\mathrm{B} T \frac{\zeta(5/2)}{\zeta(3/2)} \left(1 - \frac{N_0}{N}\right)$	$\frac{3}{2} k_\mathrm{B} T \frac{\mathrm{Li}_{5/2}(z)}{\mathrm{Li}_{3/2}(z)}$
Specific heat capacity	$\frac{15}{4} k_\mathrm{B} \frac{\zeta(5/2)}{\zeta(3/2)} \left(1 - \frac{N_0}{N}\right)$	$\frac{15}{4} k_\mathrm{B} \frac{\mathrm{Li}_{5/2}(z)}{\mathrm{Li}_{3/2}(z)} - \frac{9}{4} k_\mathrm{B} \frac{\mathrm{Li}_{3/2}(z)}{\mathrm{Li}_{1/2}(z)}$
Pressure	$n k_\mathrm{B} T \frac{\zeta(5/2)}{\zeta(3/2)} \left(1 - \frac{N_0}{N}\right)$	$n k_\mathrm{B} T \frac{\mathrm{Li}_{5/2}(z)}{\mathrm{Li}_{3/2}(z)}$

Table 2.1.: *Temperature dependence of thermal averages for the free ideal Bose gas in the macroscopic limit.*

For any macroscopic system with typical particle numbers around 10^{24}, this is a reasonable approximation. In this limit, eqs. (2.5) and (2.9) give the same results for $T > T_\mathrm{c}$, as the ground state occupation N_0 is finite and, thus, negligible in an infinite system. But unlike its predecessor, eq. (2.9) has a solution for $T < T_\mathrm{c}$. The chemical potential is obviously zero in this region and one may write

$$N(T, V, \mu) = N_0 + \frac{V}{\lambda^3} \zeta(3/2) \qquad \text{for } T \leq T_\mathrm{c}. \tag{2.11}$$

The right-hand term can be simplified by using eq. (2.7). The temperature dependence of the ground state occupation $N_0(T)$ then reads

$$\frac{N_0}{N} = \begin{cases} 1 - \left(\frac{T}{T_\mathrm{c}}\right)^{3/2}, & T \leq T_\mathrm{c} \\ 0, & T > T_\mathrm{c} \end{cases} \tag{2.12}$$

Note that the fraction of particles collecting in the ground state becomes non-zero at a *finite* temperature T_c. This is far from obvious and indeed a specialty of the three-dimensional free Bose gas. As initially mentioned, Einstein discovered this effect by an analogue investigation, which established the denotation as *Bose-Einstein condensation* (BEC).

Occurrence of BEC shows all characteristics of a phase transition with the condensate fraction acting as the order parameter. The quantitative behavior of the system changes, as condensed particles no longer contribute to any physical observables. Table 2.1 collects the temperature dependence of the most important thermal averages. They can be easily derived from the thermal energy which itself can be calculated from eq. (2.2) with an analogue procedure as used for the particle number.

It is not naturally given that every imaginable Bose gas has a BEC phase at sufficiently low temperatures. For example, one can try to follow the same reasoning used above for the one- and two-dimensional free Bose gas, respectively. The corresponding expressions for the

thermal particle number in these systems then read

$$N = \frac{V}{\lambda^2}\,\mathrm{Li}_1(z) \quad (2\mathrm{D}), \qquad\qquad N = \frac{V}{\lambda}\,\mathrm{Li}_{1/2}(z) \quad (1\mathrm{D}). \tag{2.13}$$

In both cases the polylogarithm for $z = 1$ is infinite, so there exists no critical De Broglie wave length below which these expressions would loose their validity. Here, a BEC phase simply does not exist.

2.1.2. The ideal Bose gas in a harmonic trap

The ideal Bose gas confined in a harmonic trap does also show Bose-Einstein condensation. The thermal particle number in the system is calculated as before

$$N = \sum_{n_x,n_y,n_z=0}^{\infty} \bar{n}_{n_x n_y n_z}, \tag{2.14}$$

where $\bar{n}_{n_x n_y n_z}$ denotes the Bose distribution function with the energy eigenvalues $\epsilon_{n_x n_y n_z}$. These read for particles confined in an arbitrarily shaped harmonic trap:

$$\epsilon_{n_x n_y n_z} = \hbar\omega_x\left(n_x + \frac{1}{2}\right) + \hbar\omega_y\left(n_y + \frac{1}{2}\right) + \hbar\omega_z\left(n_z + \frac{1}{2}\right). \tag{2.15}$$

The ground state has the energy $\epsilon_{000} = \frac{3}{2}\hbar\overline{\omega}$, where $\overline{\omega}$ denotes the arithmetic mean of the trapping frequencies. The transition point at which a macroscopic occupation of the ground state occurs, is, therefore, determined by $\mu \to \mu_\mathrm{c} = \epsilon_{000}$. An evaluation of eq. (2.14) by replacing the sum with an integral with special regard to the ground state occupation N_0 yields

$$N = \begin{cases} \left(\frac{k_\mathrm{B}T}{\hbar\widetilde{\omega}}\right)^3 \mathrm{Li}_3(z), & T > T_\mathrm{c}, \\ N_0 + \left(\frac{k_\mathrm{B}T}{\hbar\widetilde{\omega}}\right)^3 \zeta(3), & T \leq T_\mathrm{c}, \end{cases} \tag{2.16}$$

where $\widetilde{\omega}$ is the geometric mean of the trapping frequencies and $z = \exp(\beta(\mu - \epsilon_{000}))$. The transition temperature T_c can be read off either expression by setting $z = 1$ or $N_0 = 0$, respectively:

$$k_\mathrm{B}T_\mathrm{c} = \hbar\widetilde{\omega}\left(\frac{N}{\zeta(3)}\right)^{1/3}. \tag{2.17}$$

The temperature dependence of the condensate fraction becomes

$$\frac{N_0}{N} = 1 - \left(\frac{T}{T_\mathrm{c}}\right)^3, \tag{2.18}$$

which has a deviating exponent regarding eq. (2.12) for the free bosons. This constitutes the most obvious difference as it affects all thermal quantities accordingly. They are listed in Table 2.2. Note that the ground state energy ϵ_{000} vanishes in the thermodynamic limit, so, as before, only non-condensed particles do contribute. Thereby, the correct thermodynamic limit for a trapped system reads

$$N \to \infty, \qquad \hbar\omega \to 0, \qquad n \propto N(\hbar\omega)^3 = \mathrm{const.} \tag{2.19}$$

Quantity	$T \leq T_\mathrm{c}$	$T > T_\mathrm{c}$
Condensate fraction	$1 - \left(\frac{T}{T_\mathrm{c}}\right)^3$	0
Energy per particle	$3k_\mathrm{B}T\frac{\zeta(4)}{\zeta(3)}\left(1-\frac{N_0}{N}\right)$	$3k_\mathrm{B}T\frac{\mathrm{Li}_4(z)}{\mathrm{Li}_3(z)}$
Specific heat capacity	$12k_\mathrm{B}\frac{\zeta(4)}{\zeta(3)}\left(1-\frac{N_0}{N}\right)$	$12k_\mathrm{B}\frac{\mathrm{Li}_4(z)}{\mathrm{Li}_3(z)} - 9k_\mathrm{B}\frac{\mathrm{Li}_3(z)}{\mathrm{Li}_2(z)}$
Pressure	$nk_\mathrm{B}T\frac{\zeta(4)}{\zeta(3)}\left(1-\frac{N_0}{N}\right)$	$nk_\mathrm{B}T\frac{\mathrm{Li}_4(z)}{\mathrm{Li}_3(z)}$

Table 2.2.: *Temperature dependence of thermal averages for the 3D ideal Bose gas confined in the harmonic trap.*

Eq. (2.17) yields a finite value at the transition temperature T_c in this limit.

Another significant difference has proved to be of major importance for the experimental detection of BEC. All condensed particles in the free Bose gas have zero momentum. They are, thus, evenly spread in coordinate space and inseparable from the thermal cloud of non-condensed atoms. In contrast, the Bose-Einstein condensate in a harmonic trap has Gaussian like density distribution around the trap center in both coordinate and momentum space which is determined by the corresponding single-particle ground state wave functions. Additionally, as the ground state is macroscopically occupied and all other states are not, the condensate density sharply peaks in the flatly distributed cloud of non-condensed particles. Occurrence of such a peak in dilute gases at low temperatures is a strong indication of onsetting Bose-Einstein condensation [5]. Detection methods can be further improved by putting the trapping frequencies out of tune, i.e., creating an asymmetrically shaped trap. The condensate density will copy that shape accordingly, but the thermal atoms will still form a cloud with radial symmetry in momentum space because of $E \propto p^2$.

Interestingly, BEC is possible for the two-dimensional Bose gas in a harmonic trap. The corresponding transition temperature und the temperature dependence of the condensate fraction then read

$$k_\mathrm{B}T_\mathrm{c} = \hbar\widetilde{\omega}\left(\frac{N}{\zeta(2)}\right)^{1/2}, \tag{2.20}$$

$$\frac{N_0}{N} = 1 - \left(\frac{T}{T_\mathrm{c}}\right)^2. \tag{2.21}$$

This opens the possibility to create Bose-Einstein condensates in layered structures as considered within the scope of this diploma thesis. One of the most promising candidates for an experimental realization are composite electron-hole bosons, called *excitons*, in semiconductor heterostructures [6]. Due to their very small masses compared to atoms, the transition temperature of such a system should be larger by several orders of magnitude (see e.g., reviews [7, 8]).

2.2. Superfluidity

The original experimental observation of superfluid helium is due to two groups, Pyotr Kapitsa's in Moscow and Don Misener's in Cambridge, and was made in 1937. It had been already known for several years that helium remains fluid even at absolute zero due to zero-point fluctuations. Helium develops some peculiar characteristics when cooled below a certain transition temperature T_c, which became known as the *lambda point* due to the peculiar shape of the specific heat capacity (resembling the form of the small Greek letter λ). With different experimental setups and aims both groups could proof the existence of two different liquid phases of helium. In the so-called He-I phase above T_c, helium behaves like a conventional fluid, while the viscosity in the He-II phase below T_c is at least a factor 1500 smaller. For this ability to flow without apparent friction Kapitsa coined the term *superfluidity*.

Within a few months of the experimental detection Fritz London gave a qualitative explanation based on the concept of Bose-Einstein condensation. BEC was originally believed to be a special pathology of the non-interacting Bose gas which contradicts an application to a strongly correlated fluid. However, London's key argument was the predicted transition temperature of about 3.3 K for a gas with the particle mass and density of ^{4}He within BEC theory. This complies rather nicely to the measured lambda point at 2.2 K. Shortly after, Laszlo Tisza expanded London's idea by noting that the observed flow behavior could be qualitatively understood by assuming two fluid components. In his model, the Bose-Einstein condensed fraction of the helium atoms is accountable for the superfluid properties, while the rest behaves like an ordinary liquid.

Probably ignorant of Tisza's earlier work Lev Landau developed a phenomenological two-fluid description of liquid He-II which he published in a paper 1941. Landau posited superfluidity as a property of the ground state of a Bose liquid. He further introduced the concept of quasiparticles as collective excitations whose discrete momenta and energies sum up to the total momentum and energy of condensed matter at low temperatures. A gas of these quasiparticles is thought to form the normalfluid component of He-II. This conceptual basis for superfluidity is remarkably useful due to its intuitive approach to both the superfluid properties and the excitation spectrum.

Interestingly, Landau's theory does not directly need the concept of Bose-Einstein condensation. It even conflicts with BEC as a non-interacting Bose gas cannot be superfluid according to his theory. Oliver Penrose and Lars Onsager circumvented this problem in 1949 by generalizing the concept of BEC to interacting systems. Richard Feynman independently discovered the same theory two years later. In general consensus, these physicists are viewed as fathers of the modern theory of superfluidity.

Landau's theory will be reviewed in section 2.2.1, before the connection to Bose-Einstein condensation is investigated in section 2.2.2. Section 2.2.3 provides the two commonly used theoretical approaches within the theory of the dilute, weakly interacting Bose gas. Section 2.2.4 closes with an overview over the current status of research concerning the possible existence of superfluid solid, called *supersolids*.

2.2.1. Two-fluid model

Landau's two-fluid model divides the liquid into a normal and a superfluid component. Unlike the normalfluid, the superfluid flows frictionless through capillaries and is responsible for the observed peculiar properties of He-II. However, both fluid components are thought to interpenetrate completely and an experimental separation is impossible.

Instead of proving the frictionless flow of a moving fluid, one can demonstrate the impossibility to put a resting fluid into motion: If one considers the laminar flow of an ordinary fluid through a capillary, the dissipation loss from the friction between fluid and confining walls will slow down the movement at the fluid boundary. It ultimately leads to the formation of a paraboloidal shaped velocity field with the strongest flow in the capillary center and zero movement at the boundary layer. The same progression viewed from the initial rest frame of the fluid shows a gradual development of movement starting at the boundary.

In Landau's model, the normalfluid component is thought as made up from quasiparticles which are collective excitations out of the resting ground state. The key question is whether the kinetic energy of the moving fluid is sufficient to excite a quasiparticle in the rest frame of the fluid. In order to answer it one needs the relations for the total momentum and energy of the fluid between laboratory frame (unprimed) and the fluid rest frame (primed), which moves with velocity $\mathbf{v}$ against the laboratory frame. These can be easily derived using the Galilei transformations for position $\mathbf{x} = \mathbf{x}' + \mathbf{v}t$ and momentum $\mathbf{p} = \mathbf{p}' + m\mathbf{v}$ of a particle with mass m,

$$\mathbf{P} = \mathbf{P}' + M\mathbf{v}, \qquad E = E' + \mathbf{P}'\mathbf{v} + \frac{1}{2}M\mathbf{v}^2. \tag{2.22}$$

Here, quantities denoted with a capital letter correspond to the whole system.

Suppose the system is in its ground state having the energy E_g which will be the case at $T = 0$. Then, the total energy and momentum in both reference frames will become

$$\text{rest frame} \qquad E_1' = E_\mathrm{g}, \qquad \mathbf{P}_1' = 0, \tag{2.23}$$

$$\text{laboratory frame} \qquad E_1 = E_\mathrm{g} + \frac{1}{2}M\mathbf{v}^2, \qquad \mathbf{P}_1 = M\mathbf{v}. \tag{2.24}$$

An excitation of a quasiparticle with momentum $\mathbf{p}$ and energy $\epsilon(\mathbf{p})$ alters these relations to

$$\text{rest frame} \qquad E_2' = E_\mathrm{g} + \epsilon(\mathbf{p}), \qquad \mathbf{P}_2' = \mathbf{p}, \tag{2.25}$$

$$\text{laboratory frame} \qquad E_2 = E_\mathrm{g} + \epsilon(\mathbf{p}) + \mathbf{p}\mathbf{v} + \frac{1}{2}M\mathbf{v}^2, \qquad \mathbf{P}_2 = \mathbf{p} + M\mathbf{v}. \tag{2.26}$$

The excitation of quasiparticles is possible, when the energy difference $\Delta E = E_2 - E_1 = \epsilon(\mathbf{p}) + \mathbf{p}\mathbf{v}$ is negative. The least possible value for ΔE is achieved, when momentum of the quasiparticle and velocity of the fluid stand anti-parallel to each other. This implies that v must be greater than $\frac{\epsilon(\mathbf{p})}{p}$. If there exists a critical velocity

$$v_\mathrm{c} = \min_\mathrm{p} \frac{\epsilon(\mathbf{p})}{p} > 0, \tag{2.27}$$

then it is impossible to excite a quasiparticle in a system which flows slower than v_c. Hence, the fluid flows without friction and will not slowdown when viewed from the laboratory

frame. A linear dispersion relation, meaning an energy spectrum of acoustic phonons, meets equation (2.27), i.e., $\epsilon(\mathbf{p}) = c\mathbf{p}$. He-II itself has a slightly more complex energy spectrum with an additional so-called *roton* minimum, but one still can issue a critical velocity which empirically confirms the validity of above considerations.

The necessity of an acoustic phonon type spectrum has an important implication. As the spectrum of the non-interacting Bose gas is that for free particles $\epsilon(\mathbf{p}) = \mathbf{p}^2/2m$ there does not exist a critical velocity and, hence, a non-interacting Bose gas cannot be superfluid. This directly negates a general equality of condensate and superfluid fraction as originally devised by Tisza's two-fluid model. It further states that inter-particle interaction is a requirement for superfluidity.

So far, the system has been regarded at absolute zero. At a finite temperature above zero the fluid partly consists of quasiparticles emerged from thermal excitations. For energy dissipation due to friction between capillary boundary and fluid, the reasoning above still holds true, as only the formation of additional quasiparticles is of importance. On the other hand, a supposable friction between superfluid and normalfluid component now has to be taken into account.

In this case, one has to consider the relative movement of the quasiparticle gas against the fluid. Suppose that the velocity is $\mathbf{v}$ viewed from the rest frame of the fluid. As it can be easily seen by comparing eq. (2.24) to eq. (2.26), the excitation of a quasiparticle with energy $\epsilon(\mathbf{p})$ in the rest frame of the fluid adds a quasiparticle with energy $\epsilon(\mathbf{p}) - \mathbf{p}\cdot\mathbf{v}$ in the rest frame of the gas. In thermal equilibrium the quasiparticle energies are distributed according to Bose statistics. The total momentum of the gas viewed from the rest frame of the fluid can, therefore, be calculated via

$$\mathbf{P} = \sum_i \mathbf{p}_i \, n(\epsilon(\mathbf{p}_i) - \mathbf{p}_i \cdot \mathbf{v}). \tag{2.28}$$

Evaluating the sum with an integral over phase space and expanding the distribution in a Taylor series yields

$$\mathbf{P} = -\int \mathbf{p}(\mathbf{p}\cdot\mathbf{v})\frac{\mathrm{d}n(\epsilon)}{\mathrm{d}\epsilon}\,\mathrm{d}\tau = \frac{\mathbf{v}}{3}\int\left(-\frac{\mathrm{d}n(\epsilon)}{\mathrm{d}\epsilon}\right)p^2\,\mathrm{d}\tau, \tag{2.29}$$

where $\mathrm{d}\tau$ denotes the volume element. The last step is made by averaging over the orientations of $\mathbf{p}$.

Several conclusions can be drawn from this result. Most importantly, the relative movement of the gas against the fluid is connected with mass transportation. The effective mass can be directly read off the right-hand side of eq. (2.29). The remaining mass must be carried by the fluid. The relative movement of both components to one another is stable and, thus, frictionless since it has been obtained in thermodynamical equilibrium. Unlike the fluid, however, nothing prevents the gas of quasiparticles to collide with the capillary walls which causes friction. This constitutes Landau's view of a normalfluid as a gas made up from quasiparticles.

2.2.2. Modern theory

In the modern theory of superfluidity the underlying fundamental assumption is that the superfluid phase is connected to Bose-Einstein condensation in the following sense: At any

given time it is possible to find a complete orthonormal basis of single-particle states such that one (and only one) of these states is occupied by finite fraction of particles, which make up the *condensate*. The corresponding single-particle wave function,

$$\chi_0(\mathbf{x},t) = \sqrt{n_0(\mathbf{x},t)}\, e^{i\phi(\mathbf{x},t)}, \tag{2.30}$$

is referred to as the *condensate wave function* [9]. The condensate wave function provides phase-coherence over macroscopic distances. Yang showed that this concept can be traced back to a peculiar characteristic of the density matrix, namely *off-diagonal long-range order (ODLRO)* [10].

The connection to superfluidity is quite simple. Calculation of the current density by using the continuity equation yields

$$\mathbf{j}_0(\mathbf{x},t) = \frac{i\hbar}{2m}(\chi\nabla\chi^* - \chi^*\nabla\chi) = \frac{\hbar}{m} n_0(\mathbf{x},t)\nabla\phi(\mathbf{x},t), \tag{2.31}$$

from which the flow velocity of the condensate can be read off as

$$v_\mathrm{s}(\mathbf{x},t) = \frac{\hbar}{m}\nabla\phi(\mathbf{x},t). \tag{2.32}$$

As this motion can occur in thermodynamical equilibrium, it is frictionless and, therefore, defines the *superfluid velocity*. It should be emphasized that this does not imply the equality of condensate and superfluid fraction which has already been excluded in the preceding section.

Equation (2.32) immediately leads to the conclusion that superfluid flow is irrotational, because there exists a velocity potential field proportional to the phase of the condensate wave function. However, as the phase and, thus, the potential is periodic, circulating flow around regions which are infinite in one dimension and where $|\chi_0(\mathbf{x},t)|$ vanishes is not forbidden in general. For the integral over (2.32) around a circuit enclosing one of such regions Stokes' theorem can no longer be applied, because the region is not simply connected. But as the phase of the condensate wave function in the surrounding space must be single-valued modulo 2π, the integral leads to the *Onsager-Feynman quantization condition*

$$\oint \mathbf{v}_\mathrm{s}\cdot\mathrm{d}\mathbf{l} = \frac{h}{m}n, \qquad n\in\mathbb{Z}. \tag{2.33}$$

This condition can be satisfied by a pattern of flow with $v_\mathrm{s} \propto r^{-1}$. Such a pattern is called *vortex* or, more precisely, *vortex line*. As the hypothesis $|\chi_0(\mathbf{x},t)|$ vanishes in the core and, thus, v_s is undefined, the appearing singularity of the vortex center is physically irrelevant. In finite confinements, vortex lines end at the boundary of the liquid. The energy and angular momentum of a vortex in the center of cylindrical confinement with radius R and height h can be calculated to

$$E_\mathrm{vortex} = n^2\rho_\mathrm{s}h\pi\ln R/a, \tag{2.34}$$

$$L_\mathrm{vortex} = n\rho_\mathrm{s}h\pi R^2, \tag{2.35}$$

where a is the radius of the vortex core.

Similar to the maximum translational flow velocity as discussed in the previous chapter, the occurrence of vortices limit the angular velocity in rotating systems. Consider a bucket in which a fluid rotates with $\boldsymbol{\omega}$. The relations for the total angular momentum and energy of the fluid between laboratory frame (unprimed) and the fluid rest frame (primed) are

$$\mathbf{L} = \mathbf{L}' + I\boldsymbol{\omega}, \tag{2.36}$$

$$E = E' + \mathbf{L}' \cdot \boldsymbol{\omega} + \frac{1}{2} I\omega^2, \tag{2.37}$$

which can be obtained using the Galilei transformations for angle and angular momentum of a single particle. I denotes the rotational inertia of the whole system.

With no vortices the system shall have the energy E_g. Then, the total energy and angular momentum in both reference frames will become

$$\text{rest frame} \qquad E_1' = E_\mathrm{g}, \qquad \mathbf{L}_1' = 0, \tag{2.38}$$

$$\text{laboratory frame} \qquad E_1 = E_\mathrm{g} + \frac{1}{2} I\omega^2, \qquad \mathbf{L}_1 = I\boldsymbol{\omega}. \tag{2.39}$$

Occurrence of a single vortex with angular momentum $\mathbf{l}$ and energy $\epsilon(\mathbf{l})$ changes above relations to

$$\text{rest frame} \qquad E_2' = E_\mathrm{g} + \epsilon(\mathbf{l}), \qquad \mathbf{L}_2' = \boldsymbol{\omega}, \tag{2.40}$$

$$\text{laboratory frame} \qquad E_2 = E_\mathrm{g} + \epsilon(\mathbf{l}) + \mathbf{l} \cdot \boldsymbol{\omega} + \frac{1}{2} I\omega^2, \qquad \mathbf{L}_2 = \mathbf{l} + I\boldsymbol{\omega}. \tag{2.41}$$

Hence, the excitation of a vortex is energetically impossible for

$$\omega < \omega_\mathrm{c} = \min_{\mathbf{l}} \frac{\epsilon(\mathbf{l})}{l}. \tag{2.42}$$

Inserting expressions (2.34) and (2.35) yields for the critical angular velocity

$$\omega_\mathrm{c} = \frac{\hbar}{mR^2} \ln \frac{R}{a}. \tag{2.43}$$

A fluid circulating at this speed has exactly one vortex line with $n = 1$. At k-times ω_c there are k such vortex lines, which array themselves in a hexagonal pattern. As an angular velocity of at least $\omega \geq 3\omega_\mathrm{c}$ is needed to form vortices with $n > 1$, these are unstable against decay into multiple $n = 1$ vortices. Each vortex contributes one angular momentum quantum to the fluid.

An important effect for both experimental detection and numerical investigations is the *Hess-Fairbank effect* or *non classical rotational inertia (NCRI)*. A slow rotation of the confining bucket with an angular velocity $\omega < \omega_\mathrm{c}$ will be completely ignored by the superfluid fraction because vortex lines cannot be excited. In thermodynamic equilibrium only the normalfluid fraction rotates with ω and, thus, contribute to the moment of inertia of the whole system. As the moment of inertia is proportional to the mass density, the superfluid fraction can be calculated as follows

$$\frac{\rho_\mathrm{s}}{\rho} = 1 - \frac{I}{I_0}, \tag{2.44}$$

where I_0 denotes the expected value for the rotational inertia of the whole system.

Last but not least, it should be mentioned that vortex lines do not necessarily be straight. Particularly in capillaries, the ends of vortex lines may connect to vortex rings similar to smoke rings. Their excitation energies are typically much smaller than those of phonons and, thus, can further reduce the critical velocity of superfluid flow.

2.2.3. Weakly interacting Bose-gases

So far, the theory of superfluidity has been developed based on assumptions for the underlying physical system without an explicit connection to existing systems. As mentioned several times before, the ideal Bose gas considered in section 2.1 lacks the ability to show superfluidity. Inter-particle interaction is necessary and has to be introduced into the system. Unfortunately, an exact analytical investigation of the interacting Bose gas is impossible. However, the dilute, weakly interacting Bose gas allows for certain approximations which lead to the desired theoretical justification of superfluidity. Two different approaches are presented in this section, the *Bogoliubov theory* and the *Gross-Pitaevskii mean-field theory*. Each provides a different set of puzzle pieces, which complement one another to form the frame for understanding superfluidity (see e.g., reviews [11, 12])

Bogoliubov-approach

The Hamiltonian of a free interacting system in second quantization and momentum representation reads

$$\hat{H} = \sum_{\mathbf{k}} \frac{\hbar^2 k^2}{2m} \hat{a}^\dagger_{\mathbf{k}} \hat{a}_{\mathbf{k}} + \frac{1}{2V} \sum_{\mathbf{k},\mathbf{p},\mathbf{q}} W_{\mathbf{q}} \hat{a}^\dagger_{\mathbf{p}+\mathbf{q}} \hat{a}^\dagger_{\mathbf{k}-\mathbf{q}} \hat{a}_{\mathbf{p}} \hat{a}_{\mathbf{k}}, \tag{2.45}$$

where the Fourier transformation of the 2-particle interaction potential, $W(\mathbf{r}) = W(\mathbf{r}_2 - \mathbf{r}_1)$, is used

$$W_{\mathbf{q}} = \int \mathrm{d}^3\mathbf{r}\, e^{-i\mathbf{q}\cdot r} W(\mathbf{r}). \tag{2.46}$$

The Bogoliubov approach makes two major assumptions regarding the nature of the system, namely that

1. the system has a Bose-Einstein condensed phase and
2. the gas is dilute and only weakly interacting.

This allows for certain approximations (see appendix A), which results in a Hamiltonian of the following form

$$\hat{H} = {\sum_{\mathbf{k}}}' \frac{\hbar^2 k^2}{2m} \hat{a}^\dagger_{\mathbf{k}} \hat{a}_{\mathbf{k}} + \frac{N^2}{2V} W_0 + \frac{N}{V} {\sum_{\mathbf{k}}}' W_{\mathbf{k}} \hat{a}^\dagger_{\mathbf{k}} \hat{a}_{\mathbf{k}} + \frac{N}{2V} {\sum_{\mathbf{k}}}' W_{\mathbf{k}} \left(\hat{a}^\dagger_{\mathbf{k}} \hat{a}^\dagger_{-\mathbf{k}} + \hat{a}_{\mathbf{k}} \hat{a}_{-\mathbf{k}} \right). \tag{2.47}$$

It was Bogoliubov's main achievement to devise a convenient method in order to diagonalize this Hamiltonian [13]. He introduced a new set of operators $\hat{b}^\dagger_{\mathbf{k}}$ and $\hat{b}_{\mathbf{k}}$, which obey

the Bose commutation rules and correspond to the creation and the annihilation of a quasiparticle, respectively. Their relation to the original operators

$$\begin{aligned} \hat{a}_{\mathbf{k}} &= u_{\mathbf{k}}\hat{b}_{\mathbf{k}} + v_{\mathbf{k}}\hat{b}^{\dagger}_{-\mathbf{k}}, \\ \hat{a}^{\dagger}_{\mathbf{k}} &= u_{\mathbf{k}}\hat{b}^{\dagger}_{\mathbf{k}} + v_{\mathbf{k}}\hat{b}_{-\mathbf{k}} \end{aligned} \qquad \text{with } u_{\mathbf{k}}^2 - v_{\mathbf{k}}^2 = 1,\ u_{\mathbf{k}} = u_{-\mathbf{k}},\ v_{\mathbf{k}} = v_{-\mathbf{k}} \tag{2.48}$$

is called *Bogoliubov transformation*. The transformation was originally introduced by Holstein and Primakoff[14] within the theory of complex spin waves in 1940 and later rediscovered by Bogoliubov in 1947 [15].

If one chooses $u_{\mathbf{k}}$ and $v_{\mathbf{k}}$ according to

$$\begin{aligned} u_{\mathbf{k}}^2 &= \frac{\epsilon_{\mathbf{k}} + \left(\frac{k^2}{2m} + nW_{\mathbf{k}}\right)}{2\epsilon_{\mathbf{k}}}, \\ v_{\mathbf{k}}^2 &= \frac{-\epsilon_{\mathbf{k}} + \left(\frac{k^2}{2m} + nW_{\mathbf{k}}\right)}{2\epsilon_{\mathbf{k}}}, \end{aligned} \tag{2.49}$$

where $\epsilon_{\mathbf{k}}$ is used as shortcut for

$$\epsilon_{\mathbf{k}} = \sqrt{\left(\frac{\hbar^2 k^2}{2m} + nW_{\mathbf{k}}\right)^2 - (nW_{\mathbf{k}})^2}. \tag{2.50}$$

the off-diagonal term in eq. (2.47) vanishes. This leads to the final result

$$\hat{H} = \frac{1}{2}nNW_0 - \frac{1}{2}{\sum_{\mathbf{k}}}'\left(\frac{\hbar^2 k^2}{2m} + nW_{\mathbf{k}} - \epsilon_{\mathbf{k}}\right) + {\sum_{\mathbf{k}}}'\epsilon_{\mathbf{k}}\hat{b}^{\dagger}_{\mathbf{k}}\hat{b}_{\mathbf{k}}. \tag{2.51}$$

Equation (2.50) describes the energy spectrum of the quasiparticles and is, therefore, referred to as *dispersion relation*. It can be estimated to an acoustic phonon type spectrum $\epsilon_{\mathbf{k}} = c\hbar k$ with a sound velocity of $c = \sqrt{nW_0/m}$ for small wave vectors $\mathbf{k}$. Excitations to large wave vectors obey a dispersion relation comparable to free particles $\epsilon_{\mathbf{k}} = \frac{\hbar^2 k^2}{2m}$.

Complying to the definitions issued in the preceding sections, one would expect a weakly interacting Bose gas to show superfluidity. Indeed, the recent experimental realizations of BEC in dilute alkali gases verified this prediction. However suggestive, the comparison to He-II is misleading as the interaction strength in fluids is far from weak. Nevertheless, this result underlines the importance of inter-particle interactions for the occurrence of superfluidity.

A quantity of special interest is the thermal expectation value for the number of condensed particles N_0. For its computation, consider the particle number operator

$$\hat{N} = \sum_{\mathbf{k}}\hat{a}^{\dagger}_{\mathbf{k}}\hat{a}_{\mathbf{k}} = N_0 + {\sum_{\mathbf{k}}}'\hat{a}^{\dagger}_{\mathbf{k}}\hat{a}_{\mathbf{k}}. \tag{2.52}$$

Rewriting this operator into quasiparticle representation and calculating the thermodynamic expectation value yields

$$N = N_0 + {\sum_{\mathbf{k}}}'v_{\mathbf{k}}^2 + {\sum_{\mathbf{k}}}'\bar{n}_{\mathbf{k}}\left(u_{\mathbf{k}}^2 + v_{\mathbf{k}}^2\right), \tag{2.53}$$

where $\bar{n}_{\mathbf{k}}$ denotes the expected number of excited quasiparticles. Because of their bosonic nature without particle number conservation, $\bar{n}_{\mathbf{k}}$ equals the Bose-Einstein distribution with $\mu = 0$.

The ground state can be defined by demanding $\hat{b}_{\mathbf{k}} |0\rangle = 0$ for all wave vectors. This corresponds to a state without excited quasiparticles. Altering the above equation accordingly, one obtains for the condensate fraction

$$\frac{N_0}{N} = 1 - \frac{\nu}{(2\pi\hbar)^3} \int v_{\mathbf{k}}^2 \, \mathrm{d}^3\mathbf{k}. \tag{2.54}$$

Equation (2.54) implies that even when the system is in its ground state, not all particles are condensed. This effect is called *condensate depletion*. On the other hand, the system is 100 % superfluid in its ground state, which emphasizes the difference between condensate and superfluid fraction.

Equation (2.54) predicts the existence of a critical density, $n_\mathrm{c} = \frac{1}{(2\pi\hbar)^3} \int v_{\mathbf{k}}^2 \, \mathrm{d}^3\mathbf{k}$. Denser gases do not show a BEC phase. This self-consistently confirms the initial assumption of a dilute gas.

The restriction of the inter-particle interaction to a pure contact potential type with s-wave scattering length a allows one to issue quantitative predictions for the condensate depletion. The condensate density will become

$$n_0 = \begin{cases} n - \frac{8}{3\sqrt{\pi}}(na)^{3/2}, & T = 0\,\mathrm{K} \\ n - \frac{8}{3\sqrt{\pi}}(na)^{3/2} \left(1 + 6\int_0^\infty \mathrm{d}y \frac{x}{e^{\gamma y} - 1}\right), & T > 0\,\mathrm{K} \end{cases} \tag{2.55}$$

Phonons with $\epsilon_{\mathbf{k}} = c\hbar k$ are the only quasiparticles, which can be excited at very low temperatures. This yields a parabolic increase of the condensate depletion with rising temperature in first-order approximation:

$$n_0(T) = n_0(0) - \frac{m}{12c}(k_B T)^2. \tag{2.56}$$

Further investigations can be found e.g., in [15] or [16].

Gross-Pitaevskii mean-field approach

So far, the Bogoliubov approach made it possible to draw the connection between Bose-Einstein condensation and superfluidity. It demonstrates the role of inter-particle interactions for a phonon type spectrum and explains the inequality of condensate and superfluid fraction. However, it does not explain the dynamical properties of the condensate. In particular, it lacks a reasonable explanation for the condensate wave function assumed in chapter 2.2.2.

A different approach to the theory of the weakly-interacting Bose gas is the Gross-Pitaevskii mean-field ansatz [17, 18]. The basic assumptions are identical to those made in the Bogoliubov theory, but its starting point is Hamiltonian in second quantization and space representation, i.e.,

$$\begin{aligned} \hat{H} = &\int \mathrm{d}\mathbf{r}_1 \, \hat{\Psi}^\dagger(\mathbf{r}_1) \left(-\frac{\hbar^2}{2m} \nabla_{\mathbf{r}_1}^2 + V(\mathbf{r}_1) \right) \hat{\Psi}(\mathbf{r}_1) \\ &+ \frac{1}{2} \iint \mathrm{d}\mathbf{r}_1 \mathrm{d}\mathbf{r}_2 \, \hat{\Psi}^\dagger(\mathbf{r}_1) \hat{\Psi}^\dagger(\mathbf{r}_2) W(\mathbf{r}_1 - \mathbf{r}_2) \hat{\Psi}(\mathbf{r}_2) \hat{\Psi}(\mathbf{r}_1). \end{aligned} \tag{2.57}$$

The main idea is to replace the field operators by a new set of operators, which do only act on condensed particles. In particular, these new *condensate operators* $\hat{\Xi}, \hat{\Xi}^\dagger$ shall change the number of particles in the condensate by 1. Under the imposed restriction that the ground state is occupied by a macroscopic number of particles, a change of this number does not have any major impact on the physical behavior. One can, therefore, assume that the condensate operators do not change state of the system. This assertion is strictly valid in the thermodynamic limit. Thus, the condensate operators are defined as follows

$$\lim_{N\to\infty} \langle m, N|\hat{\Xi}|m, N+1\rangle = \Xi, \tag{2.58}$$

$$\lim_{N\to\infty} \langle m, N+1|\hat{\Xi}^\dagger|m, N\rangle = \Xi^*. \tag{2.59}$$

Here, $|m, N\rangle$ and $|m, N+1\rangle$ denote "identical" system states, which only differ in the number of particles in the system.

Calculating the thermodynamic expectation value of the condensate particles operator gives the condensate density

$$\langle\hat{\Xi}^\dagger\hat{\Xi}\rangle = \Xi^*\Xi = |\Xi|^2 = n_0. \tag{2.60}$$

In general, the gas is neither homogeneous nor stationary, so Ξ is a function of space and time. It then is the wave function for a particle in the condensate. Obviously, the wave functions for each condensate particle are identical, so it has the meaning of the condensate wave function

$$\Xi(\mathbf{r}, t) = \sqrt{n_0(\mathbf{r}, t)}\, e^{i\Phi(\mathbf{r},t)}, \tag{2.61}$$

which is exactly the same as in eq. (2.30).

The original field operators can be issued in the form

$$\hat{\Psi} = \hat{\Xi} + \hat{\Psi}', \qquad \hat{\Psi}^\dagger = \hat{\Xi}^\dagger + \hat{\Psi}^{\dagger\prime}, \tag{2.62}$$

where $\hat{\Psi}', \hat{\Psi}^{\dagger\prime}$ describe the "remaining" operators, which act on non-condensed particles. Consequently, they transfer the non-condensate part of a state $|m, N\rangle$ into a thereto orthogonal state, i.e.,

$$\lim_{N\to\infty} \langle m, N|\hat{\Psi}'|m, N+1\rangle = 0, \tag{2.63}$$

$$\lim_{N\to\infty} \langle m, N+1|\hat{\Psi}^{\dagger\prime}|m, N\rangle = 0. \tag{2.64}$$

The equation of motion for the field operators reads

$$\begin{aligned} i\hbar\frac{\partial}{\partial t}\hat{\Psi}(\mathbf{r}, t) = &\left\{-\frac{\hbar^2}{2m}\nabla^2 + V(\mathbf{r})\right\}\hat{\Psi}(\mathbf{r}, t) \\ &+ \int \mathrm{d}\mathbf{r}'\, \hat{\Psi}^\dagger(\mathbf{r}', t)W(\mathbf{r}-\mathbf{r}')\hat{\Psi}(\mathbf{r}', t)\,\hat{\Psi}(\mathbf{r}, t). \end{aligned} \tag{2.65}$$

In zeroth-order approximation the field operators can be substituted by the condensate wave function. This leads to the *Gross-Pitaevskii equation* (GPE)

$$\begin{aligned} i\hbar\frac{\partial}{\partial t}\Xi(\mathbf{r}, t) = &\left\{-\frac{\hbar^2}{2m}\nabla^2 + V(\mathbf{r})\right\}\Xi(\mathbf{r}, t) \\ &+ \Xi(\mathbf{r}, t)\int \mathrm{d}\mathbf{r}'\, |\Xi(\mathbf{r}', t)|^2 W(\mathbf{r}-\mathbf{r}'). \end{aligned} \tag{2.66}$$

Assuming that the wave function $\Xi(\mathbf{r},t)$ changes slowly on atomic spacings and the inter-particle interaction $W(\mathbf{r}-\mathbf{r}')$ is short ranged (e.g., contact potential), one can approximate the pair interaction by pulling $\Xi(\mathbf{r},t)$ out of the integral. The effect of the pair interaction then reduces to a simple factor λ. Using the time evolution of the stationary wave-function, i.e.,

$$\Xi(\mathbf{r},t) = \Xi(t)e^{-i\frac{\hbar}{\mu}t}, \tag{2.67}$$

one arrives at the *stationary Gross-Pitaevskii equation*

$$\left\{-\frac{\hbar^2}{2m}\nabla^2 + \lambda|\Xi(\mathbf{r})|^2\right\}\Xi(\mathbf{r}) = \mu\Xi(\mathbf{r}). \tag{2.68}$$

This equation has the form of a non-linear Schrödinger equation. The inter-particle interaction is taken into account by an additional mean-field term. Neglecting this term results in the normal Schrödinger equation.

As a closing note, two applications of the stationary GPE for systems with contact interaction ($\lambda = W_0$, $\mu = nW_0$) are presented

Acoustic phonons. A standing wave ansatz, i.e.,

$$\Xi = \sqrt{n} + Ae^{i(\mathbf{k}\cdot\mathbf{r}-\omega t)} + Be^{-i(\mathbf{k}\cdot\mathbf{r}-\omega t)}, \tag{2.69}$$

describing small density oscillations leads to known dispersion relation (eq. (2.50)) derived within Bogoliubov theory.

Vortex lines. An ansatz of the form

$$\Xi(r,\phi) = \sqrt{n}\, f\left(\frac{r}{r_0}\right) e^{i\phi}, \tag{2.70}$$

models the superfluid density distribution around a straight vortex line. By introducing the reduced units $x = r/r_0$ with $r_0 = \sqrt{\hbar/8\pi an}$ one obtains a conditional equation for the radial part of the wave function, i.e.,

$$\frac{1}{x}\frac{d}{dx}\left(x\frac{df}{dx}\right) - \frac{f}{x^2} + f - f^3 = 0. \tag{2.71}$$

The differential equation itself can be only solved numerically. But an investigation of its asymptotic behavior yields

$$f \propto x \to 0, \qquad \text{for } x \to 0, \tag{2.72}$$

$$f \approx 1 - 1/2x^2, \qquad \text{for } x \to \infty. \tag{2.73}$$

This complies to the initial assumption that superfluidity is completely suppressed in the vortex core, whereas far away from the center the superfluid density of the resting fluid is assumed. The length r_0 characterizes the size of the vortex core and is called *healing length*, as it corresponds to the analogous quantity for magnetic flux lines in type-II superconductors. For dilute, weakly interacting gases, r_0 is large in comparison to inter-particle distances, in contrast to the atomic dimensions of vortices in liquids [16].

2.2.4. Superfluidity in the solid phase

The occurrence of superfluidity in the fluid and gas phase of matter have led to speculations whether macroscopically ordered states like solids could exhibit superfluidity, too. The debate was initiated by a paper from Leggett published in 1970 [19]. He considered a rotating solid confined in a cylindrical annulus. Thereby, he defines "solid" as a system of atoms, whose pair correlation function in the ground state does not tend to a constant value even deep inside the sample, i.e., showing strong variations over distances of the order of atomic spacing. This definition does not imply that the many body wave function of the ground state must be clearly disconnected, which would correspond to the conventional picture of a solid with its localized atoms on lattice sites. If one allows for the possibility of atoms to exchange places, one cannot exclude the occurrence of the NCRI-effect. Such potentially superfluid solids became known as *supersolids* in literature.

A potential mechanism for particle exchange was given by Chester[20] a little time earlier in the same year. He suggested that in a Bose solid a non-zero fraction of atoms may occupy the zero momentum state. The existence of a Bose-Einstein condensate certainly allows for the assumption of particle exchange. Another interesting possibility would be the condensation of crystal defects as proposed by Andreev and Lifshits in 1969[21]. However, Leggett issues a tentative upper limit to the expectant superfluid fraction. The value lies at $\sim 3 \cdot 10^{-4}$, which would explain why the effect had so far escaped notice.

The topic grew hot again in 2004, when Kim and Chan reported their discovery of the NCRI-effect observed for helium confined in porous materials, namely Vycor[22] and gold[23], and later in bulk helium confined in an annulus channel[24]. Their detection method of choice is a torsion experiment with a high mechanical quality factor ($2 \cdot 10^6$) of the oscillation. The sample is confined under high pressure (up to 66 bar) in a cell attached to a rod hanging below the ceiling. The cylindrical drive and detection electrodes are each coupled capacitively to planar electrodes attached as fins on the cell. A lock-in amplifier keeps the oscillation of the cell in resonance, which is about $\tau \approx 1\,\mathrm{ms}$ and can be measured with an accuracy of $\Delta\tau \approx 1\,\mathrm{ns}$.

In the experiment, the resonance frequency ω_0 slips from its classically expected value when the system is cooled below 230 mK. Since ω_0 of the cell is directly coupled to its moment of inertia, Kim and Chan relate the drop to the NCRI-effect implying that solid helium must be partly superfluid. Interestingly, they receive values for superfluid fraction ranging up to 1.7 %. However, several authors criticize these results and propose alternative explanations for the drop of the moment of inertia. For instance, Dash and Wettlaufer[25] suggest to take slippage of the solid, due to grain boundary premelting between the solid and densely adsorbed layers at the container wall, into account for the missing rotational inertia. Such an intermediate liquid layer of helium could also be superfluid accounting for the NCRI-effect in the Vycor experiments, where slippage is impossible because helium is pinned in the Vycor matrix. Numerical investigations from Khairallah and Ceperley[26] using the path-integral Monte-Carlo method based on first principles (see chapter 3) provide further evidence for such a superfluid layer. Bulk helium itself seems to consist of perfectly localized atoms. A partly delocalized and, thus, superfluid layer is found only in between the mismatching bulk surface and densely absorbed layer at the Vycor boundary inside a pore.

Nevertheless, Kim and Chan's announcement revived the interest in supersolids. Some recent theoretical works are devoted to provide necessary preconditions which must be fulfilled in order to observe the phenomenon. Prokof'ev and Svistunov[27] prove that the solid must be incommensurate, meaning it is to have zero-point vacancies, or interstitial atoms, or both as an integral part of the ground state. In the same spirit, Shi[28] provides a general derivation of the NCRI-effect as consequence of off-diagonal long-range order (ODLRO) in an interacting Bose system. Particularly, he demonstrates explicitly that NCRI cannot be possessed in absence of defects. Both groups argue against supersolidity in bulk helium, since an overwhelming part of experimental work suggests helium to be commensurate (see e.g., review [29]).

A number of groups[30, 31, 32, 33] investigated a model system with hard-core bosons on a triangular lattice and next-neighbor hopping. Such a system does exhibit a stable supersolid phase, if the lattice points are nearly half occupied with bosons. Depending on the filling factor ρ, either the bosons ($1/3 < \rho < 1/2$) or the vacancies ($1/2 < \rho < 2/3$) form a crystalline structure which is completely interpenetrated by a Bose-Einstein condensate consisting of the corresponding complementary part. Interestingly, one does not find a stable supersolid phase on a square lattice regardless of the filling factor. Here, the system splits up into solid clusters separated from one another by superfluid interfaces [34].

In very recent history, a different supersolid phase was found by Boninsegni, Prokof'ev and Svistunov[35] using numerical PIMC simulations with the newly created worm-algorithm extension developed by the same group [36]. They created an amorphous phase of ^{4}He by quenching the system from its liquid phase into a frozen meta-stable state. Such a highly disordered state possesses off-diagonal long-range order and is, thus, superfluid. Due to its glass like nature, this state of matter has been named *superglass*.

3. The path integral Monte Carlo method

Richard Feynman introduced the path integral representation of the quantum system in 1948 which generalizes the action principle of classical mechanics. Within this theory, each quantum particle is considered as a series of positions forming a closed trajectory in space. The particle "moves" along this trajectory obeying a law similar to the classical action. The physics of the system itself are derived from an functional integration over all possible paths.

However, the explicit calculation of physical observables is somewhere limited, as huge amounts of computational time are needed in order to perform the integration. The combination with Monte Carlo integration method remedies this issue and constitutes the *path integral Monte Carlo (PIMC)* method. It is suited for statistical investigations of a quantum system at any temperature. In principle, all errors due to necessary approximations can be made arbitrarily small, which makes PIMC a powerful numerical method based on first principles.

3.1. Calculation of thermal averages with path integrals

Any quantum system is fully described by its density operator [37], which in the canonical ensemble reads

$$\hat{\rho} = \sum_i e^{-\beta E_i} |i\rangle \langle i| = e^{-\beta \hat{H}}, \tag{3.1}$$

where $|i\rangle$ denotes an eigenstate of the Hamiltonian $\hat{H}$ to the energy eigenvalue E_i, i.e., $\hat{H}|i\rangle = E_i|i\rangle$. The trace over $\hat{\rho}$ yields the partition function

$$Z = \sum_i e^{-\beta E_i} = \operatorname{Tr} \hat{\rho}. \tag{3.2}$$

The thermal average of an observable $\hat{A}$ in thermodynamic equilibrium is determined by

$$\langle \hat{A} \rangle = \frac{\sum_i e^{-\beta e_i} \langle i|\hat{A}|i\rangle}{\sum_i e^{-\beta e_i} \langle i|i\rangle} = \frac{\operatorname{Tr} \hat{\rho}\hat{A}}{\operatorname{Tr} \hat{\rho}} = \frac{\operatorname{Tr} \hat{\rho}\hat{A}}{Z}. \tag{3.3}$$

The corresponding density matrix in coordinate representation reads

$$\rho(R, R'; \beta) \equiv \langle R|e^{-\beta \hat{H}}|R'\rangle = \sum_i \phi_i^*(R) e^{-\beta E_i} \phi_i(R'), \tag{3.4}$$

with $R = (\mathbf{r}_1, \ldots, \mathbf{r}_N)$, where $\mathbf{r}_i$ denotes the position of the ith particle. The partition function (3.2) in this basis is

$$Z = \int \mathrm{d}R\, \rho(R, R; \beta), \tag{3.5}$$

and the thermal average (3.3) is calculated as

$$\langle \hat{A} \rangle = \frac{1}{Z} \int \mathrm{d}R \, \langle R|\rho\hat{A}|R\rangle = \frac{1}{Z} \int \mathrm{d}R \int \mathrm{d}R' \, \rho(R, R'; \beta) \, \langle R|\hat{A}|R'\rangle \, . \tag{3.6}$$

The basic idea behind path integrals relies on the group property of the density operator, i.e.,

$$\hat{\rho}(\beta) = e^{-\beta\hat{H}} = \left[e^{-\frac{\beta}{M}\hat{H}}\right]^M = [\hat{\rho}(\beta/M)]^M \, , \tag{3.7}$$

where M is a positive integer number. With equation (3.7), the density operator can be expressed in terms of the density operatar at a M times higher temperature. In order to derive an expression for the density matrix in coordinate representation, one has to insert $M-1$ identity operators resulting in an integration over $M-1$ intermediate points, i.e.,

$$\rho(R, R'; \beta) = \int \mathrm{d}R_1 \mathrm{d}R_2 \ldots \mathrm{d}R_{M-1} \, \rho(R, R_1; \tau)\rho(R_1, R_2; \tau) \cdots \rho(R_{M-1}, R'; \tau), \tag{3.8}$$

with $\tau = \beta/M$. This is called the *discrete time path integral* representation of the density matrix. It deviates from the original path integral with its functional integration as introduced by Feynman, but is more suitable for the system in question.

The term "time" refers to a number of notations commonly used in path integral specific language in allusion to classical analogons. The similarity of the density operator to the time propagator in quantum mechanics suggests to regard the inverse temperature β as an *imaginary time*. The particles move along a *path* or *trajectory* given by their corresponding positions, called *beads*, from the sequence of points $R_0, R_1, \ldots, R_{M-1}, R_M$ in discrete *time steps* $\tau = \beta/M$. A single R_k is referred to as the kth *time slice*. A *link* m is a pair of consecutive time slices (R_{m-1}, R_m) separated by the time τ. The *action* of a link is defined as

$$S^m \equiv S(R_{m-1}, R_m; \tau) = -\ln\left[\rho(R_{m-1}, R_m; \tau)\right] , \tag{3.9}$$

where $\rho(R_{m-1}, R_m; \tau)$ denotes the exact density matrix. By introducing this shortcut the exact path integral expression becomes

$$\rho(R, R'; \beta) = \int \mathrm{d}R_1 \mathrm{d}R_2 \ldots \mathrm{d}R_{M-1} \, \exp\left[-\sum_{m=1}^{M} S^m\right] . \tag{3.10}$$

Further notations can be found in [38].

Equation (3.8) is exact for any finite M provided that the exact expression for the N-particle density matrix is used. However, finding this expression means solving the N-particle Schrödinger equation, which is only possible in a few special cases like non-interacting systems. This problem can be circumvented by introducing approximations to the density matrix. The simplest approach is to split the Hamiltonian into its kinetic and potential part, i.e., $\hat{H} = \hat{T} + \hat{V}$, and use the *primitive approximation*

$$e^{-\tau\hat{T}} e^{-\tau\hat{V}} = e^{-\tau(\hat{T}+\hat{V}) + \frac{\tau^2}{2}[\hat{T},\hat{V}]} \approx e^{-\tau(\hat{T}+\hat{V})}, \tag{3.11}$$

obtained by neglecting the commutators $[\hat{T}, \hat{V}]$ from the exact operator identity. The error is proportional to τ^2 and vanishes in the limit $M \to \infty$ in eq. (3.11), but in the infinite product

in eq. (3.7) the infinitesimal errors might build up to a finite error. However, according to Trotter [39] the formula

$$e^{-\beta(\hat{T}+\hat{V})} = \lim_{M\to\infty}\left[e^{-\tau\hat{T}}e^{-\tau\hat{V}}\right]^M, \tag{3.12}$$

holds as long as the operators $\hat{T}$, $\hat{V}$ and $\hat{T}+\hat{V}$ are self-adjoint and make sense separately which is the case if their spectrum is bounded below (see [40]).

Taken in position space with the primitive approximation, the kinetic and potential parts of the density matrix can be evaluated separately, i.e.,

$$\rho(R,R';\beta) \equiv \langle R|e^{-\beta(\hat{T}+\hat{V})}|R'\rangle \approx \int \mathrm{d}R_1\ \langle R|e^{-\beta\hat{T}}|R_1\rangle\,\langle R_1|e^{-\beta\hat{V}}|R'\rangle\,. \tag{3.13}$$

This is trivial for the potential operator since it is diagonal in the position representation, and the kinetic operator can be computed by a momentum eigenstate expansion:

$$\rho_{\mathrm{pot}}(R,R';\tau) \equiv \langle R|e^{-\beta\hat{V}}|R'\rangle = e^{-\beta V(R)}\delta(R-R'), \tag{3.14}$$

$$\begin{aligned}\rho_{\mathrm{kin}}(R,R';\tau) &\equiv \langle R|e^{-\beta\hat{T}}|R'\rangle = \int \mathrm{d}P\ \langle R|P\rangle\, e^{-\beta\sum_{i=1}^{N}\frac{\mathbf{p}_i^2}{2m_i}}\,\langle P|R'\rangle \\ &= \lambda_\beta^{-3N}\, e^{-\frac{\pi}{\lambda_\beta^2}(R-R')^2},\end{aligned} \tag{3.15}$$

where $\lambda_\beta = \sqrt{2\pi\hbar^2\beta/m}$ is the thermal De Broglie wave length and the explicit expressions for plain waves have been inserted for $\langle R|P\rangle$ and $\langle P|R'\rangle$. Insertion of eqs. (3.13)–(3.15) into eq. (3.8) yields the discrete time path integral in primitive approximation

$$\rho(R,R';\beta) \approx \int \mathrm{d}R_1\mathrm{d}R_2\ldots\mathrm{d}R_{M-1}\, e^{-\sum_{i=0}^{M-1}\frac{\pi}{\lambda_\tau^2}(R_i-R_{i+1})^2}\, e^{-\sum_{i=0}^{M-1}\tau V(R_i)}, \tag{3.16}$$

with $R = R_0$ and $R' = R_M$.

It can be seen from eq. (3.16) that only particles within the same time slice interact with each other and the kinetic energy depends on the moved distance during a time step. Closed particle trajectories correspond to diagonal elements of the density matrix. Thus, the full density matrix is obtained by integration over all possible path configurations with fixed endpoints.

So far, only quantum systems with spinless particles have been considered. The spin part of the quantum states can be ignored as long as the Hamiltonian does not depend on it, but the statistical effects related to spin—namely Bose and Fermi statistics—cannot. The many body wave function for bosons and fermions has to be symmetric or antisymmetric under particle exchange, respectively. As Feynman shows [37], the corresponding density matrix can be obtained as follows

$$\rho^{\mathrm{S}}(R,R';\beta) = \frac{1}{N!}\sum_{P\in S_N}\rho(R,PR';\beta) \qquad \text{symmetric,} \tag{3.17}$$

$$\rho^{\mathrm{A}}(R,R';\beta) = \frac{1}{N!}\sum_{P\in S_N}\mathrm{sgn}(P)\rho(R,PR';\beta) \qquad \text{antisymmetric,} \tag{3.18}$$

where ρ is the density matrix defined in eq. (3.1). For the corresponding path integral, the permutation of particle positions occurs at a single time slice only, as one can easily see by applying the group property to eqs. (3.17) and (3.18). In principle, this time slice can be arbitrarily chosen, but one usually takes the R_Mth corresponding to the permutation of the endpoints of the particle trajectories. Howsoever, a given permutation mends the paths of multiple particles into a single one and one has to sum over all possible inter-connections. Such multi-particle trajectories correspond to off-diagonal elements of the density matrix.

3.2. Solving high-dimensional integrals with the Monte Carlo method

Path-integrals provide an elegant access to thermal quantities of a many-body quantum system. With them, the physical part of the problem is set—what remains is a numerical issue, which effectively prevents any use of path integrals until an efficient computational method for solving high-dimensional integrals is found. The simplest approach to compute an one-dimensional integral chops the integration interval into n parts of equal length Δx and estimates the integral as the sum of rectangular areas, each spanned by Δx and the function's value at a chosen point x_i from within Δx. This method can be easily generalized to N-dimensional integrations, i.e.,

$$\int_{a_1}^{b_1} \mathrm{d}x_2 \int_{a_2}^{b_2} \mathrm{d}x_1 \ldots \int_{a_N}^{b_N} \mathrm{d}x_N \, f(\mathbf{x}) \approx \frac{(b_1 - a_1)(b_1 - a_1)\ldots(b_N - a_N)}{n_1 n_2 \ldots n_N} \sum_{j_1=1}^{n_1} \sum_{j_2=1}^{n_2} \ldots \sum_{j_N=1}^{n_N} f(x_{j_1}, \ldots, x_{j_N}), \quad (3.19)$$

where n_j denotes the number of integration points in the jth dimension. Various extensions like e.g., the Simpson's rule advance the convergence and hence improve the accuracy for a fixed number of integration points when compared to the simple calculation rule above. Nevertheless, those improvements do not remedy the fact that the needed computational time scales with $\mathcal{O}(n^N)$ sustaining the same accuracy as a one-dimensional integration would have. Even the most powerful computer would eventually choke on the task to compute the $3NM$-dimensional path integral, if the number of particles N or beads M grew much larger than 1. Much for the worse, the inclusion of spin statistics boosts this number by a factor of $N!$.

The *Monte Carlo (MC)* integration effectively tackles the scaling problem by sampling over randomly distributed points $\tilde{\mathbf{x}}_i$ from the integration basis, instead of sampling function values with points from regular integrals Δx. This means

$$\int \mathrm{d}\mathbf{x} \, f(\mathbf{x}) = \int \mathrm{d}\mathbf{x} \, \frac{f(\mathbf{x})}{p(\mathbf{x})} \, p(\mathbf{x}) \approx \frac{1}{M} \sum_{i=1}^{M} \frac{f(\tilde{\mathbf{x}}_i)}{p(\tilde{\mathbf{x}}_i)}, \quad (3.20)$$

where the probability of sampled points $\tilde{\mathbf{x}}_i$ is given by $p(\mathbf{x})\mathrm{d}\mathbf{x}$. One may consider the integral as the expectation value of the function $f(\mathbf{x})/p(\mathbf{x})$.

In principle, the probability distribution $p(\mathbf{x})$ can be chosen arbitrarily. With the simplest possible choice, i.e., uniformly distributed points according to $p(\mathbf{x}) = \prod_i 1/(b_i - a_i)$, the MC method is said to use *straightforward sampling*. However, for strongly non-uniform integrands $f(\mathbf{x})$ (e.g., peaked functions etc.) it is obviously advisable to choose $p(\mathbf{x})$ to follow the general shape of $f(\mathbf{x})$, since places where the integrand is larger yield larger contributions to the integral. This is called *importance sampling*. One can show that the optimal choice which minimizes the error of the approximation reads $p(\mathbf{x}) = c|f(\mathbf{x})|$, where c is a constant (see, e.g., [41]). Unfortunately, to find the function $F(y)$ which generates a sequence of points distributed according to $p(\mathbf{x})$ requires solving the integral

$$F(y) = \int_{-\infty}^{y} \mathrm{d}\mathbf{x}\, p(\mathbf{x}). \tag{3.21}$$

This is exactly the unknown integral in eq. (3.20). Thus, the central issue with the importance sampling method is the search for a simple, but good matching probability $p(\mathbf{x})$.

Reconsidering eq. (3.6), the preferred probability density for an application to canonical ensembles is evidently given by the normalized Boltzmann factor $p_\mathrm{B} = e^{-\beta \hat{H}}/Z$. This guarantees to do the averaging only with microstates which are in thermodynamical equilibrium, providing a high efficiency of the Monte Carlo method. Unfortunately, the partition function Z is needed to generate microstates distributed according to p_B, but is unknown a priori. A convenient method to overcome this problem was devised by Metropolis *et al.* [42]. He proposed using the *Markov chain* in such a way that, starting from an initial state R_0, all further states are generated with p_B. One then needs to specify the transition probability $p(R_i \to R_{i+1})$ from one state to the next. Some restrictions are placed on $p(R_i \to R_{i+1})$ to ensure that the generated states are distributed according to p_B:

- *Conservation*: $\sum_{R_{i+1}} p(R_i \to R_{i+1}) = 1$, for all R_i.
- Convergence of $p_\mathrm{B}(R_i)$ to the *unique equilibrium state*: $\sum_{R_i} p_\mathrm{B}(R_i) p(R_i \to R_{i+1}) = p_\mathrm{B}(R_{i+1})$.
- *Ergodicity*: Any possible microstate is reached in a finite number of steps.
- All transition probabilities are *non-negative*: $p(R_i \to R_{i+1}) \geq 0$

The evolution of the probability p_B is governed by $p(R_i \to R_{i+1})$ and can be described by the *Master equation*, whose stationary solution is fulfilled when the more strict *detailed balance*

$$p_\mathrm{B}(R_i) p(R_i \to R_{i+1}) = p_\mathrm{B}(R_{i+1}) p(R_{i+1} \to R_i) \tag{3.22}$$

is met. Eq. (3.22) obviously does not specify $p(R_i \to R_{i+1})$ uniquely, but the commonly chosen solution reads

$$p(R_i \to R_{i+1}) = \frac{p_\mathrm{B}(R_{i+1})}{p_\mathrm{B}(R_i)} = \min\left[1, e^{-\beta \Delta U(R)}\right], \tag{3.23}$$

where $\Delta U(R) = U(R_{i+1}) - U(R_i)$ is the energy difference of subsequent microstates. A new configuration is always accepted when its energy is lower than before, or else with a probability proportional to the Boltzmann factor. The first guarantees the system to converge to an energy minimum, whereas the latter guarantees that the system will not be stuck in a local energy minimum. A detailed derivation can be found in [41].

3.3. Path-integral Monte Carlo (PIMC)

3.3.1. General algorithm

In order to solve path integrals with the Monte Carlo method, a more generalized Metropolis procedure is used nowadays. The transition probability $p(s \to s')$ is written as a product of a *sampling distribution* $T(s, s')$ and an *acceptance probability* $A(s, s')$, i.e., $p(s \to s') = T(s, s')A(s, s')$.

$T(s, s')$ determines the preference of the system to try a move from state s to s'. In the original Monte Carlo method, $T(s, s')$ is a constant distribution inside a cube and zero outside. In contrast, the more sophisticated *smart Monte Carlo* for classical systems marks particle displacements in direction of the potential gradient as preferable (see e.g., [43]). The acceptance probability $A(s, s')$ has to satisfy the detailed balance eq. (3.22), which is fulfilled by choosing

$$A(s, s') = \min\left[1, \frac{T(s', s)p(s')}{T(s, s')p(s)}\right]. \tag{3.24}$$

Each of the different move types in a PIMC simulation has its particular sampling distribution $T(s, s')$.

In general, the path integral Monte Carlo simulation implements the following procedure

1. Initialize the system
   - Read system parameters like particle number, temperature, beads, number of Monte Carlo steps, etc.
   - Randomly assign starting positions to particles
   - Initialize variables for physical observables
2. Monte Carlo step: Find a new system configuration with the generalized Metropolis algorithm
   - Choose and attempt one of the available methods to sample a new path configuration s'
   - Check with the corresponding $A(s, s')$, if the move is accepted. If not, stay in the old configuration s.
3. Calculate the contribution of the current configuration to the physical observables.
4. Jump back to step 2 unless the maximum number of Monte Carlo steps has been reached.
5. Output the calculated thermal averages.

Physical observables are not recorded from the start, but after a number of initial Monte Carlo steps needed to reach thermal equilibrium.

The main difference to classical Monte Carlo methods is the more sophisticated scheme to sample new configurations. The classical approach to repeatedly choose a random particle and displace it by some distance works out poorly when applied to single beads of the

path integral. The then needed displacement attempts to acquire a configuration which is uncorrelated to its predecessor scales with $(NM)^2$. Thus, the method is inefficient for simulations at low temperatures, where larger numbers of time slices are needed.

An improved method tries to move several beads at once. For such a move, the transition $T(s, s')$ and acceptance $A(s, s')$ probabilities must be defined and the satisfaction of the detailed balance condition ensured. The common move types for indistinguishable particles are

Whole particle displacement. A random particle is chosen and its whole trajectory displaced by some distance in position space. As in classical Monte Carlo simulations, $T(s, s')$ can be defined as a uniform distribution inside a cube with the corresponding $A(s, s')$ as in the standard Metropolis algorithm (eq. (3.23)).

Multilevel move. Chooses a random particle and deforms its trajectory on all time slices between the kth and $(k + m_0 - 1)$th (with $m_0 = 2^{l_0-1}$, $l_0 \in \mathbb{N}$), where k is also randomly chosen. The deformation is carried out by displacing the middle bead in the section and recursively proceeding with each of the two subintervals until the whole path is reconstructed. The acceptance of the new configuration is checked on each level, i.e., before even finer bisections are made. Rejection immediately aborts the further construction, which saves computational time elsewise wasted on the futile sampling of intermediate points.

The transition and acceptance probabilities for the lth level read

$$T_l(s_l, s_l') = \frac{p_l(s_l')}{p_l(s_l)}, \tag{3.25}$$

$$A_l(s_l, s_l') = \min\left[1, \frac{T_l(s_l)p_l(s_l')p_{l-1}(s_{l-1})}{T_l(s_l')p_l(s_l)p_{l-1}(s_{l-1}')}\right]. \tag{3.26}$$

Permutation change. Selects all particles whose indices are to be changed in a chosen permutation, and simultaneously samples new trajectories to the permuted endpoints with the multilevel method. One may restrict the method to the endpoint exchange of only 2 particles, since any permutation can be reached by pair transpositions.

The probabilities to pick a certain permutation $T(P, P')$ and finally accept the move $A(P, P')$ are

$$T(P, P') = \frac{\rho_{\text{kin}}(R_i, PR_{i+i_0}; i_0\tau)}{W(P)}, \tag{3.27}$$

$$A(P, P') = \min\left[1, \frac{W(P)}{W(P')}\right], \tag{3.28}$$

where $W(P) = \sum_P \rho_{\text{kin}}(R_i, PR_{i+i_0}; i_0\tau)$ is the normalization factor obtained by summing over all possible endpoint permutations of the kinetic density matrix (eq. (3.15)).

For the efficiency of the Metropolis algorithm an overall acceptance ratio of about 0.5 for proposed configurations is preferable. For much lower ratios it takes more attempts to

find new configurations as most are rejected. If the acceptance ratio is too high, successive configurations are strongly correlated. In both cases, more Monte Carlo steps are needed to acquire a sufficient number of independent configurations. The acceptance ratio can be controlled by adjusting the maximum displacement length in classical Monte Carlo simulations. The corresponding parameter for multilevel moves is the maximum number of blocks l_0.

3.3.2. Estimators

Thermodynamic averages of a quantum system can be computed directly from eq. (3.6) or as derivatives of the partition function Z. There are usually different ways to obtain a single property. A specific formula is called an *estimator*. For example, the *thermodynamic estimator* of energy reads

$$E = -\frac{\partial}{\partial\beta}\ln Z = -\frac{1}{Z}\frac{\partial Z}{\partial\beta}. \tag{3.29}$$

In case of a d-dimensional, N-particle quantum system (without Bose/Fermi statistics), this estimator takes the following form in high temperature representation of the density matrix [44]:

$$E = \frac{dMN}{2\beta} - \left\langle \sum_{k=0}^{M-1} \frac{Nm}{2\hbar^2\beta^2}(R_{k+1} - R_k)^2 \right\rangle + \left\langle \frac{1}{M}\sum_{k=0}^{M-1} V(R_k) \right\rangle \tag{3.30}$$

For numerical reasons, this estimator is usually not used in PIMC simulations, since the kinetic energy is calculated as a difference of two large terms diverging in the limit of infinite temperature. A better choice is the *virial energy estimator* [45].

The derivation of many useful estimators can be found in, e.g., [41, 38] and will not be discussed in detail here. However, of particular interest for the application to quantum systems is the possibility to calculate the superfluid density γ_s since the superfluid fraction of a trapped system can be defined via its response to slow rotations of the confining bucket. Only the normalfluid component of the liquid rotates rigidly with the walls, effectively decreasing the energy needed to spin up the container. The deviation of the rotational inertia I_qm from its classically expected value I_class is directly related to the superfluid density, i.e.,

$$\gamma_\mathrm{s} = \frac{\rho_\mathrm{s}}{\rho} = 1 - \frac{I_\mathrm{qm}}{I_\mathrm{class}}. \tag{3.31}$$

Chapter 2.2 introduced this effect as non classical rotational inertia (NCRI).

The quantum mechanical moment of inertia I_qm can be defined as the work done by an infinitesimally small rotation rate, i.e.,

$$I_\mathrm{qm} = \left.\frac{\mathrm{d}\left\langle \hat{L}_z \right\rangle}{\mathrm{d}\omega}\right|_{\omega=0} = \frac{1}{Z}\,\mathrm{Tr}\left[\hat{L}_z \frac{\mathrm{d}\hat{\rho}}{\mathrm{d}\omega}\right]\Bigg|_{\omega=0}, \tag{3.32}$$

where $\hat{L}_z$ is the total angular momentum operator along the rotation axis (chosen as the z-axis). $\hat{L}_z$ reads in cylindrical coordinates

$$\hat{L}_z = i\hbar\sum_{i=0}^{N}\frac{\partial}{\partial\phi_i}, \tag{3.33}$$

where ϕ_i is the angular coordinate of ith particle.

Equation (3.32) requires to calculate the derivative of the density matrix with respect to ω. This can be most easily obtained in the rest frame of the rotating fluid where the Hamiltonian is of the form

$$\hat{H}_\omega = \hat{H}_0 - \omega \hat{L}_z. \tag{3.34}$$

Here, $\hat{H}_0$ is the Hamiltonian at rest. In order to find an appropriate estimator for discrete-time path integrals consider the operator identity

$$\frac{\mathrm{d}}{\mathrm{d}x} e^{\hat{A}} = \frac{1}{M} \sum_{k=1}^{M} e^{k\hat{A}/M} \frac{\mathrm{d}\hat{A}}{\mathrm{d}x} e^{(M-k)\hat{A}/M}. \tag{3.35}$$

The application to equation (3.32) gives

$$I_{\mathrm{qm}} = \frac{1}{Z} \operatorname{Tr} \left[\tau \sum_{k=1}^{M} \hat{L}_z e^{-(M-k)\tau\hat{H}_0} \hat{L}_z e^{-k\tau\hat{H}_0} \right], \tag{3.36}$$

This expression can be explicitly evaluated when the high temperature approximation of the density matrix is inserted. After some algebra one arrives at

$$\gamma_{\mathrm{s}} = \frac{2m \left\langle A_z^2 \right\rangle}{\beta\lambda I_{\mathrm{class}}}, \tag{3.37}$$

where two functions of a given path are introduced, namely the projected area

$$\mathbf{A} = \frac{1}{2} \sum_{i=1}^{N} \sum_{k=0}^{M-1} \mathbf{r}_k^{(i)} \times \mathbf{r}_{k+1}^{(i)}, \tag{3.38}$$

and the classical moment of inertia

$$I_{\mathrm{class}} = \left\langle \sum_{i=1}^{N} \sum_{k=0}^{M-1} m_i \mathbf{r}_{k,\perp}^{(i)} \cdot \mathbf{r}_{k+1,\perp}^{(i)} \right\rangle. \tag{3.39}$$

Equation (3.37) is referred to as *area formula* in literature. It relates the superfluid fraction to the ratio of the covered area by the particle trajectories to the cross-sectional area of the whole system. It obviously emphasizes the importance of particle exchange, since a N-particle permutation trajectory naturally covers more area. However, also single-particle paths have a finite extension, which gives rise to a non-bosonic contribution to superfluidity in finite systems. This is one of the points which will be thoroughly discussed in the following chapters.

3.3.3. Basic tests

The efficiency of the PIMC algorithm corresponds to the ratio of the number of uncorrelated system configurations to the computational time needed. Naturally, the latter scales with

[1] The definition of the coupling parameter λ and other reduced units is given by eqs. (4.3)–(4.6)

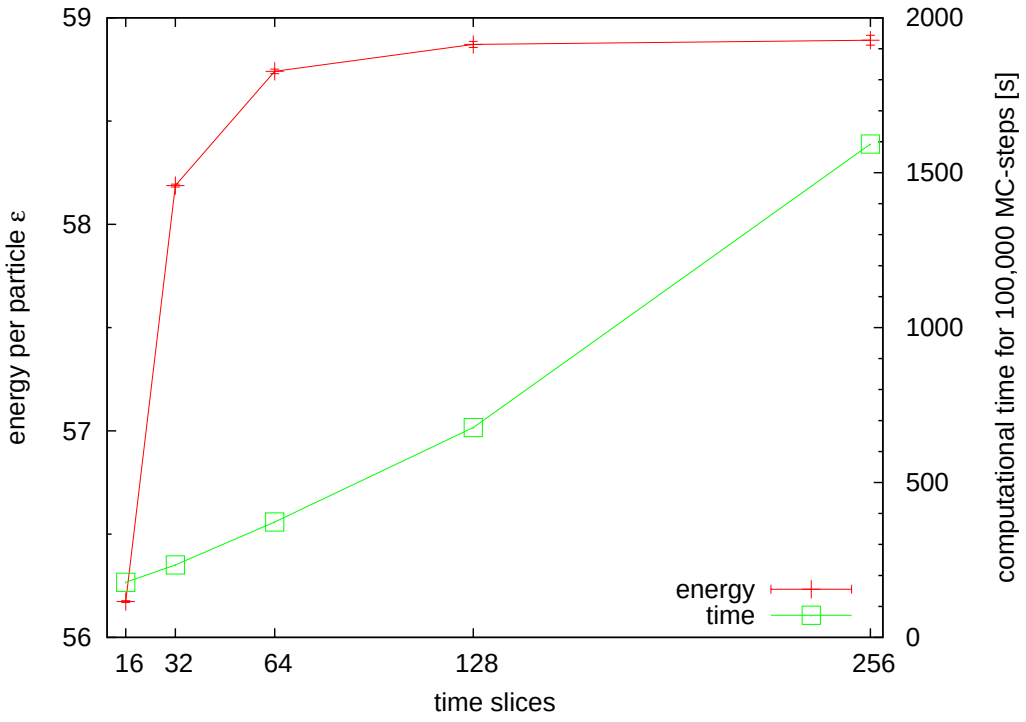

Figure 3.1.: *Performance of the PIMC simulation (8 bosons, $t = 0.1$, $\lambda = 10$)[1]. This example shows the accuracy of the energy calculation depending on the number of time slices M used (red line) in comparison to the computational time needed (green line). The error of the energy increases with M, as more MC-steps are needed in order to get uncorrelated configurations. Simulations for more than $M = 64$ yield an improvement of less than 1 % to the energy, so this is an appropriate choice for the current parameters.*

the number of time slices M which is, thus, desired to be as low as possible. Improvements like accurate actions (better than the primitive approximation) may vastly decrease M, but tests are still needed in order to find its optimal value. If M is too low, the calculation of physical quantities will be biased, the energy, e.g., is typically underestimated in this case. If M is chosen larger than needed on the other hand, there will be no improvements to any quantities, but the simulation needs longer to calculate them to the same accuracy. Figure 3.1 shows this interplay. In this example, an appropriate choice for M would be 64. Once calculated for a specific temperature, appropriate values for M can be simply derived by considering eq. (3.7): At half the temperature, M must be doubled and vice versa.

Aside from this general premise, the simulation must be of sufficient length to keep the statistical error small which scales with the number of *uncorrelated* Monte Carlo steps according to $\sqrt{N}$. For most quantities, a total number of Monte Carlo steps of about $500,000$ is sufficient. Unfortunately, the inclusion of Bose statistics may vastly increase this number, particularly when changes to the permutation configuration are rare. This poses a problem at low temperatures, since the probability of such a change decreases with M. Especially quantities like the superfluid density γ_s which are sensible to Bose statistics may need simulation lengths of $5 \cdot 10^6$ Monte Carlo steps and more (see fig. 3.2).

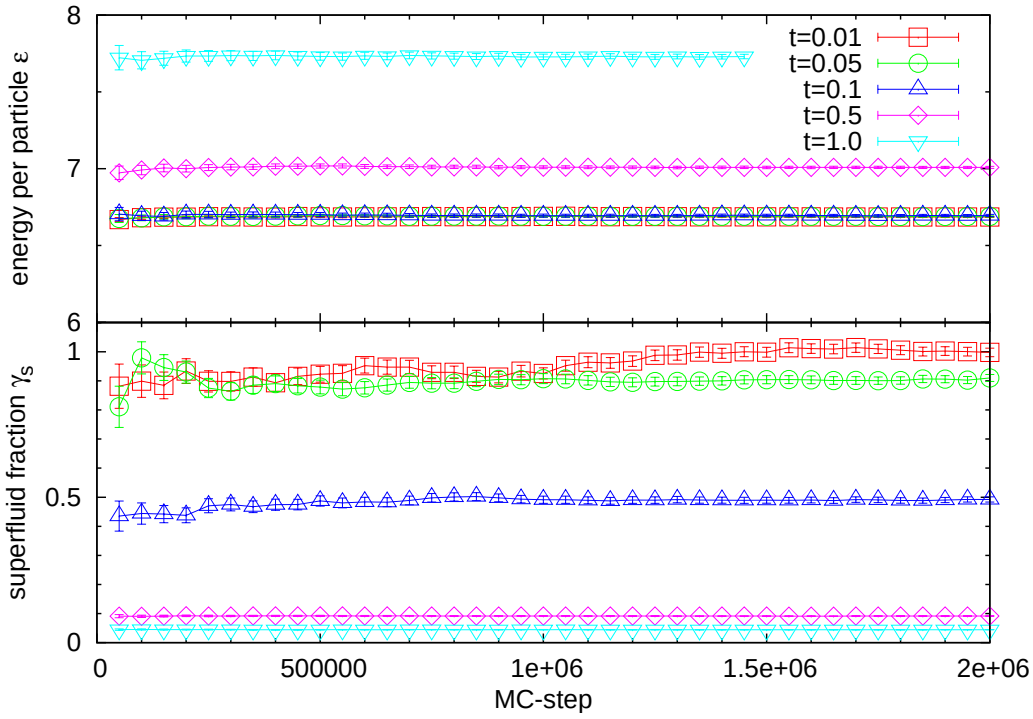

Figure 3.2.: *Convergence of the energy and superfluid fraction γ_s of a PIMC simulation (2 bosons, $\lambda = 30$)[1]. Since the exchange energy is small in comparison to the inter-particle interaction in this case, the energy computation is largely unaffected by exchange events. $500,000$ MC-steps are sufficient for its convergence. On the other hand, exchange events become rare at low temperatures which results in strong fluctuations of γ_s throughout the whole simulation. A length of $2,000,000$ MC-steps seems to be the lower limit for its convergence.*

4. Mesoscopic Bose gases in harmonic traps

4.1. Introduction

In chapter 2, systems in the thermodynamic limit have been considered. However, any experimental setup can naturally contain only a finite number of particles. Especially BEC experiments with dilute gases in harmonic traps have been limited to a few ten thousand particles up to date. In this regime, finite size effects gain importance.

Strictly speaking, a finite system does not display a true phase transition, which is by definition an abrupt change in its physical behavior. A clearly defined transition temperature T_c does not exist anymore, as the system smoothly glides from its condensate phase into the high-temperature gas phase. Nevertheless, assuming that the exponent of the order parameter (the condensate fraction) far below the transition regime remains unchanged, one usually defines T_c by extrapolating this low-temperature curve to zero. Compared to the analytically calculated expressions for the transition temperature (see eqs. (2.17) and (2.20)), the experimentally observed T_c shifts to lower values. The shift can be calculated analytically by introducing first-order corrections in the grand canonical partition function.

One has to bear in mind that expectation values calculated with micro-canonical, canonical and grand-canonical ensembles no longer yield identical results. Indeed, thermal averages can differ dramatically in small systems with up to a few hundred particles [46]. For the system in question with its fixed number of particles at a given temperature, the correct choice is a canonical approach. Since the Bose-Einstein distribution (2.1) follows from grand-canonical considerations, one must find a different approach. The straightforward method is a direct evaluation of the N-particle partition function as the trace over the symmetrized N-particle density matrix, i.e., (see eqs. (3.17) and (3.5))

$$Z(N,T,V) = \int \mathrm{d}R\, \rho^\mathrm{S}(R,R;\beta) = \frac{1}{N!} \sum_{P\in S_N} \int \mathrm{d}R\, \rho(R,PR;\beta). \tag{4.1}$$

The following chapter 5 provides an exact method to evaluate this expression for the ideal Bose gas. It is based on the idea that any permutation can be decomposed into exchange cycles. Since the particles are indistinguishable and non-interacting, only the length of such a cycle may have an effect on the system's physics. Chapter 6 introduces inter-particle Coulomb repulsion into the system. As the low-temperature N-particle density matrix for such a system is unknown, the path-integral representation of (4.1) with high-temperature approximation is used and numerically evaluated with Monte-Carlo methods (PIMC), as described in chapter 3.

4.2. System specification

The Hamiltonian for a system of N equally charged bosons in a harmonic trap reads

$$\hat{H} = \sum_{i=1}^{N} \left(-\frac{\hbar^2}{2m} \nabla_{\mathbf{r}_i}^2 + \frac{m}{2} \omega^2 \mathbf{r}_i^2 \right) + \sum_{i<j}^{N} \frac{1}{4\pi\epsilon_\mathrm{b}\epsilon_0} \frac{q^2}{|\mathbf{r}_i - \mathbf{r}_j|}, \tag{4.2}$$

where m is the mass and q the charge of a particle. It is advisable to reduce the Hamiltonian to a dimensionless form by introducing

Reduced length	$\mathbf{x} = \mathbf{r}/l_0,$	(4.3)
Reduced energy	$\epsilon = E/\epsilon_0,$	(4.4)
Reduced temperature	$t = k_\mathrm{B}T/\epsilon_0,$	(4.5)
Coupling parameter	$\lambda = l_0/a_\mathrm{B},$	(4.6)

where $l_0 = \sqrt{\hbar/m\omega}$ is the harmonic oscillator length, $\epsilon_0 = \hbar\omega$ is the energy level spacing and $a_\mathrm{B} = 4\pi\epsilon_\mathrm{b}\epsilon_0\hbar^2/mq^2$ is the effective Bohr radius. The reduced Hamiltonian reads

$$\hat{H}_\mathrm{red} = \frac{1}{2} \sum_{i=1}^{N} \left(-\nabla_{\mathbf{x}_i}^2 + \mathbf{x}_i^2 \right) + \lambda \sum_{i<j}^{N} \frac{1}{|\mathbf{x}_i - \mathbf{x}_j|}, \tag{4.7}$$

with $\hat{H}_\mathrm{red} |i\rangle = \varepsilon_i |i\rangle$.

The coupling parameter λ measures the relative interaction strength. The limit $\lambda \to 0$ formally makes the transition to an ideal system, while for $\lambda \to \infty$ the particles are strongly correlated. Because of $\lambda \propto \omega^{-1/2}$, the trap frequency ω effectively controls the coupling between particles. As it also effects the density of the system, the transition to an ideal system corresponds to the high density limit.

Equations (4.3)–(4.6) do not represent the only possibility to introduce reduced units. In particular, simulations with a strong reference to experiments usually take the Hartree $\epsilon_\mathrm{Ha} = \hbar^2/ma_\mathrm{B}$ as energy unit and the effective Bohr radius a_B as length unit. The specific advantage lies in the independence of these units from the trap frequency ω, which would otherwise be affected when using ω to control the coupling between the particles.

Nevertheless, oscillator units are used throughout this diploma thesis since they constitute the natural unit scales in which interesting effects occur. Additionally, these units have a special numerical advantage regarding PIMC simulations: The number of time slices needed for a simulation at a given temperature t does not depend on λ, in contrast to simulations with a fixed temperature $k_\mathrm{B}T/\epsilon_\mathrm{Ha}$. Note that some statements considering the t-λ-dependence of physical quantities might change compared to experiments using a trap frequency controlled λ.

4.3. Superfluidity in finite systems

In chapter 2.2, superfluidity is introduced as a ground state property of macroscopic systems with a acoustic phonon type energy spectrum. Thus, it is inseparably connected to interparticle interactions. The central topic of this diploma thesis is the question, how the concept

of superfluidity translates to systems with a finite particle number. The chapters 5 and 6 will give quantitative answers for specific systems. Here, some general issues and pitfalls will be discussed.

First of all, the proposal of Bose-Einstein condensation and superfluidity in finite systems is questionable. In the macroscopic limit, Bose-Einstein condensation is a phase, where a finite fraction of particles collects in the ground state of an infinite system at a finite temperature. In finite systems on the other hand, the ground state (and any other state) is obviously *always* occupied by a finite fraction of particles regardless of the temperature. Under these circumstances, one should rather speak of a *predominant ground state occupation* (which can be defined as a state where $\langle N_0 \rangle$ passes over a certain threshold like, e.g., 1 in very small clusters). In the following, the term *Bose-Einstein condensation* is meant in this sense.

A different problem arises with superfluidity. One usually defines the superfluid part as the fraction of particles, which does not show a response to a rotation of the external potential. This is introduced in chapter 2.2.2 as the NCRI effect (eq. (2.44)). Its appearance depends on the possibility (or rather impossibility) to excite vortices, which bring in friction and, thus, slow the fluid. However, in a confined finite system, the excitation spectrum is discrete, meaning there are gaps between energy levels. Here, the NCRI effect will be *always* present at low temperatures, since the excitation of condensed particles requires a certain threshold energy to overcome the lowest lying energy gap. Consequently, superfluidity is not exclusively linked to inter-particle interactions anymore [47]. Nevertheless, the NCRI will be assumed to make up the superfluid fraction in the following chapters. The closing discussion in section 6.4.1 will review this definition.

Bear in mind that these finite size effects are an essential part of the system's physics and do not pose a bias like, e.g., in simulations for macroscopic systems using periodic boundary conditions. One has to accept the oddities as long as they obey the correspondence principle and vanish in thermodynamic limit.

5. Analytical results for ideal systems

This chapter is devoted to the analysis of the finite non-interacting bose gas. As Feynman shows, particle exchange can be handled in a convenient way when described by permutation cycles. It will be shown in this chapter that any N-particle quantity can be computed from its corresponding single-particle quantity and the thermal average of the cycle length probabilities.

5.1. Partition function

The starting point is the partition function computed as the trace over the symmetrized density matrix $\rho^{\mathrm{S}}(R, R; \beta)$ (see eq. (4.1)), i.e.,

$$Z_N(\beta) = \int \mathrm{d}R\, \rho^{\mathrm{S}}(R, R; \beta) = \frac{1}{N!} \sum_{P \in S_N} \int \mathrm{d}R\, \rho(R, PR; \beta). \tag{5.1}$$

For the non-interacting Bose gas the total Hamiltonian is a sum over independent single-particle Hamiltonians. The partition function can be written as a product of N independent integrals—each containing only the single-particle density matrix

$$Z_N(\beta) = \frac{1}{N!} \sum_{P \in S_N} \int \prod_{i=1}^{N} \mathrm{d}^d\mathbf{x}_i\, \rho_1(x_i, x_{\pi_i}; \beta). \tag{5.2}$$

Any permutation can be broken into cycles. Each permutation can be viewed as a set $\{\, C_1, C_2, \ldots, C_N \,\}$, where C_q denotes the number of cycles with length q. As the particles are unlabeled, different permutations resulting in identical cycle configurations give identical contributions to the partition function. One may rewrite the sum over permutations as a sum over cycle configurations with an additional factor to take the number of possible realizations into account. The partition function becomes

$$Z_N(\beta) = \frac{1}{N!} \sum_{\{\, C_q \,\}} M(\{\, C_q \,\}) \prod_{q=1}^{N} (h_q)^{C_q}, \tag{5.3}$$

where h_q is introduced as a shortcut for the integral over the single-particle density matrices connected with a cycle of length q. It reads

$$\begin{aligned} h_q &= \int \mathrm{d}\mathbf{x}_1 \mathrm{d}\mathbf{x}_2 \ldots \mathrm{d}\mathbf{x}_q\, \rho_1(x_1, x_2; \beta) \rho_1(x_2, x_3; \beta) \ldots \rho_1(x_q, x_1; \beta) \\ &= \int \mathrm{d}\mathbf{x}_1\, \rho_1(x_1, x_1; q\beta), \\ &= Z_1(q\beta). \end{aligned} \tag{5.4}$$

The integral has been reduced using the group property of the density matrix (eq. (3.7)).

With the following expression for the combinatorial factor (compare e.g., [37, 48]),

$$M(\{C_q\}) = \frac{N!}{\prod_q C_q! q^{C_q}}, \tag{5.5}$$

one arrives at the final result for the partition function

$$Z_N(\beta) = \sum_{\substack{\{C_q\} \\ \text{restr.}}} \prod_{q=1}^{N} \frac{Z_1(q\beta)^{C_q}}{C_q! q^{C_q}}, \tag{5.6}$$

where

$$\sum_{q=1}^{N} qC_q = N \tag{5.7}$$

poses the restriction for the possible cycle configurations in a N-particle system. The restriction can be lifted by introducing a chemical potential. This implies switching from canonical to grand canonical statistics as the total number of particles is no longer kept constant. This is done e.g., in [48] and ultimately leads to the recursion relation for the canonical partition function shown in eq. (5.11). In the following a different ansatz is used, which does not leave canonical grounds.

With an analog argumentation as for the partition function itself, one can evidently define $\langle C_q \rangle$ as

$$\langle C_q \rangle (\beta) = \frac{1}{Z_N(\beta)} \sum_{\substack{\{C_r\} \\ \text{restr.}}} \prod_{r=1}^{N} \frac{Z_1(r\beta)^{C_r}}{C_r! r^{C_r}} C_q. \tag{5.8}$$

Note that terms with $C_q = 0$ do not contribute. Splitting the product into the factors with $r \neq q$ and the factor $r = q$ yields

$$\langle C_q \rangle (\beta) = \frac{1}{Z_N(\beta)} \frac{Z_1(q\beta)}{q} \sum_{\substack{\{C_r\} \\ \text{restr.}}} \frac{Z_1(q\beta)^{C_q - 1}}{(C_q - 1)! r^{C_q - 1}} \prod_{\substack{r=1 \\ r \neq q}}^{N} \frac{Z_1(r\beta)^{C_r}}{C_r! r^{C_r}}. \tag{5.9}$$

The substitution of $C_q - 1$ by C_q alters the restriction condition from $\sum_q qC_q = N$ to $\sum_q qC_q = N - q$. Thus, the remaining sum in the equation above can be identified as the partition function of a system with q particles less. One ends up with the final formula for the mean cycle occupation number

$$\langle C_q \rangle (\beta) = \frac{Z_{N-q}(\beta)}{Z_N(\beta)} \frac{Z_1(q\beta)}{q}. \tag{5.10}$$

Inserting this formula into the constraint (eq. (5.7)) immediately yields the recursion relation for the partition function

$$Z_N(\beta) = \frac{1}{N} \sum_{q=1}^{N} Z_{N-q}(\beta) Z_1(q\beta). \tag{5.11}$$

Equations (5.10) and (5.11) provide an exact and numerically undemanding access to non-interacting Bose systems.

5.2. Thermodynamic averages

5.2.1. Energy

One obtains the average energy of a system in the canonical ensemble as follows

$$\langle E \rangle (\beta) = \tau^2 \frac{\partial \ln Z_N(\tau)}{\partial \tau}. \tag{5.12}$$

where $\tau = \beta^{-1}$. With eq. (5.6), the derivative of the full partition function becomes

$$\begin{aligned}
\frac{\partial Z_N(\tau)}{\partial \tau} &= \sum_{\{C_q\}} \sum_{r=1}^{N} \left(\prod_{q=1}^{r-1} \frac{Z_1(\tau/q)^{C_q}}{C_q! q^{C_q}} \right) \frac{1}{C_r! r^{C_r}} \frac{\partial (Z_1(\tau/r)^{C_r})}{\partial \tau} \left(\prod_{q=r+1}^{N} \frac{Z_1(\tau/q)^{C_q}}{C_q! q^{C_q}} \right) \\
&= \sum_{\{C_q\}} \left(\prod_{q=1}^{N} \frac{Z_1(\tau/r)^{C_r}}{C_r! r^{C_r}} \right) \sum_{r=1}^{N} \frac{\partial \ln \left(Z_1(\tau/q)^{C_r} \right)}{\partial \tau} \\
&= \sum_{r=1}^{N} \frac{\partial \ln \left(Z_1(\tau/r) \right)}{\partial \tau} \sum_{\{C_q\}} \left(\prod_{q=1}^{N} \frac{Z_1(\tau/q)^{C_q}}{C_q! q^{C_q}} C_r \right).
\end{aligned}$$

The desired expression for the derivative in eq. (5.12) follows by applying eq. (5.8)

$$\frac{\partial \ln Z_N(\tau)}{\partial \tau} = \sum_{r=1}^{N} \frac{\partial \ln \left(Z_1(\tau/r) \right)}{\partial \tau} \langle C_r \rangle . \tag{5.13}$$

If one reuses eq. (5.12) to replace the derivation of the single-particle partition function by the single-particle energy, one arrives at the final formula for the average energy

$$\langle E \rangle (\beta) = \sum_{q=1}^{N} E_1(q\beta) \langle q C_q \rangle . \tag{5.14}$$

5.2.2. Single-particle density

The integration of the diagonal density matrix over all coordinates except one yields the single-particle density

$$n(\mathbf{x}_1, \beta) = \frac{1}{N!} \sum_{P \in S_N} \int \mathrm{d}^d \mathbf{x}_2 \mathrm{d}^d \mathbf{x}_3 \ldots \mathrm{d}^d \mathbf{x}_N \, \frac{\rho(R, PR; \beta)}{Z_N(\beta)}. \tag{5.15}$$

One can split the sum over all permutations up into multiple parts $\sum_P = \sum_{q=1}^{N} \sum_{P_q}$, where each P_q contains only permutations in which particle 1 sits in a cycle of length q. The integration over such a cycle can be separated from the rest and reduces to the single-particle

density matrix with the group property. It follows

$$\begin{aligned} n(\mathbf{x}_1,\beta) &= \sum_{q=1}^{N} \frac{1}{N!}\frac{1}{Z_N(\beta)} \sum_{P_q} \int \mathrm{d}^d\mathbf{x}_2 \mathrm{d}^d\mathbf{x}_3 \ldots \mathrm{d}^d\mathbf{x}_N \prod_{i=1}^{N} \rho_1(\mathbf{x}_i, \mathbf{x}_{\pi_i};\beta) \\ &= \sum_{q=1}^{N} \frac{M_q}{N!}\frac{1}{Z_N(\beta)} \rho_1(\mathbf{x}_1,\mathbf{x}_1;q\beta) \sum_{P_q} \int \prod_{i=q}^{N} \mathrm{d}^d\mathbf{x}_i\, \rho_1(\mathbf{x}_i,\mathbf{x}_{\pi_i};\beta) \\ &= \sum_{q=1}^{N} \frac{M_q(N-q)!}{N!}\frac{Z_{N-q}(\beta)}{Z_N(\beta)} \rho_1(\mathbf{x}_1,\mathbf{x}_1;q\beta), \end{aligned}$$

where $M_q = (N-1)!/(N-q)!$ is the number of possible realizations for q-cycles containing particle 1. Using eq. (5.10) yields

$$n(\mathbf{x},\beta) = \frac{1}{N}\sum_{q=1}^{N} \frac{\rho_1(\mathbf{x},\mathbf{x};q\beta)}{Z_1(q\beta)} \langle qC_q\rangle = \frac{1}{N}\sum_{q=1}^{N} n_1(\mathbf{x},q\beta)\langle qC_q\rangle\,. \tag{5.16}$$

The result is normalized to the particle number. An integration over the remaining coordinate directly leads to the restriction conditions eq. (5.7).

5.2.3. Heat capacity

The heat capacity is defined as follows

$$C_N(\tau) = \frac{\partial E_N(\tau)}{\partial \tau}. \tag{5.17}$$

Together with eq. (5.14) one obtains

$$C_N(\tau) = \sum_{q=1}^{N} C_1(\tau/q)\langle C_q\rangle + E_1(\tau/q)\frac{\partial\langle qC_q\rangle}{\partial\tau}. \tag{5.18}$$

The derivative of the mean cycle occupation number with respect to τ can be most easily obtained by using the recursion relation (eq. (5.11)). This gives

$$\begin{aligned} \frac{\partial\langle C_q\rangle}{\partial\tau} &= \langle C_q\rangle \frac{\partial \ln\langle C_q\rangle}{\partial\tau} \\ &= \left(-\frac{\partial \ln Z_N(\tau)}{\partial\tau} + \frac{\partial \ln Z_{N-q}(\tau)}{\partial\tau} + \frac{1}{q}\frac{\partial \ln Z_1(\tau/q)}{\partial(\tau/q)}\right)\langle C_q\rangle \\ &= \frac{1}{\tau^2}\left(-E_N(\tau) + E_{N-q}(\tau) + qE_1(\tau/q)\right)\langle C_q\rangle\,. \end{aligned} \tag{5.19}$$

The definition for the energy eq. (5.12) was reused in the last step.

5.2.4. Condensate fraction

The occupation number N_i of an arbitrary energy level E_i can be calculated as the derivative of the partition function with respect to βE_i (see [46]), i.e.,

$$\langle N_i \rangle (\beta) = -\frac{1}{Z_N(\beta)} \frac{\partial Z_N(\beta)}{\partial(q\beta)}. \tag{5.20}$$

Application to eq. (5.6) and using the fact $Z_1(\beta) = \sum_i e^{-\beta E_i}$ yields

$$\langle N_i \rangle = \sum_{q=1}^{N} \frac{e^{-q\beta E_i}}{Z_1(q\beta)} \langle qC_q \rangle . \tag{5.21}$$

This formula can easily be adjusted to compute the condensate fraction when taken at the ground state energy E_0

$$\frac{N_0}{N} = \frac{1}{N} \sum_{q=1}^{N} \frac{e^{-q\beta E_0}}{Z_1(q\beta)} \langle qC_q \rangle . \tag{5.22}$$

5.2.5. Superfluid fraction

The NCRI effect relates the normal fluid fraction of a rotating Bose system to fraction of quantum mechanical to classical moment of inertia (see (2.44)). One can compute the quantum mechanical moment of inertia as the response to rotations. In non-rotating situations with $\langle \hat{L}_z \rangle = 0$ this yields (compare eq. (3.32))

$$I_{\mathrm{qm}} = \beta \langle \hat{L}_z^2 \rangle . \tag{5.23}$$

The classical moment of inertia is defined as

$$I_{\mathrm{class}} = m \sum_{j=1}^{N} \langle x_j^2 + y_j^2 \rangle . \tag{5.24}$$

In order to obtain $\langle \hat{L}_z^2 \rangle$, consider a system in a trap which is invariant to rotations around the z-axis. The single-particle Hamiltonian $\hat{h}$ and the single-particle angular momentum operator $\hat{l}_z$ then have the same eigenfunctions as the operators commute. This gives

$$\hat{h} \, |n_r, m, n_z\rangle = \epsilon_{n_r m n_z} \, |n_r, m, n_z\rangle , \qquad \hat{l}_z \, |n_r, m, n_z\rangle = m\hbar \, |n_r, m, n_z\rangle , \tag{5.25}$$

where the eigenfunctions are classified by three quantum numbers for the radial $n_r = 0, 1, 2, \ldots$, rotational $m = 0, \pm 1, \ldots$, and axial $n_z = 0, 1, 2, \ldots$ degrees of freedom. The total Hamiltonian $\hat{H}$ and total angular momentum operator $\hat{L}_z$ are given by the sum over their corresponding single-particle operators for each particle. The expression for the thermal average $\langle \hat{L}_z^2 \rangle$ reads

$$\langle \hat{L}_z^2 \rangle = \frac{\mathrm{Tr}\, \hat{\rho} \hat{L}_z^2}{Z_N} = \frac{1}{Z_N} \frac{1}{N!} \sum_{P \in S_N} \sum_{n_1, \ldots, n_N} \langle n_1, \ldots, n_N | \sum_{j,k=1}^{N} \hat{l}_z^{(j)} \hat{l}_z^{(k)} e^{-\beta \hat{H}} | n_{\pi_1}, \ldots, n_{\pi_N} \rangle , \tag{5.26}$$

where the sum over all states is carried out in the basis of single-particle states $n_j = (n_{r,j}, m_j, n_{z,j})$. The matrix element factorizes to a sum of matrix elements for only one particle, where each of the elements takes one of the following forms:

$$\langle n_j | e^{-\beta \hat{h}^{(j)}} | n_{\pi_j} \rangle = e^{-\beta \epsilon_{n_j}} \delta_{n_j, n_{\pi_j}}, \tag{5.27}$$

$$\langle n_j | \hat{l}_z^{(j)} e^{-\beta \hat{h}^{(j)}} | n_{\pi_j} \rangle = \hbar m_j e^{-\beta \epsilon_{n_j}} \delta_{n_j, n_{\pi_j}}, \tag{5.28}$$

$$\langle n_j | (\hat{l}_z^{(j)})^2 e^{-\beta \hat{h}^{(j)}} | n_{\pi_j} \rangle = (\hbar m_j)^2 e^{-\beta \epsilon_{n_j}} \delta_{n_j, n_{\pi_j}}. \tag{5.29}$$

Due to the Kronecker-δ's in each of these factors, only permutation cycles whose participating particles are in the same state contribute to the thermal averaging in eq. (5.26). The sum over one such q-cycle depends on the number of angular momentum operators associated to it, so there are again three different possibilities:

$$\sum_{n_j} e^{-q\beta \epsilon_{n_j}} = Z_1(q\beta), \tag{5.30}$$

$$\sum_{n_j} \hbar m_j e^{-q\beta \epsilon_{n_j}} = 0, \qquad \text{because } \epsilon_{n_r, m, n_z} = \epsilon_{n_r, -m, n_z}, \tag{5.31}$$

$$\sum_{n_j} (\hbar m_j)^2 e^{-q\beta \epsilon_{n_j}} = \frac{2\hbar^2 e^{-q\beta\hbar\omega_\perp}}{(1 - e^{-q\beta\hbar\omega_\perp})^2} Z_1(q\beta). \tag{5.32}$$

The factor in the third expression follows by using the explicit expression for the energy eigenvalues $\epsilon_{n_r, m, n_z} = \hbar\omega_\perp (2n_r + |m| + 1) + \hbar\omega_\parallel (n_z + 1/2)$.

For a given number C_q of q-cycles there are qC_q particles in these cycles and each can be paired with q other particles on their own cycle (including itself). So there are $q^2 C_q$ ways of pairing two angular momentum operators resulting in eq. (5.32). With this combinatorial factor eq. (5.26) can be rewritten as

$$\langle \hat{L}_z^2 \rangle = \frac{1}{Z_N} \frac{1}{N!} \sum_{\substack{\{C_q\} \\ \text{restr.}}} M(\{C_q\}) \sum_{q=1}^{N} \frac{2\hbar^2 e^{-q\beta\hbar\omega_\perp}}{(1 - e^{-q\beta\hbar\omega_\perp})^2} q^2 C_q \prod_{r=1}^{N} Z_1(r\beta)^{C_r}, \tag{5.33}$$

where $M(\{C_q\})$ is defined as in eq. (5.5). Together with eqs. (5.23) and (5.8), the quantum mechanical moment of inertia becomes

$$I_{\text{qm}} = 2\hbar^2 \sum_{q=1}^{N} \frac{q\beta e^{-q\beta\hbar\omega_\perp}}{(1 - e^{-q\beta\hbar\omega_\perp})^2} \langle qC_q \rangle . \tag{5.34}$$

The classical moment of inertia can be obtained by following the analogous procedure for $\langle x_j^2 + y_j^2 \rangle$ as above. Here, the appearing matrix elements are most easily evaluated by using the eigenstates $|n_x, n_y, n_z\rangle$, i.e.,

$$\sum_{n_j} \langle n_j | (x_j^2 + y_j^2) e^{-q\beta \hat{H}} | n_j \rangle = \frac{\hbar}{m\omega_\perp} \frac{1 + e^{-q\beta\hbar\omega_\perp}}{1 - e^{-q\beta\hbar\omega_\perp}} Z_1(q\beta). \tag{5.35}$$

This leads to the following expression for the classical moment of inertia

$$I_{\text{class}} = \frac{\hbar}{\omega_\perp} \sum_{q=1}^{N} \frac{1 + e^{-q\beta\hbar\omega_\perp}}{1 - e^{-q\beta\hbar\omega_\perp}} \langle qC_q \rangle \,. \tag{5.36}$$

Eqs. (5.34) and (5.36) allow the computation of the superfluid fraction totally based on cycle occupation numbers, i.e.,

$$\frac{\rho_{\text{s}}}{\rho} = 1 - \frac{\sum_{q=1}^{N} q\beta\hbar\omega \sinh^{-2}(-q\beta\hbar\omega/2) \langle qC_q \rangle}{2\sum_{q=1}^{N} \coth(-q\beta\hbar\omega/2) \langle qC_q \rangle}. \tag{5.37}$$

5.3. Discussion

The major advantage of an access to quantum systems totally based on cycle occupation numbers is the clearly expressed effect of Bose statistics. As in the classical non-interacting gas, all thermal averages depend only on single-particle quantities: An exchange cycle of length q contributes to a thermal average like a single-particle at a q times lower temperature. Weighted with the thermal expectation value for the number of particles occupying such a cycle $\langle qC_q \rangle$, the contributions from each q-cycle sum up to the total value of the physical quantity.

As a remark, the picture of exchange cycles as single particles at lower temperatures is used in the same spirit by path-integrals—only in the opposite direction. Here, a single particle is described as a closed path, precisely a cycle, whose beads behave like particles at higher temperatures.

One can easily turn off Bose statistics in any expression for thermal averages listed above by restricting to $C_1 = N$ and C_q, $q = 2 \ldots N$. This allows only the identity permutation and, thus, switches to Boltzmann statistics. A comparison between both cases singles out effects related to Bose statistics.

So far, no specifications to the system itself have been issued besides that it is non-interacting and composed of bosons (not counting the specialized derivation for the superfluid fraction, which is only valid in a harmonic trap with axial symmetry). The expressions for the thermal averages stated above only show the reduction to single-particle quantities, which themselves depend on the single-particle partition function Z_1. Naturally, one needs its explicit expression in order to proceed with a quantitative investigation for the system in question. For 2D trapped systems, Z_1 reads

$$Z_1(\beta) = \left(2\sinh(\hbar\omega\beta/2)\right)^{-2} . \tag{5.38}$$

See appendix B or, e.g., [48] for the complete derivation.

5.3.1. Cycle distribution

Asbeforementioned, the effect of Bose statistics can be measured with a single quantity, the thermal expectation value of the cycle occupation number $\langle C_q \rangle$. Figure 5.1 shows the probability that a 2D trapped system has an exchange cycle of length q, i.e., $p_{C_q}(t) = \langle qC_q \rangle / N$.

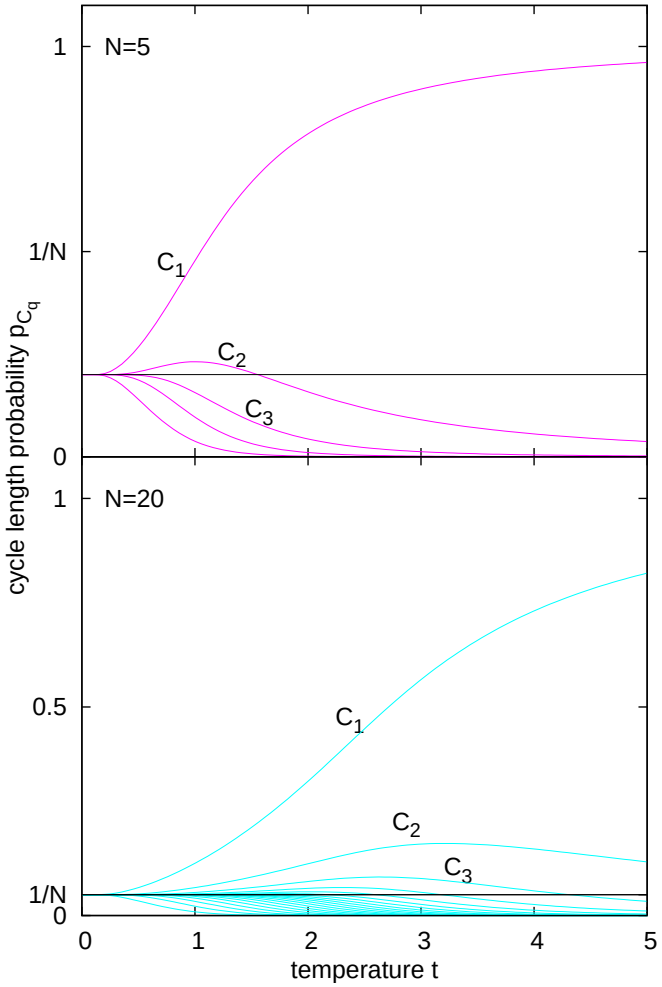

Figure 5.1: *Cycle configuration for 2D trapped systems containing 5 (top) and 20 (bottom) non-interacting bosons. The topmost line denotes the probability for the identity permutation $p_{C_1}(t)$. The second to top line denotes the probability for a particle to participate in a two-particle exchange $p_{C_2}(t)$, the third to top corresponds to the three-particle exchange $p_{C_3}(t)$ and so on. At any temperature, the sum over all cycle length probabilities is 1. The low-temperature limit where every permutation is equally probable is indicated with a horizontal black line.*

In the high-temperature limit, $p_{C_1}(t \to \infty)$ reaches unity and the probability for any other permutation becomes zero. This complies to the expectation that any quantum system should develop into a classical one at high temperatures (correspondence principle). One can issue an approximate temperature t_B below which the difference between Bose and Boltzmann statistics becomes significant, e.g., by defining t_B as the temperature, at which p_{C_1} falls below a certain threshold value (see appendix C). Adding particles to the system does not change the effective volume of an ideal system, but increases its density. This encourages particle exchange and, thus, shifts t_B to higher values. Note that the critical temperature T_c is correlated but not identical to t_B (compare figs 5.1 and 5.2).

In the low-temperature limit, every permutation of a quantum system becomes equally probable, i.e., $p_{C_q}(0) = 1/N$ for all q. At $t = 0$, every boson in an ideal system occupies its single-particle ground state level. The fully symmetrized many-body wave function equals a product of N identical single-particle wave functions. One obtains the same result for a system of boltzmannons since those do also occupy the same single-particle state in this limit. This implies that the additional inclusion of bosonic particle exchange does not alter expectation values of observables obtained for the system's ground state. Consequently,

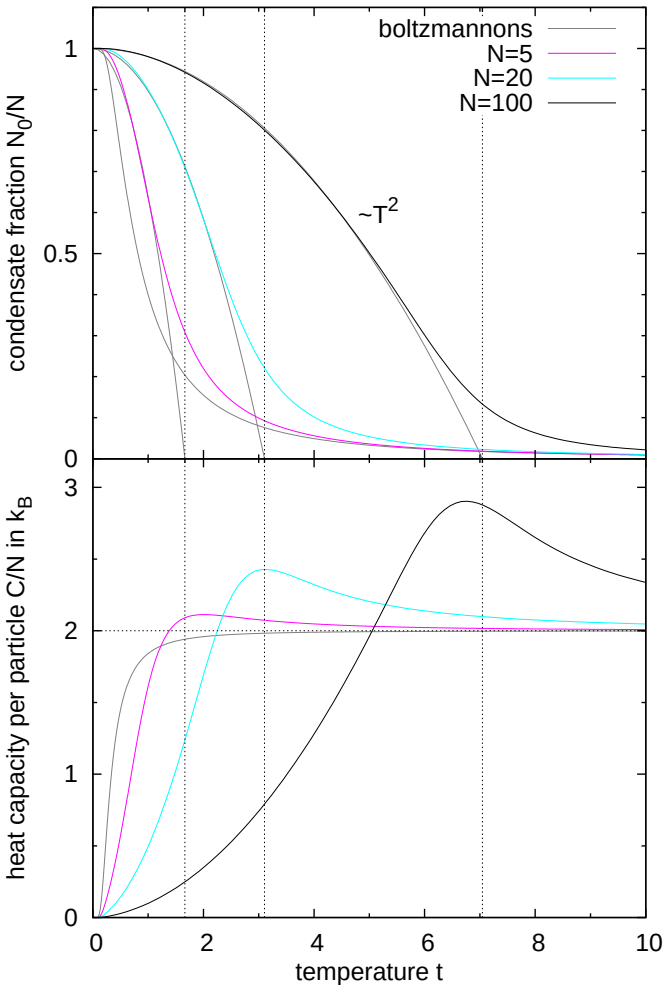

Figure 5.2: *Different possibilities to obtain the transition temperature T_c, here shown for a 2D trapped system of non-interacting bosons. In the upper figure, the function $1-(T/T_c)^2$ is fitted to the condensate fraction at low temperatures (see text). Vertical dashed lines emphasize the calculated transition temperatures for each particle number. The lower figure shows the temperature dependence of the heat capacity per particle in units of k_B. All curves converge to the high temperature limit of $C = 2k_BN$ indicated with the horizontal dashed line. The peaks of the curves roughly coincide with the T_c's from the upper figure.*

thermal averages calculated for bosonic or boltzmannonic systems must be identical for both the high- and the low-temperature limit and differences can only be expected at intermediate temperatures, i.e., for temperatures within $0 < t \lesssim t_B$. The plots for specific heat, condensate, and superfluid fraction (figs. 5.2 and 5.4) verify this predication.

5.3.2. Condensate Fraction

The temperature dependence of the condensate fraction is shown in the upper plots of the figures 5.4(a), 5.4(b) and 5.2. Naturally, the condensate fraction reaches unity at $t = 0$ and decays to zero in the high-temperature limit as consequence of particle excitation from the ground state. In the thermodynamic limit, the condensate fraction is of the form (see chapter 2.1)

$$1-(T/T_c)^x. \tag{5.39}$$

In particular, N_0/N shows a parabolic decay (i.e., $x = 2$) for the 2D trapped system. This behavior can also be found for finite systems—at least for temperatures well below the transition temperature T_c, which is broadened into an extended transition regime showing an

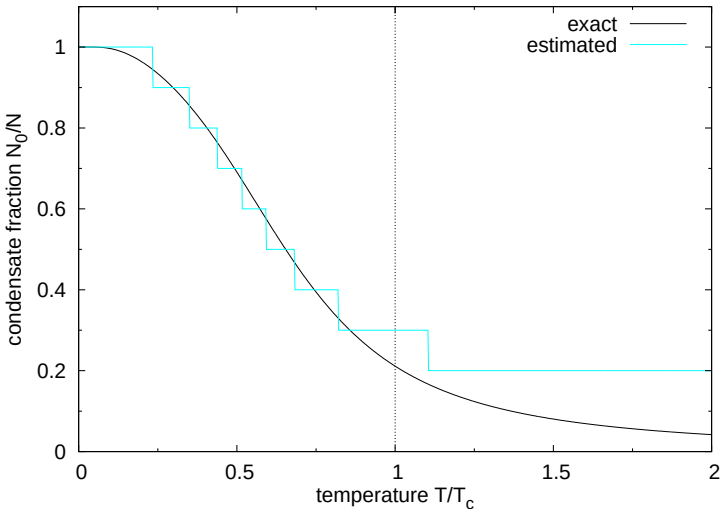

Figure 5.3: *Estimation of the condensate fraction with the cycle length threshold method. Shown is the situation for* 10 *non-interacting bosons. The solid black line corresponds to the exact condensate fraction calculated with eq.* (5.22)*. The light blue line shows the estimation from the cycle length distribution (see text) with the threshold chosen to* $x = 0.6$*. The estimation fails above the critical temperature* T_c *emphasized with the vertical dashed line in the plot.*

asymptotic decay of N_0/N to zero. However, by fitting the polynomial in eq. (5.39) with T_c as open parameter to the condensate curve, one can approximately determine the transition temperature to T_c. This procedure is compared to another method—using the "singularity" of the specific heat curve at the transition temperature—in figure 5.2. Both methods are in good agreement to each other although the assumption of a parabolic dependence is only fulfilled satisfactorily for $N \gtrsim 25$. Smaller systems mainly display the Gaussian like behavior of the extremal boltzmannonic case (which corresponds to the 1-boson case). The so obtained T_c can be compared with equation (2.20), which lies at higher temperature values. This is the temperature shift which is also observed experimentally.

The condensate fraction can be estimated from the cycle length distribution. The method uses the fact that all particles in an exchange cycle must be in the same state (see derivation of γ_s above). Since particle exchange only occurs at temperatures below t_B, one may assume that the common state is the ground state of the system. The general idea is to issue a threshold value x and define the condensate consisting of particles on the longest permutation cycle, whose probability is greater than $p_c = x/N$. The knowledge of exact analytical results for both condensate fraction and cycle length probability allows for a test of this method. It is found that the approximation reproduces the exact value of the condensate fraction quite good for $T < T_c$, when a threshold value of $x = 0.6$ is used. For temperatures above T_c, the approximation over-estimates the condensate fraction.

The major advantage of this method is its application in numerical PIMC investigations of quantum systems with inter-particle interaction. Here, a direct determination of the condensate fraction is delicate, since the energy spectrum of the system is inaccessible. On the other hand, the probability of a q-cycle can be easily computed by simply counting the number of configurations containing such a cycle. However, one thatt guarantee the validity of the empirically determined threshold value of 0.6 for interacting systems. Unfortunately, the estimation can only determine the condensed particles to integral numbers, which renders its application to very small systems ($N \lesssim 10$) practically useless.

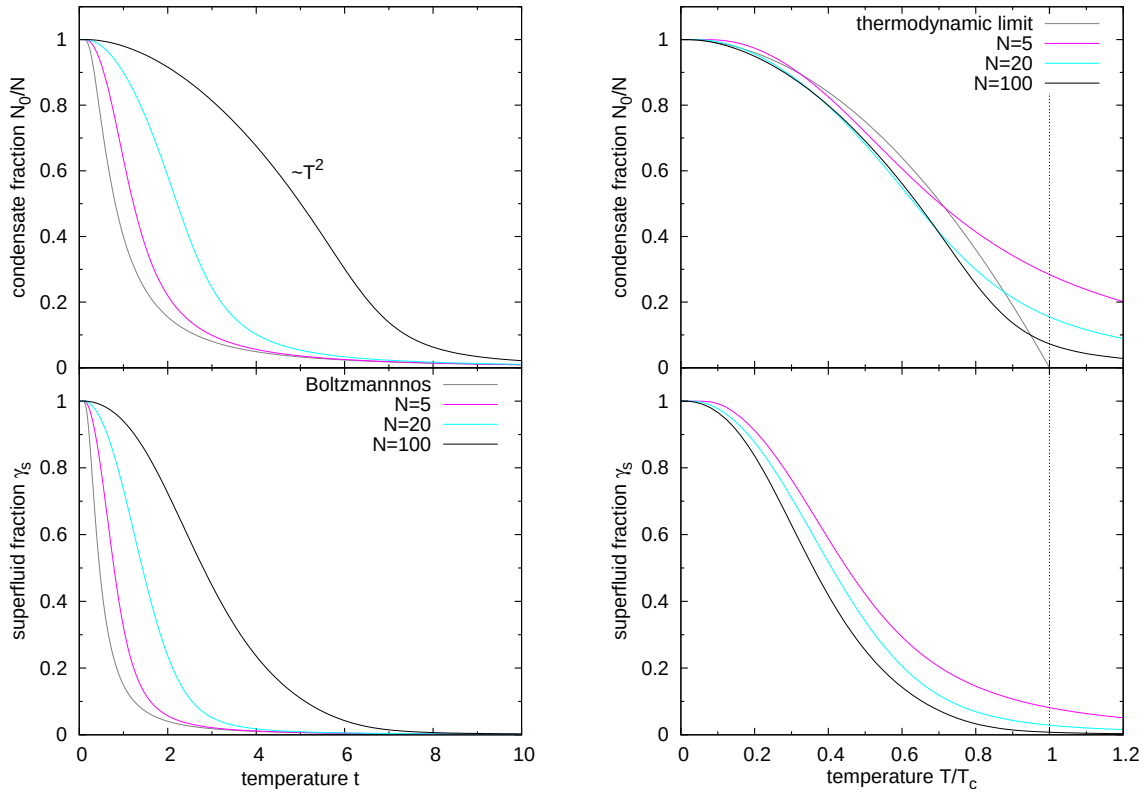

Figure 5.4.: *Temperature dependence of the condensate fraction N_0/N (top) and superfluid fraction γ_s (bottom) for 2D trapped systems with 5, 25 and 100 bosons. In the left panel, the temperature scale is normalized to oscillator units. The solid gray line indicates the results obtained for a quantum system containing an arbitrary number of boltzmannons. In the right panel, the temperature scale is normalized to the analytically calculated transition temperature from equation (2.20). The condensate fraction obtained in the thermodynamic limit is denoted with the solid gray line.*

5.3.3. Superfluid Fraction

Asbeforementioned in chapter 4.3, finite systems have a discrete spectrum with energy gaps, which allows even ideal systems to show the NCRI effect. The definition of superfluidity in confined systems is based on this effect and has been used in the derivation of expression (5.37). The results for various particle numbers with and without Bose statistics are shown in figure 5.4.

Like the condensate fraction, the superfluid fraction γ_s reaches unity at $t = 0$ and asymptotically decays to zero in the high-temperature limit, but the functional forms of both quantities differ from one another ($N_0/N \geq \gamma_s$). Justifying from figure 5.4(a), adding particles into the system seemingly increases γ_s. However, rescaling the temperature axis in units of the macroscopic transition temperature T_c (see eq. (2.20)) reverses this behavior, i.e., γ_s decreases. This complies to the expectation that an ideal system in the macroscopic limit does not exhibit superfluidity, which satisfies the correspondence principle.

Figure 5.4(a) also indicates that boltzmannonic systems produce a finite superfluid frac-

tion. This is not prohibited since superfluidity is a ground state property and, thus, not directly a consequence of Bose statistics. However, using the picture of viewing permutation cycles as single particles at lower temperatures, bosons condensate at higher temperatures into the ground state of the system. The more particles are in the system, the longer the possible permutation cycles can become and the higher the temperature with significant values for γ_s will be. In contrast, thermal averages remain unaffected when changing the number of particles in a boltzmannonic system. Hence, the difference between bosonic and boltzmannonic calculations for γ_s increases with increasing particle number.

Bose-Einstein condensation does not occur in a macroscopic system consisting of boltzmannons, or, in other words, a finite occupation of the ground state is only found at absolute zero. Thus, effects like BEC and superfluidity are solely a consequence of Bose statistics in the macroscopic limit. As explained, this statement does not hold if one transfers the concept of BEC and superfluidity to mesoscopic systems. Certainly, Bose statistics remains coupled to these effects, but is not their cause. This change of understanding has been thoroughly discussed in chapter 4.3.

6. Numerical results for systems with Coulomb-interaction

6.1. Analytical methods

An analytical access to finite bosonic systems based on the canonical ensemble is still an open question in statistical physics. As explained in chapter 3, the density matrix of interacting systems is unknown a priori, so one has to solve the N-particle Schrödinger equation in order to find it. Kleinert states in his book[48] that theoretical papers on the topic are generally in disagreement with each other and experimental results for dilute gases, respectively. Possible approaches considered for this diploma thesis are shortly discussed below.

Weakly interacting systems

Naturally, approximations must be introduced to treat the inter-particle interaction. This can be done within perturbation theory, if the interaction is weak. The method is currently under development in the Kleinert group.

Strongly interacting systems

It is known that trapped particles which strongly repel each other form ordered structures, called Wigner crystals, at low temperatures [49]–[53]. In good approximation, the particles can be considered sitting in their own local potentials centered on the classical equilibrium positions. By expanding the potential energy $\hat{V}$ around the equilibrium positions in a Taylor series, one can issue an unitary transformation into eigenmode representation which diagonalizes the Hamiltonian $\hat{H}$ [54, 55].

On the plus side, the density matrix is now known, since $\hat{H}$ describes a system of independent quasiparticles (the eigenmodes) each sitting in a harmonic trap. Unfortunately, the inclusion of Bose statistics turns out to be problematic, since one still has to symmetrize the density matrix in position space. Neglecting the fact that an exchange of particles corresponds to large displacements out of the equilibrium positions uncovered by the initial approximation, a permutation of any number of particles usually affects all modes (except the center-of-mass modes, which always remain unchanged). Thus, an elegant analysis via the cycle length decomposition as used for the ideal case is impossible. Another problem is the rotational mode with its "trapping" frequency of $\omega = 0$, for which the density matrix of the harmonic oscillator is singular. Simply excluding any rotations will not do, as permutations affect the rotational state. One encounters a similar problem in molecular physics, known as the impossibility to completely separate vibrational and rotational motion from one another [56]. A separation can only be achieved by introducing further approximations, valid e.g., in strong magnetic fields [57], which do not apply for the system in question.

Nevertheless, the method can be tried for the two particle system, where an exchange only alters the sign of the breathing mode. Unfortunately, the results are in disagreement with the PIMC simulations presented below, which reinforces Kleinert's predication. Therefore, further investigations were abandoned at this point.

6.2. 2 particles in a trap

The following sections are devoted to the numerical results obtained for 2D trapped particles. The dependence for various physical quantities on the temperature t, coupling strength λ and particle number is investigated. In total, data obtained with close to 1000 PIMC simulations has been evaluated. The needed computational time for a single run ranged from a few minutes up to several hours.

This section focuses on the 2-particle case and is restricted to a discussion of the energy, the density distribution, and the superfluid fraction. The next section broadens the spectrum of investigated quantities and takes effects related to the particle number ($N = 2 \dots 5$) into account. The most intruding results are summarized in the closing chapter.

6.2.1. Overview

The general behavior of the 2-particle system is presented in figure 6.1. Shown is the density distribution around the trap center viewed from a body fixed frame. The attachment to this frame suppresses the blurring due to rotational symmetry. Appendix D describes the procedure in detail.

One can distinguish four different "phases" of the system:

Bose-Einstein condensate. In the nearly ideal case, the particles completely overlap with one another and form a single cloud in the trap center. The radius of this cloud increases with the coupling parameter λ.

Crystal. For strongly coupled systems, the bosons form a crystal like structure at intermediate temperatures. They are strongly localized and separated by a certain distance with the trap center in between them. The distance grows with increasing λ.

Thermal excitation. At temperatures above ~ 1, thermally excited fluctuations of the particles around their equilibrium positions cause a broadening of the density distribution primarily in radial direction, which corresponds to the breathing mode of the system.

Quantum melting. At very low temperatures, the particles extend in angular direction while staying localized in the radial direction. At some point, depending on the interaction strength, the density closes into a ring with completely delocalized particles.

The plotted distributions do not differentiate whether the broadening of the density relates to thermal (vibrational) fluctuations or quantum mechanical expansion. However, rotations of the system around the trap center are suppressed leaving only the breathing mode and the two center-of-mass modes as thermally motivated contributions. Thus, an angular broadening must be due to the expansion of the particles themselves. Furthermore, one does

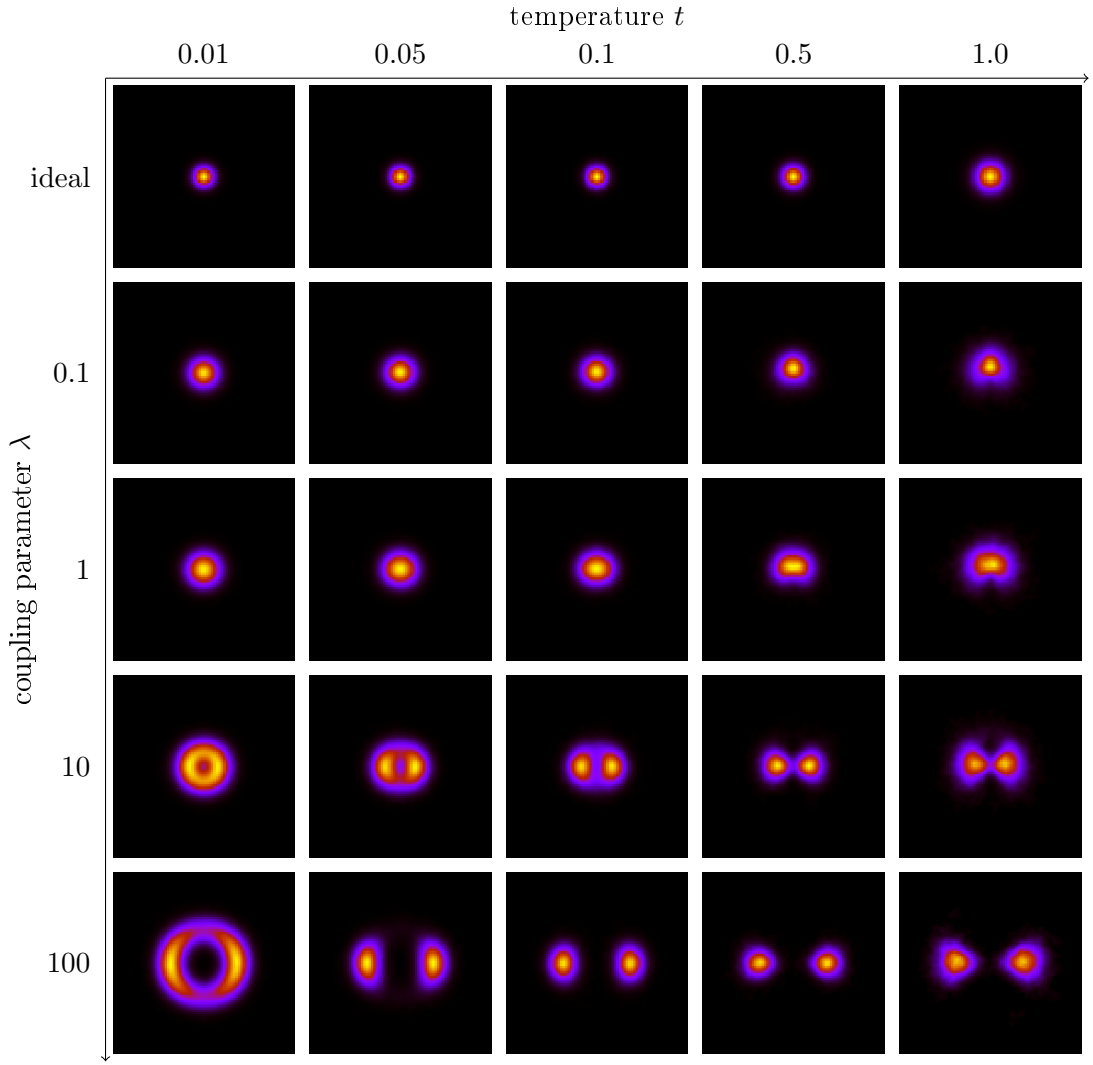

Figure 6.1.: *Density distribution for 2 bosons in a 2D harmonic trap. A section of* $16\,l_0 \times 16\,l_0$ *with the trap center in the middle is shown in each plot. The top row shows the ideal case calculated analytically with eq.* (5.16)*. The remaining rows show results from PIMC simulations obtained from an overlay of 2000 particle configurations, where the arbitrary rotation around the trap center has been suppressed. The "kink" in some of the plots from the rightmost column results from a biased suppression affecting primarily weakly correlated systems (see appendix D).*

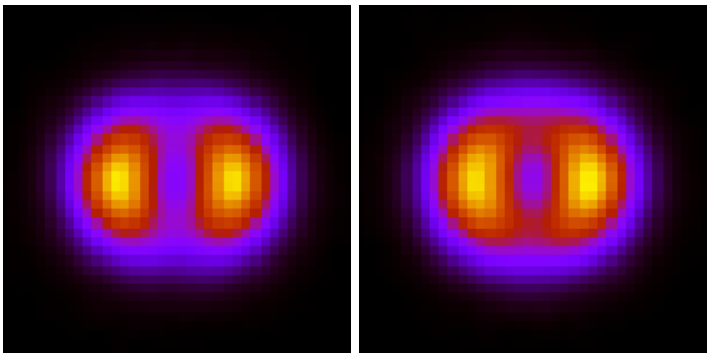

(a) Boltzmannons. (b) Bosons.

Figure 6.2.: *Comparison of the bosonic and boltzmannonic density distribution at $\lambda = 10$ and $t = 0.05$. A section of $8\,l_0 \times 8\,l_0$ is shown. The blocky appearance is an artifact due to the specific calculation of the density.*

observe the stable molecule like phase where neither of both effects occur. This stable phase is apparently situated in between.

As a remark, the quantum melting is not an effect directly related to Bose statistics. The analog density diagram for boltzmannons (very much like figure 6.1 for bosons) shows only differences at the second glance. One specific comparison for $\lambda = 10$ and $t = 0.05$ is presented in figure 6.2. In general, Bose statistics encourage ring formation but are not its cause. The additional bosonic particle exchange effectively behaves like an attractive interaction.

6.2.2. Energy

The dependence of the energy per particle on the temperature and the relative interaction strength is shown in figure 6.3. Obviously, the PIMC results reproduce the analytically computed data nicely in the limit $\lambda \to 0$.

The system reaches its ground state energy level of $\varepsilon = 1$ at approximately $t \approx 0.2$ in the ideal case. This temperature seems to be almost universal regardless of the interaction strength save a slight tendency to higher values. In good approximation, the ground state energy is proportional to $\lambda^{2/3}$ for $\lambda > 10$. A simple analysis for 2 classical point particles shows

$$x_0 = \left(\frac{\lambda}{4}\right)^{\frac{1}{3}} \qquad \varepsilon(x_0) = \frac{3}{2}\left(\frac{\lambda}{\sqrt{2}}\right)^{\frac{2}{3}}, \tag{6.1}$$

where x_0 is the classical equilibrium distance to the trap center which minimizes the potential energy. Every graph in figure 6.3(bottom) converges against this limit with increasing λ, as the system becomes locked in the strongly bounded state.

On the other hand, inter-particle interaction grows less important with increasing temperature. This is shown in figure 6.3(top) where all curves converge into the one of the ideal system at high temperatures. It can also be seen in figure 6.3(bottom) where the energies for the ideal system are marked by short gray lines. The higher the temperature, the faster the curves converge into this limit for $\lambda \to 0$.

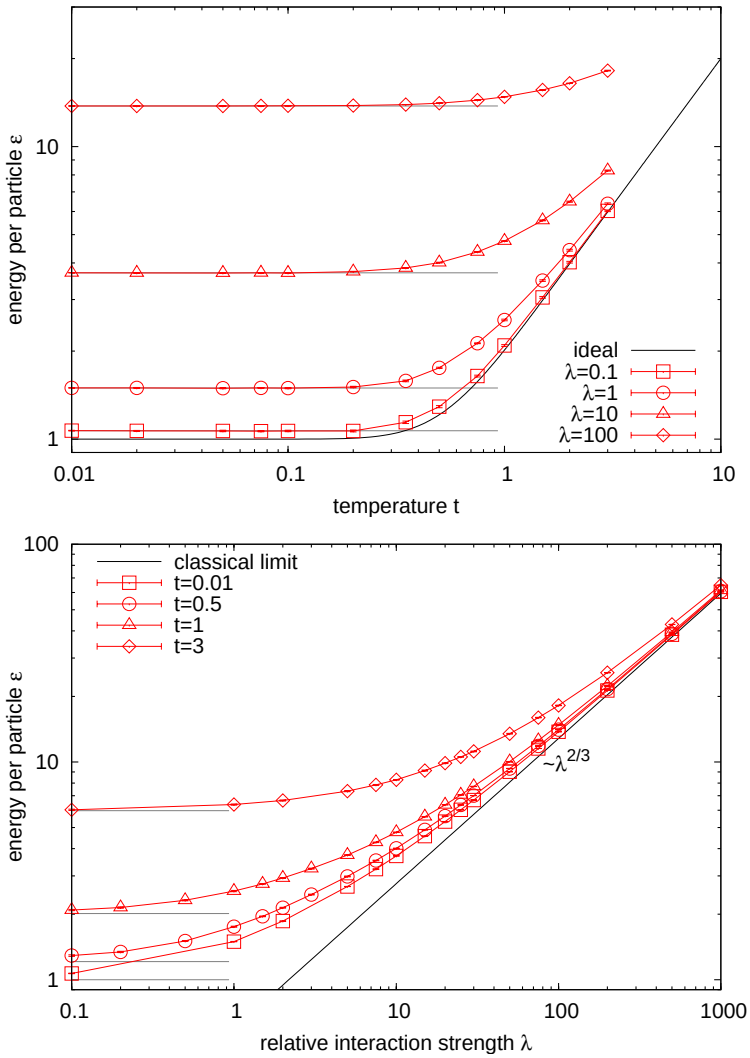

Figure 6.3.: *Energy per particle for 2 bosons. The upper figure shows the dependence on temperature for various coupling parameters λ. The ideal limit is indicated by a solid black line. Red lines connect data points obtained from PIMC simulations for the same λ. Horizontal gray lines indicate the assumed ground state energy for the corresponding λ. The lower figure displays the energy dependence on the interaction strength λ. Here, each red line corresponds to a fixed temperature. Values obtained for the ideal asymptotics are indicated by short gray lines. In good approximation, the bottommost line for $t = 0.01$ corresponds to the ground state energy which asymptotically converges into a $\lambda^{2/3}$ law (precisely eq. (6.1)) in the strongly correlated regime.*

6.2.3. Radial density distribution

The radial density $n(r)$ and pair distribution function $f(r_{12})$ reflect the behavior of the energy. When the ground state energy level is reached, both quantities, $n(r)$ and $f(r_{12})$, remain unchanged (see fig. 6.4). The peak in the radial density occurs at the classical equilibrium position x_0 of two point-particles in a trap. The distance from the trap center scales with the coupling parameter λ according to $x_0 \propto \lambda^{1/3}$ (eq. (6.1)). The pair distribution $f(r_{12})$, i.e., the probability to find a particle at the distance r_{12} from a reference particle, obviously has its maximum at $2x_0$, since the trap center lies exactly in the middle.

With increasing temperature the radial density distribution broadens and the peak height lessens due to thermal fluctuations. At the same time the density in the trap center increases. If the temperature grows sufficiently high, the peak of $n(r)$ vanishes completely and individual particles cannot be distinguished anymore. This indicates the dissociation of the crystal and a transition to a gaseous phase.

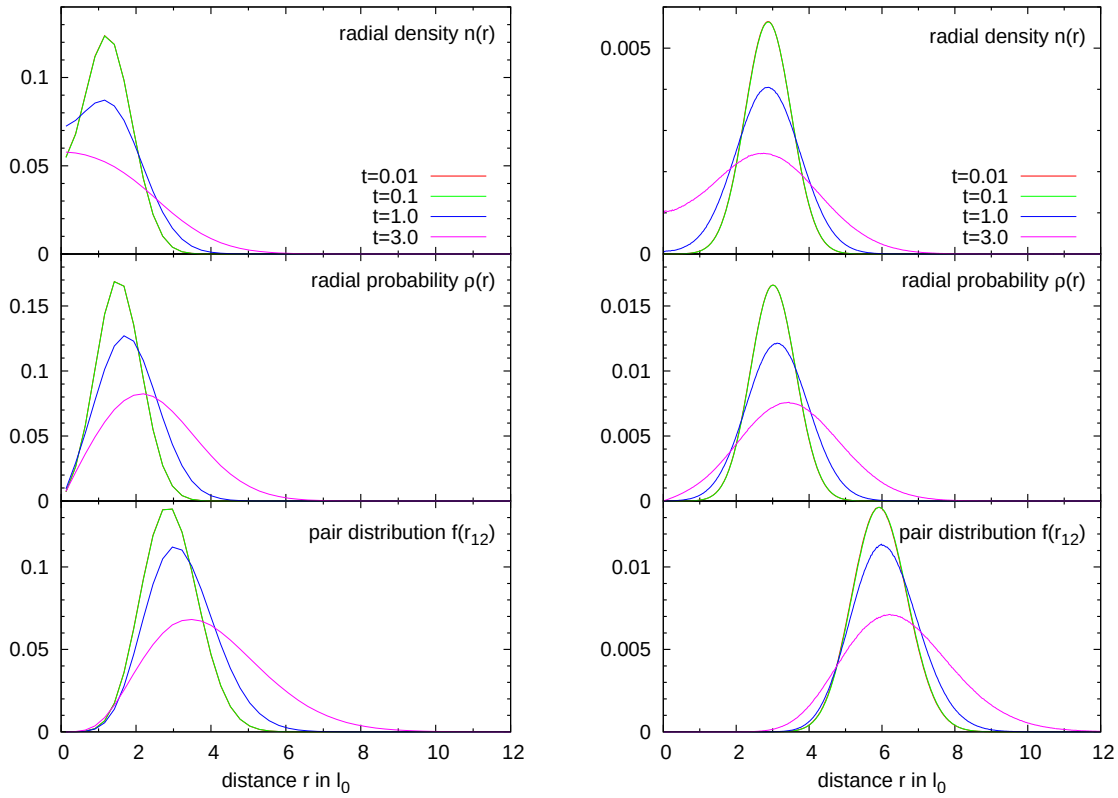

(a) $\lambda = 10$. (b) $\lambda = 100$.

Figure 6.4.: *Radial density $n(r)$ (top), radial probability $\rho(r) = 2\pi r n(r)$ (middle) and pair distribution function $f(r_{12})$ (bottom) for 2 particles with $\lambda = 10$ in the left and $\lambda = 100$ in the right panel, respectively. The distance r on the x-axis denotes the distance to the trap center in the upper two plots and the inter-particle distance in the bottom plot. The plots for $t = 0.01$ (red line) and $t = 0.1$ (green line) lie exactly on top of each other leaving only the latter visible. The graphs are valid for both Bose and Boltzmann statistics.*

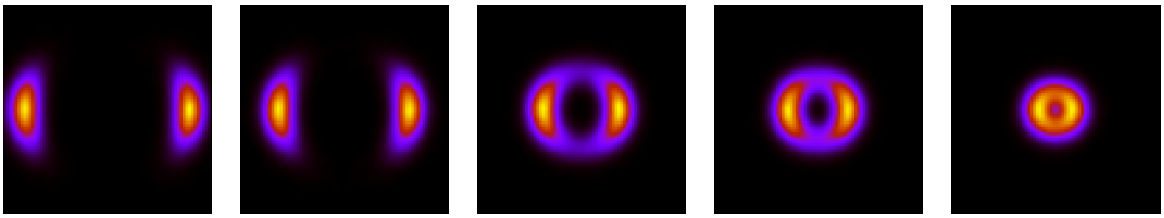

(a) $\lambda = 1000$. (b) $\lambda = 500$. (c) $\lambda = 100$. (d) $\lambda = 50$. (e) $\lambda = 10$.

Figure 6.5.: *Density distribution for 2 bosons at $t = 0.02$. From left to right the relative interacting strength λ decreases. The size and form of a cloud is seemingly independent of λ as long as the particles do not overlap.*

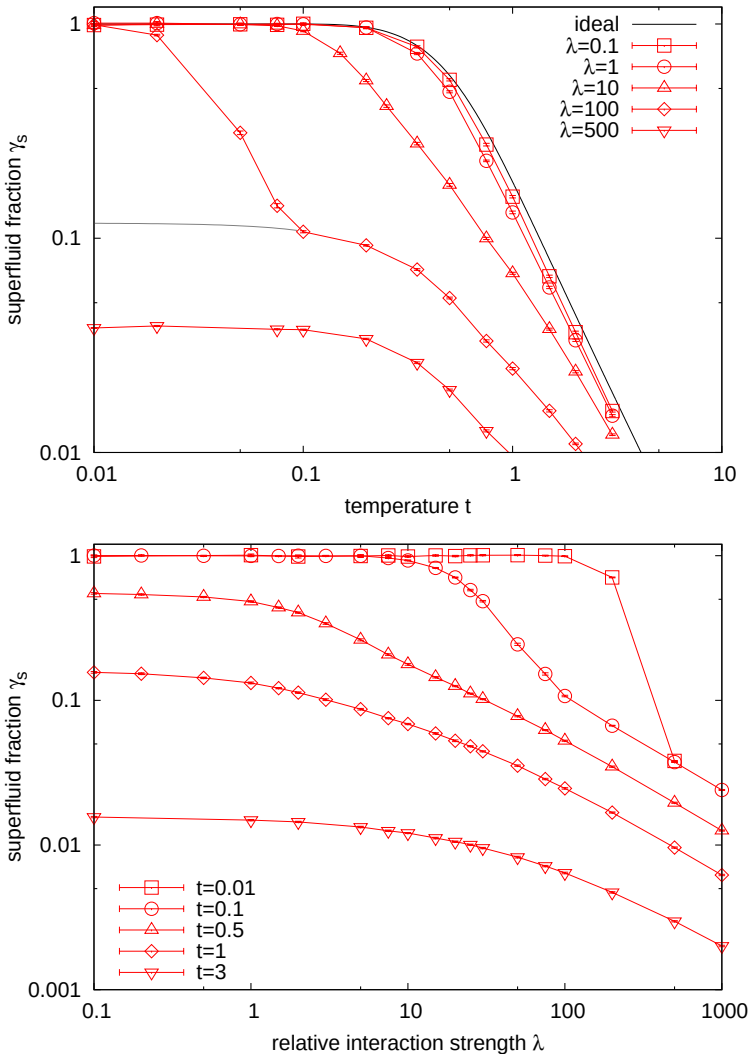

Figure 6.6.: *Superfluid fraction γ_s for 2 trapped bosons. The dependence of γ_s on the temperature is shown in the upper figure and the dependence on the interaction strengths λ in the lower figure. The solid black line indicates the result for the ideal case computed analytically with eq. (5.37). Symbols with error bars denote PIMC data. They are connected with red lines to guide the eye. In the case of $\lambda = 10$, γ_s shows a peculiar two-step behavior as a result from two different contributions to the NCRI. Only the low-temperature contribution is a ground state effect. The thermal high-temperature contribution is caused by the finite volume of the system (see text).*

With decreasing temperature, however, the crystal melts into a ring like structure with completely delocalized particles. The density only spreads along the angular direction in this procedure which leaves the radial density profile unchanged. Both radial density and pair distribution function are insensitive to the occurrence of such a phase.

6.2.4. Superfluidity

The behavior of the superfluid fraction γ_s is shown in figures 6.6–6.8. One can divide its temperature dependence into three different cases—the nearly ideal, the intermediate, and the strongly correlated regime.

Nearly ideal systems reach the 100 % superfluid state at approximately $t \approx 0.2$. Above this temperature γ_s decays asymptotically to zero. In general, the shape of the graph resembles the analytical results obtained for the ideal case (see fig. 5.4), but is shifted to lower temperatures with increasing interaction strength λ.

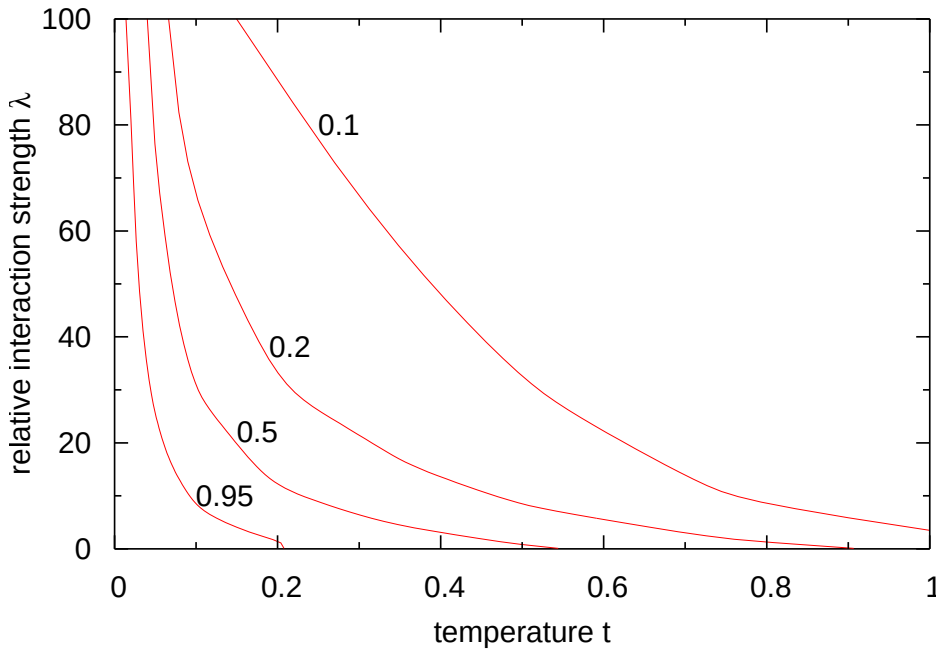

Figure 6.7.: *Topological diagram for the superfluid fraction γ_s in the 2D trapped system. Shown are the lines of equal γ_s. The corresponding values are indicated in the attached labels. Note that the lines end at a finite temperature in the limit $\lambda \to 0$, while converging asymptotically to $t = 0$ for $\lambda \to \infty$.*

A system of intermediate coupling strength displays a peculiar aspect, as the graph develops a two step behavior: When the system is cooled, γ_s first seems to saturate at some value until it has a second rise up to 1 beginning at the characteristic temperature t_B. This is exactly the point at which bosonic and boltzmannonic calculations start to differ (see fig. 6.8). The contributions to γ_s result from different origins above and below t_B.

Ground state contribution $t < t_B$. This regime is characterized by bosonic particle exchange. The cycle-picture developed in chapter 5 implies that all particles participating in the same cycle must be in the same state, presumably the ground state. The jump of γ_s with the beginning of particle exchange below t_B can, thus, be related to Bose-Einstein condensation which should obviously yield a high superfluid response considering the energy gap to the first excited state.

Thermal contribution $t > t_B$. Concluding from the reasoning above, contributions to γ_s above t_B cannot be a consequence of Bose-Einstein condensation and must, thus, be solely related to the finite size of the system. An intuitive explanation can be drawn from the area formula (eq. (3.37)) used in PIMC simulations to calculate the NCRI. The area formula relates NCRI to the ratio of the covered area to the cross section of the whole system. The latter is finite and quantum particles always have a finite extension which results in a non-zero value for the NCRI. This explanation works whether the system is in its ground state or not since also non-condensed particles have a finite extension.

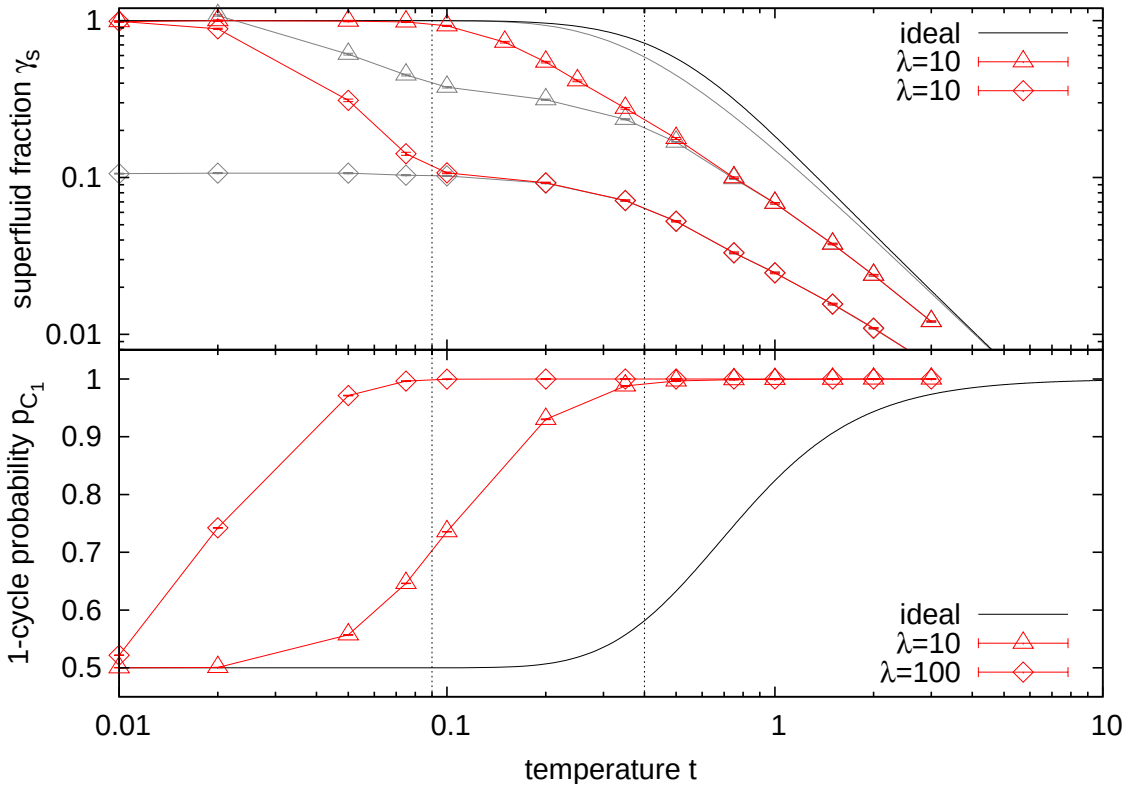

Figure 6.8.: *Two-step behavior of the superfluid fraction γ_s. The upper panel shows the difference in γ_s due to Bose (colored lines) and Boltzmann (gray lines) statistics. The calculations for three different relative interaction strengths λ are presented. The probability of the identity permutation p_{C_1} in the bosonic systems. The vertical dashed lines indicate the approximate temperature below which the bosonic and boltzmannonic calculation start to differ.*

One can extrapolate the second contribution down to $t = 0$ as shown in fig. 6.6(top) by the gray line. It represents the dominant contribution in weakly interacting systems, but decreases with increasing λ since the size of the system also increases (see fig. 6.4) while the extension of the particles remains unchanged (see fig. 6.5).

It is not implied that boltzmannonic systems only yield finite size contributions to γ_s. On the contrary, since boltzmannons condensate into the ground state at a finite temperature, the system should also experience a jump in γ_s at this point (see the $\lambda = 10$ case in fig. 6.8). This corresponds to the observation made for ideal systems that bosonic and boltzmannonic simulations may only differ in intermediate temperature regions.

In the strongly correlated regime the distance between the classical equilibrium positions becomes quite large which effectively suppresses particle exchange. Figure 6.6(top) suggests that only the finite size contribution to γ_s is at $\lambda = 500$. However, there is no "hard" transition to this behavior (which is never the case in finite systems), t_B rather converges asymptotically to zero for $\lambda \to \infty$ (see fig. 6.7). In principle, γ_s should always reach unity, but t_B grows so small for very high interaction strengths that the region becomes inaccessible with PIMC simulations.

6.3. 2–5 particles in a trap

This section is devoted to the investigation of effects related to the number of particles. For 2D systems with Coulomb interaction it is advisable to start with a small increase up to 5 particles. In these systems the particles array themselves on a ring around the trap center in their ground state configuration. Adding another particle opens a new shell with a particle in the trap center. Effects related to shell formation will not be considered within this diploma thesis since the bulk of the obtained data from PIMC simulations was biased or did not converge on time.

6.3.1. Overview

The following pages provide a general overview of the system for $N = 2, \ldots, 5$ (figs. 6.10–6.13). In the whole picture, the situation does not significantly change when more particles are added to the system. The statements issued for the 2-particle system in the previous chapter remain valid for larger N, in particular, one can again separate the parameter space into the 4 "phases". Differences are subtle and are related dominantly to the change of the density. The implications are considered separately for each quantity.

6.3.2. Energy

In a non-interacting system, the energy per particle in the ground state is independent of the particle number. For the system in question that is $\varepsilon = 1$ as seen in figure 6.9. At a finite temperature a system with more particles has a lower energy, which is a characteristic effect for bosons due to their negative exchange energy. Arguing with the picture of exchange cycles as single particles at lower temperatures, particles can condensate into the ground state at higher temperatures than distinguishable particles could. The larger the particle number, the longer the possible permutation cycles and the lower the temperature for a cycle can be. Thus, putting more bosons together effectively decreases the energy per particle.

Interestingly, this effect is reversed for strongly correlated systems. Here, more particles mean a higher energy per particle. From the classical viewpoint the repulsion forces the particles out of the trap center into a ring like structure, whose radius increases with each particle added (see figure 6.14). The farther a particle sits from the center, the higher its energy. In good approximation, each particle sits in its own harmonic potential centered around the classical equilibrium position. In quantum mechanics the point-particles are replaced with wave functions, namely the typical Gaussian for the ground state in this case. Taking Bose statistics into account does not change much, although the system in principle can lower its energy compared to a boltzmannonic system. But firstly, the possible slip from exchange energy is negligibly small against the large interaction term and secondly, the stronger localization suppresses the exchange probability (see figure 6.18).

According to figure 6.9(b), the point at which exchange and interaction energy hold the balance lies at $\lambda_{\text{rev}} \approx 0.2$ for intermediate temperatures. Bosonic exchange has no effect on the energy for $t \to 0$ and $t \to \infty$, so the transition point vanishes, as it is $\lambda \to 0$ in these cases.

Aside from the additional dependence on the particle number, the arguments issued in

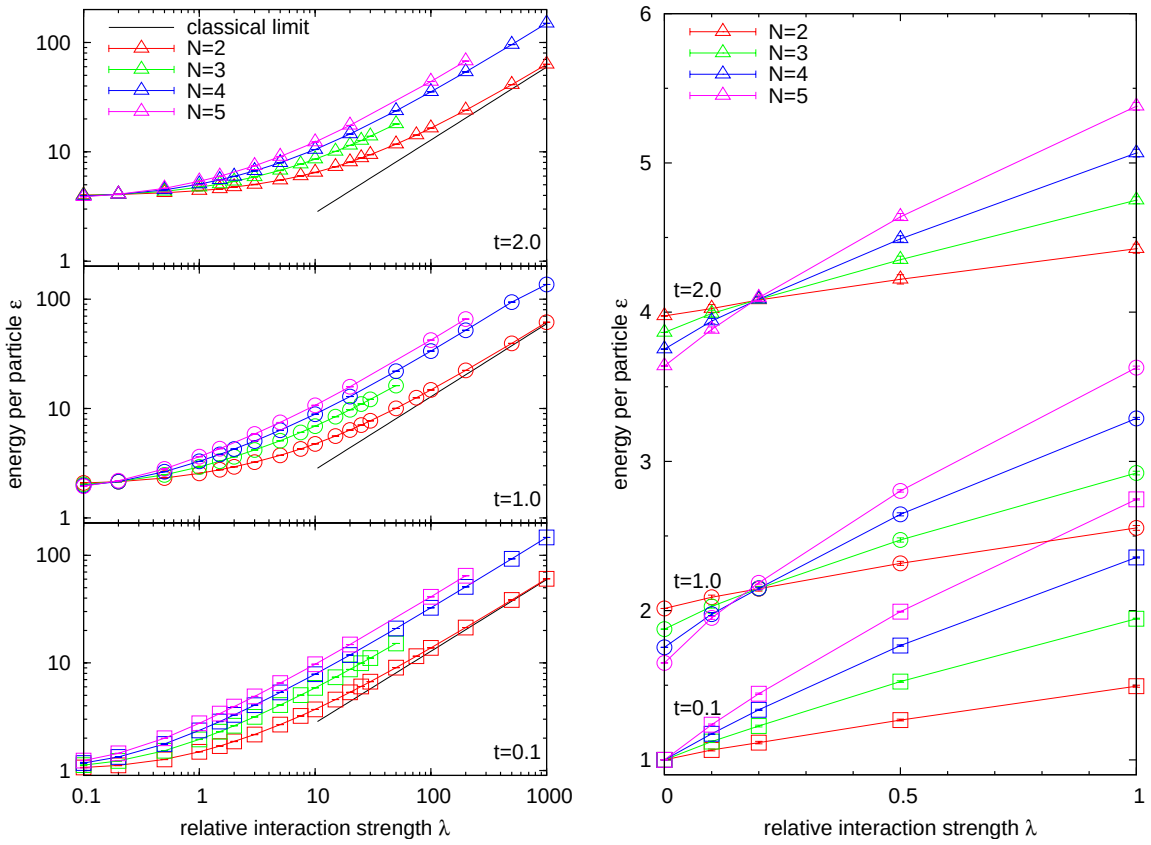

(a) General overview.

(b) Detailed view.

Figure 6.9.: *Dependence of the energy per particle ε on the relative interaction strength λ. The left-hand figure gives the general idea of the behavior. All graphs converge into the classical limit $\varepsilon \propto \lambda^{2/3}$ for $\lambda \to \infty$. The right-hand figure shows the weakly interacting case in detail. For nearly ideal systems the energy per particle is lowered in larger systems due to the the negative exchange energy. Since the inter-particle interaction is repulsive, the situation reverses with increasing λ.*

the previous section for the energy behavior with respect to temperature and interaction strength are still applicable. In summary, the energy is independent of t and proportional to $\lambda^{2/3}$ for low temperatures, and strongly correlated systems behave like an ideal system in the limit of high temperatures.

6.3.3. Radial density distribution

Figure 6.14 shows the density distribution for different particle numbers. They are compared to each other for 4 different parameter pairs (t, λ) ranging from ideal to strongly correlated setups. They are rounded out by the plots for the radial density distribution $n(r)$ shown in figure 6.15(a).

In non-interacting systems at $t = 0$ the density shows the typical Gaussian like distribution

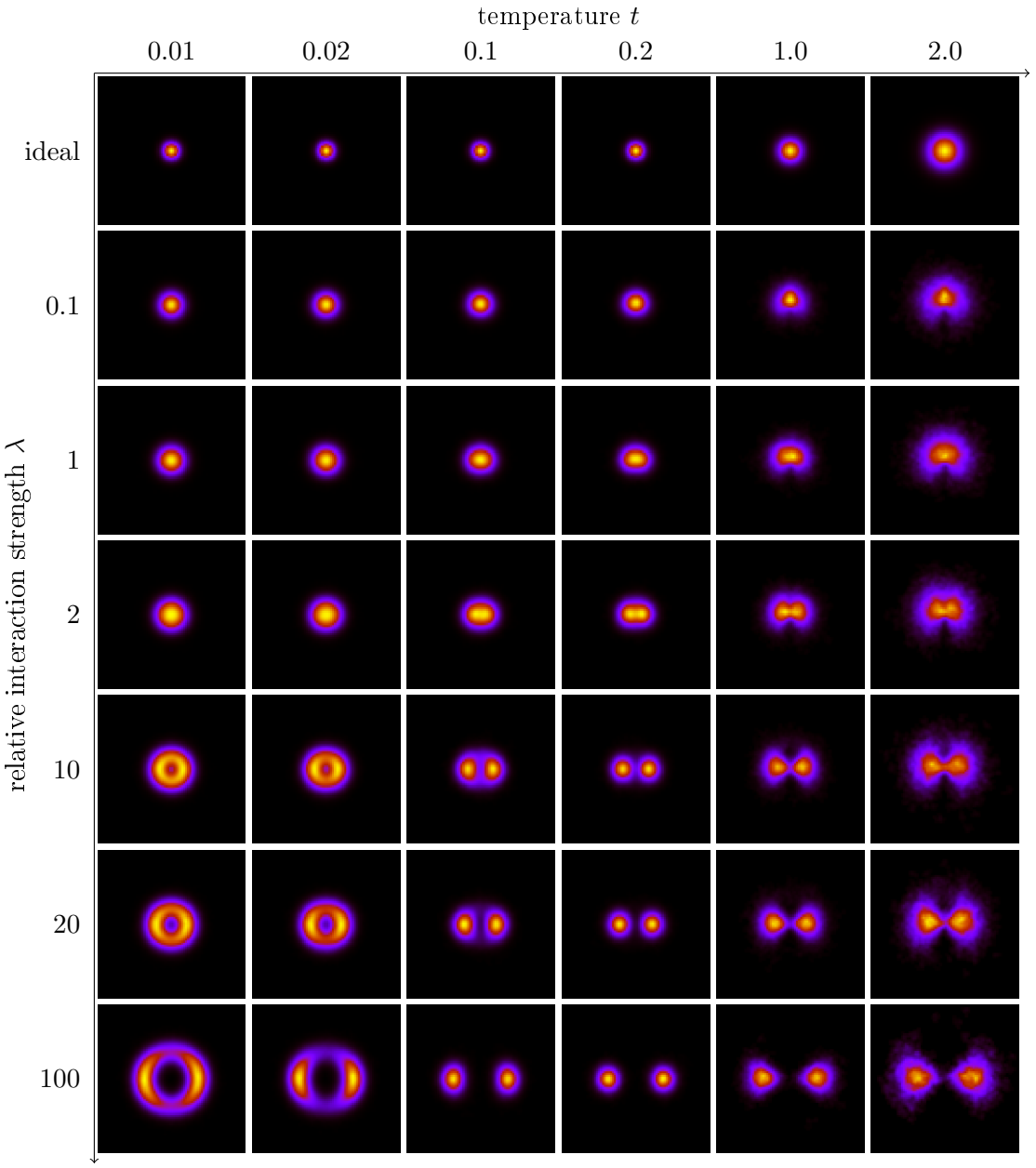

Figure 6.10.: *Density distribution for* 2 *bosons.*

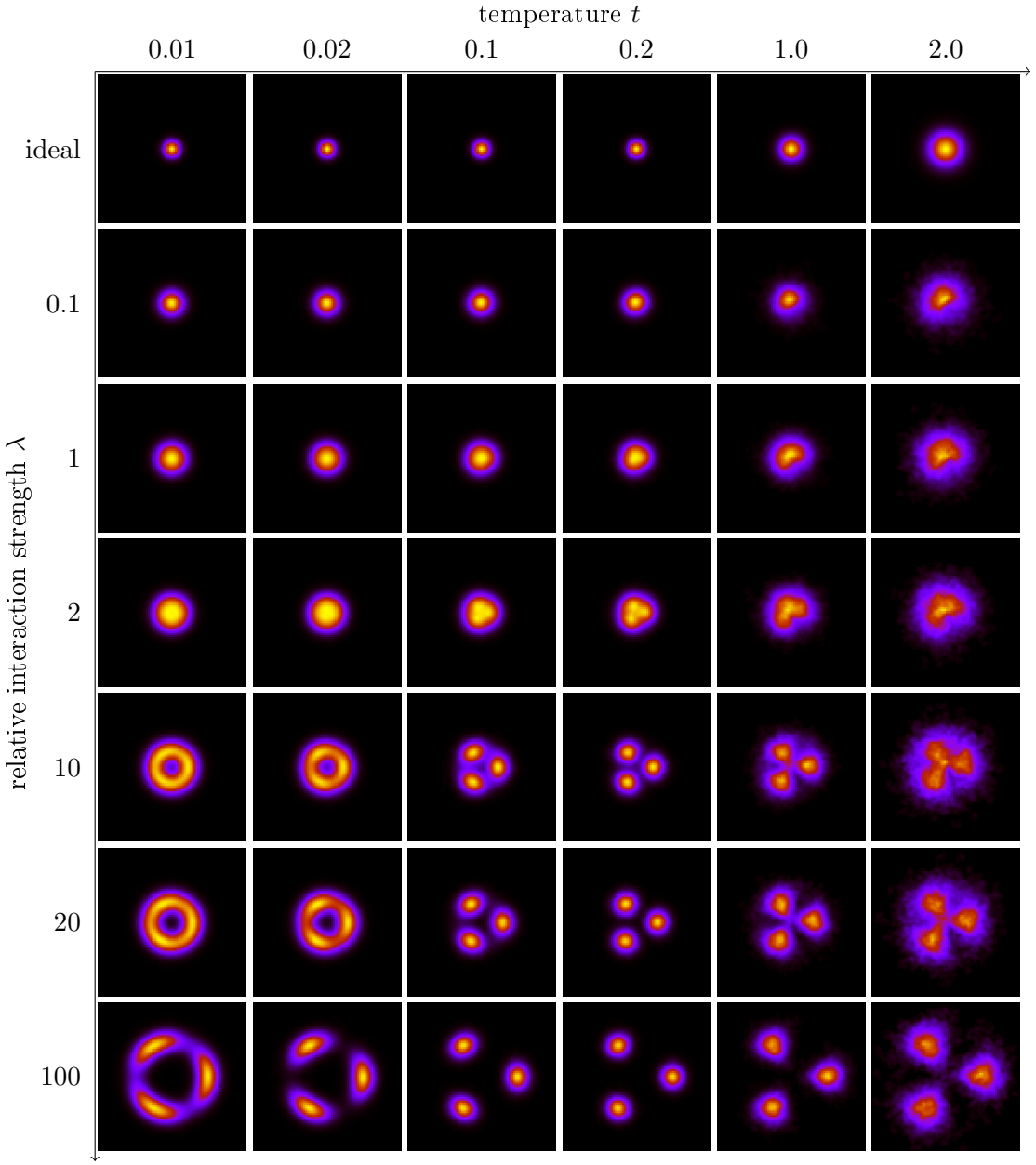

Figure 6.11.: *Density distribution for* 3 *bosons.*

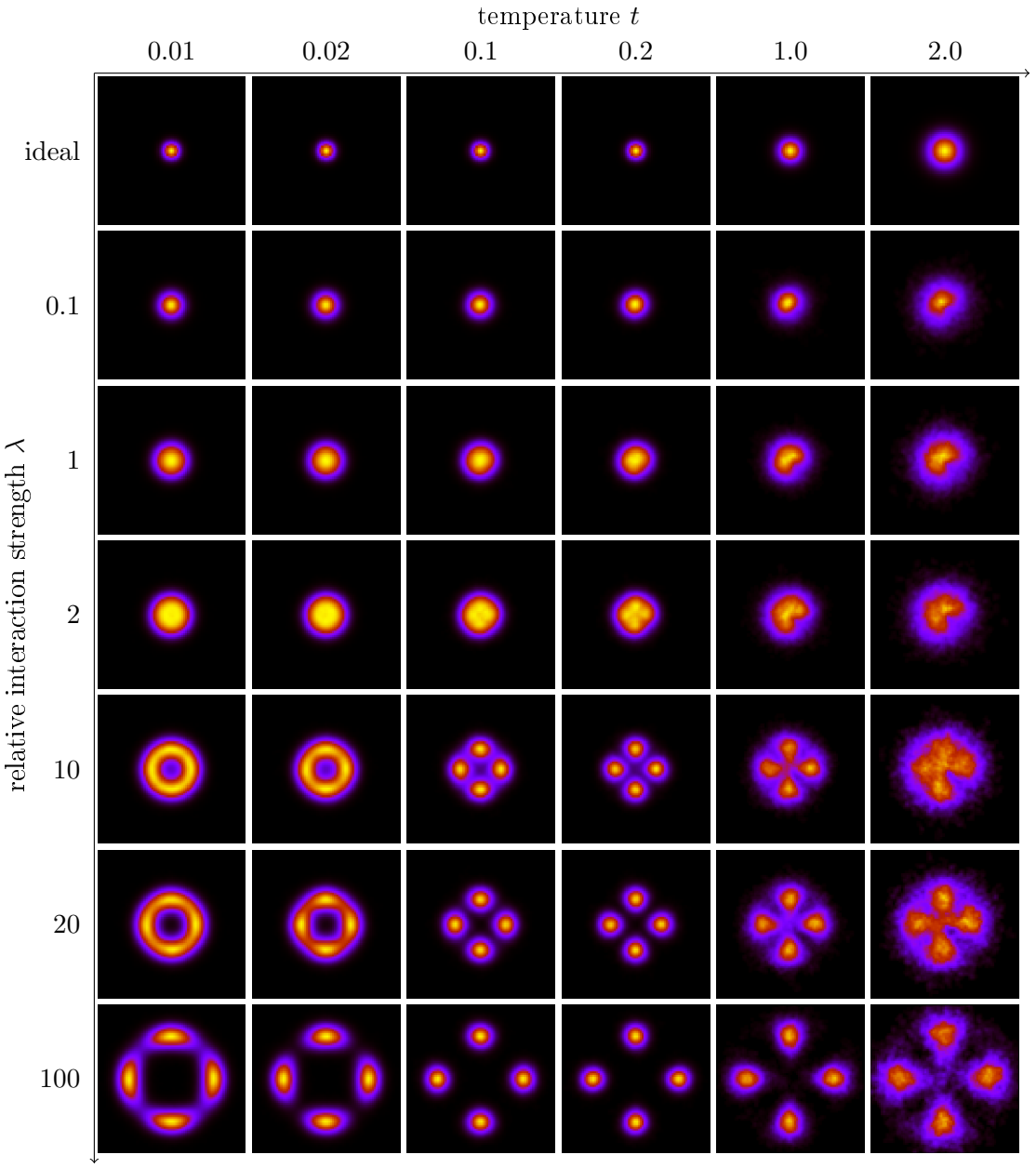

Figure 6.12.: *Density distribution for* 4 *bosons.*

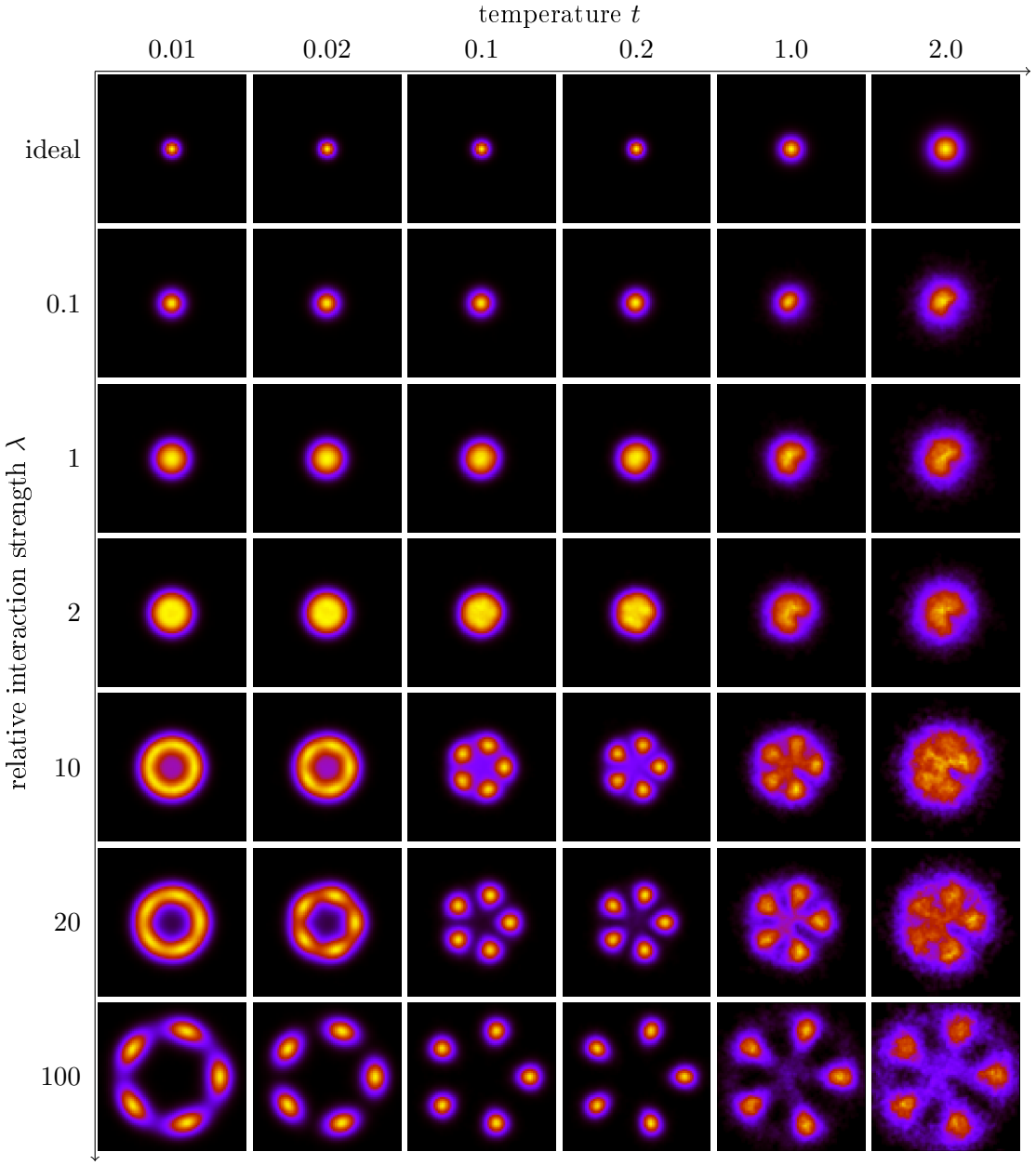

Figure 6.13.: *Density distribution for* 5 *bosons.*

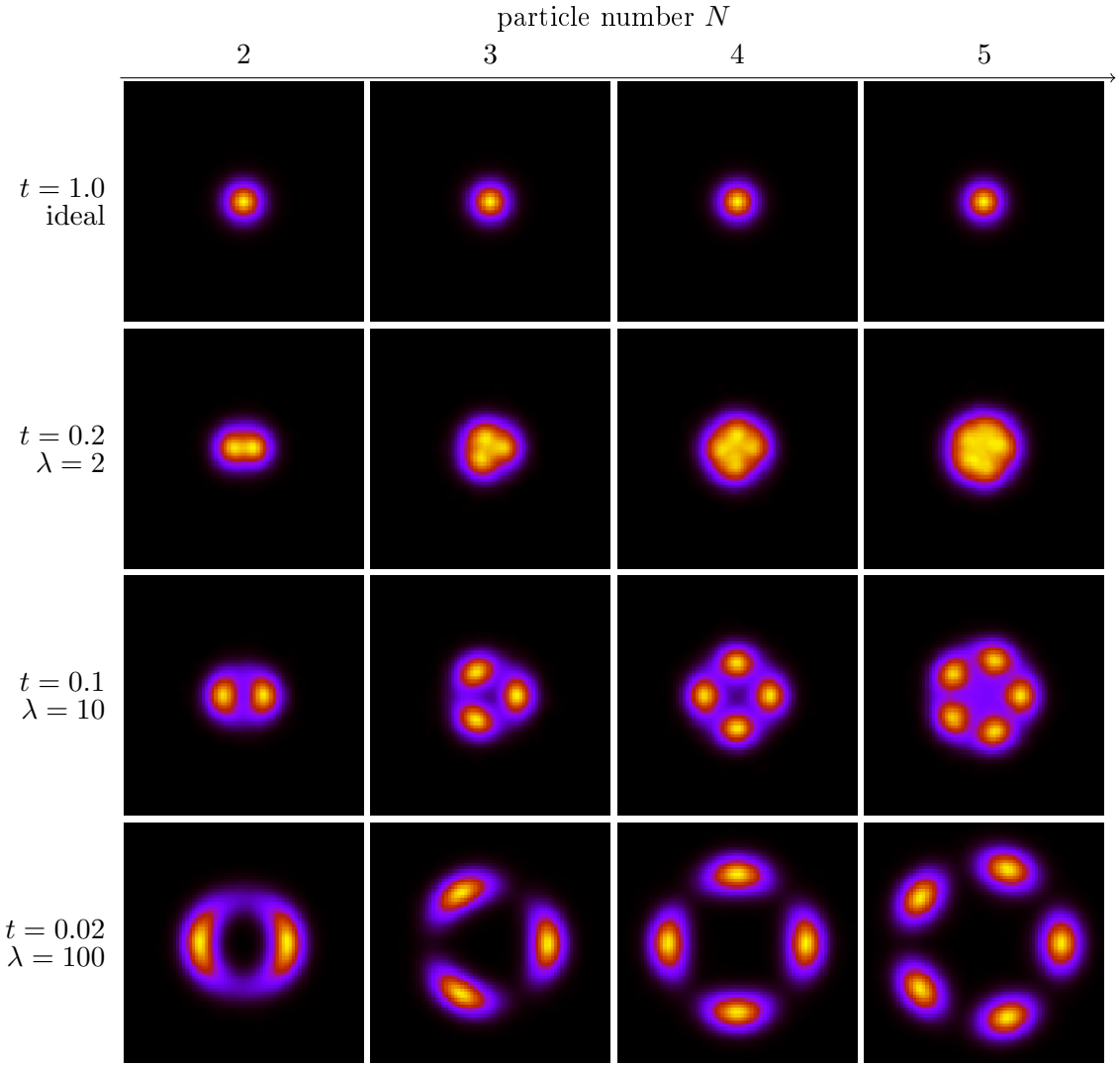

Figure 6.14.: *Direct comparison of the density distribution for $N = 2 \ldots 5$ bosons at 4 chosen parameter sets. The effective system size increases due to inter-particle repulsion. The size and the localization increase with the particle number in case of strongly correlated systems (bottom row).*

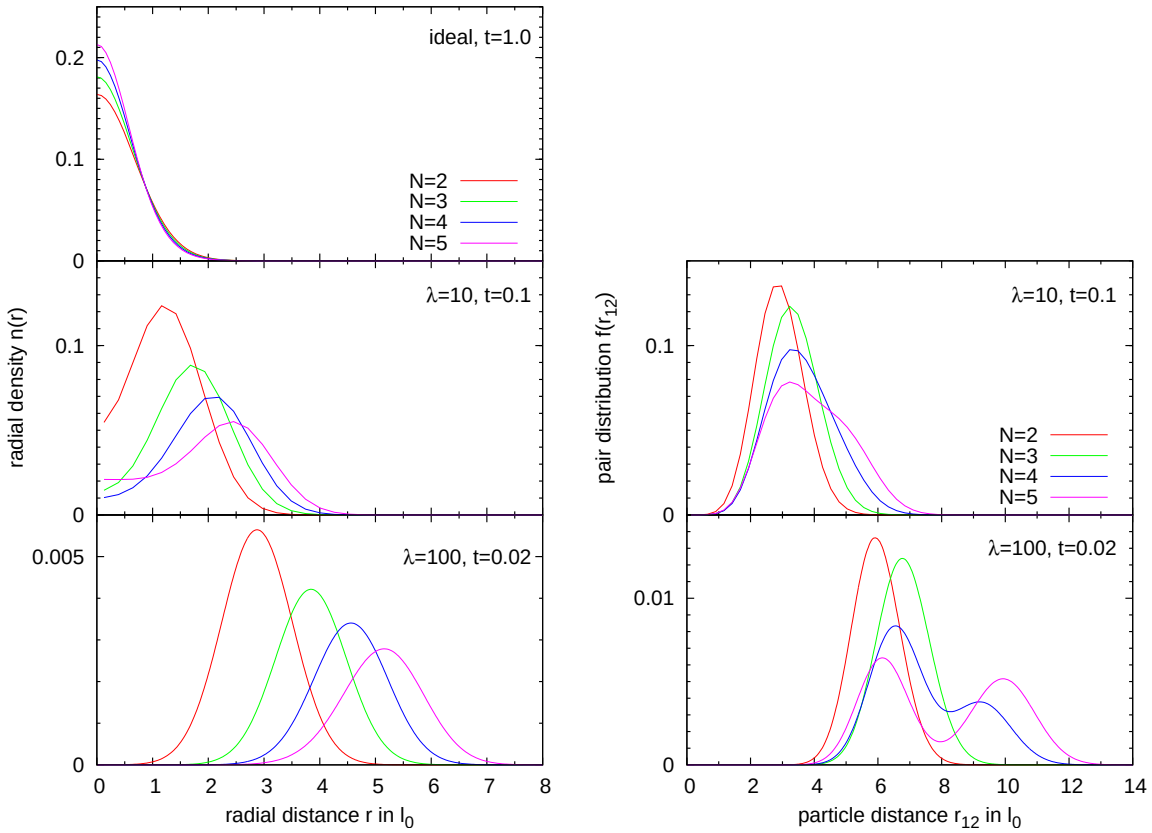

(a) Radial density distribution.

(b) Pair distribution function.

Figure 6.15.: *Comparison of the radial density distribution and the pair distribution function in 2D trapped systems for varying particle numbers ($N = 2 \ldots 5$). From top to bottom, the plots correspond to the configurations shown in the first, third and forth line of figure 6.14. The pair distribution function was not calculated for the ideal system.*

corresponding to $|\Psi|^2$ of the single-particle ground state wave function

$$\Psi(x) \propto e^{-\frac{1}{2}\left(\frac{x}{l_0}\right)^2} \tag{6.2}$$

of the quantum mechanical harmonic oscillator. The peak continuously dissolves into a flatly distributed cloud when the system is heated. It is characteristic for bosonic systems that the transition can also be invoked by changing the particle number in the system. The resolution of the planar density plots is unable to demonstrate this, but the radial density shows a small but clearly visible sharpening of its peak. For example, compare the radial density for 4 particles to the sharper peak in the 5-particle case. The latter system must acquire the same density distribution as the 4-particle system at some higher temperature since the transition is continuous. Consequently, adding more particles shifts the system further to its ground state configuration. This complies to the energy behavior discussed previously. Additionally, since the radial density plots in figure 6.15(a) are normalized to the particle number, the peak in the distribution is actually N times higher. The occurrence of an extremely sharp

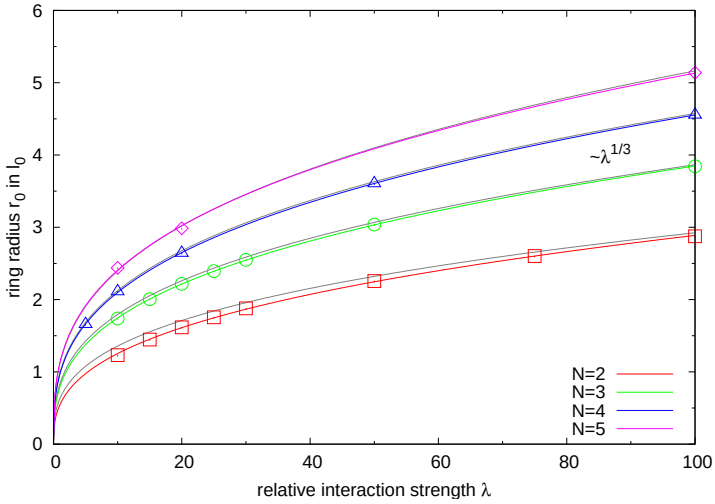

N	2	3	4	5
c	0.63	0.83	0.99	1.11

Figure 6.16.: *Dependence of the system size on the relative interaction strength λ. The lines indicate the distance of the peaks in the density distribution from the trap center. Colored and gray lines denote PIMC data and the corresponding classical equilibrium positions ($x_0 = r_0/l_0 = c\lambda^{1/3}$), respectively.*

peak in position (and momentum) space over a flatly distributed thermal cloud is the method of choice for detecting Bose-Einstein condensation in experimental setups. In these (nearly) macroscopic systems the transition occurs abrupt.

Again, the inclusion of a strongly repulsive interaction seemingly reverses the behavior of the density distribution. Adding particles broadens the width and shrinks the height of the peak in the radial density plots. What the radial distribution does not show is that, in spite of the peaks broadening, the particles actually get more localized at their classical equilibrium positions. The density's angular distribution width decreases, as more particles try to fit onto the same ring leaving less space for an individual one, although the ring's radius slightly increases (fig. 6.16).

The pair distribution function $f(r_{12})$ (fig. 6.15(b)) is a common method-of-choice in order to investigate the state of matter, at least for macroscopic systems. Clearly separated peaks indicate strong particle localization found in bounded, crystal like phases. For the system in question, its usefulness is limited since the particle number is too small for $f(r_{12})$ to develop a characteristic behavior. For example, 2- and 3-particle systems only show a single peak because the particles are equally distanced from one another. Whether the system is bound or not cannot be reliably resolved in these cases. The situation improves for 4 and 5 particles, where two different inter-particle distances occur in the bound state. According to figure 6.15(b) the system forms a crystal at $t = 0.02$, $\lambda = 100$ (lower figure), but not at $t = 0.1$, $\lambda = 10$ (upper figure). The deeper notch in the 5-particle case indicates the stronger localization in this system. The peaks are approximately of equal height since each particle has two neighbors close-by and two farther away. With 4 particles each particle has only one remote neighbor leading to a second peak with half the height of the first.

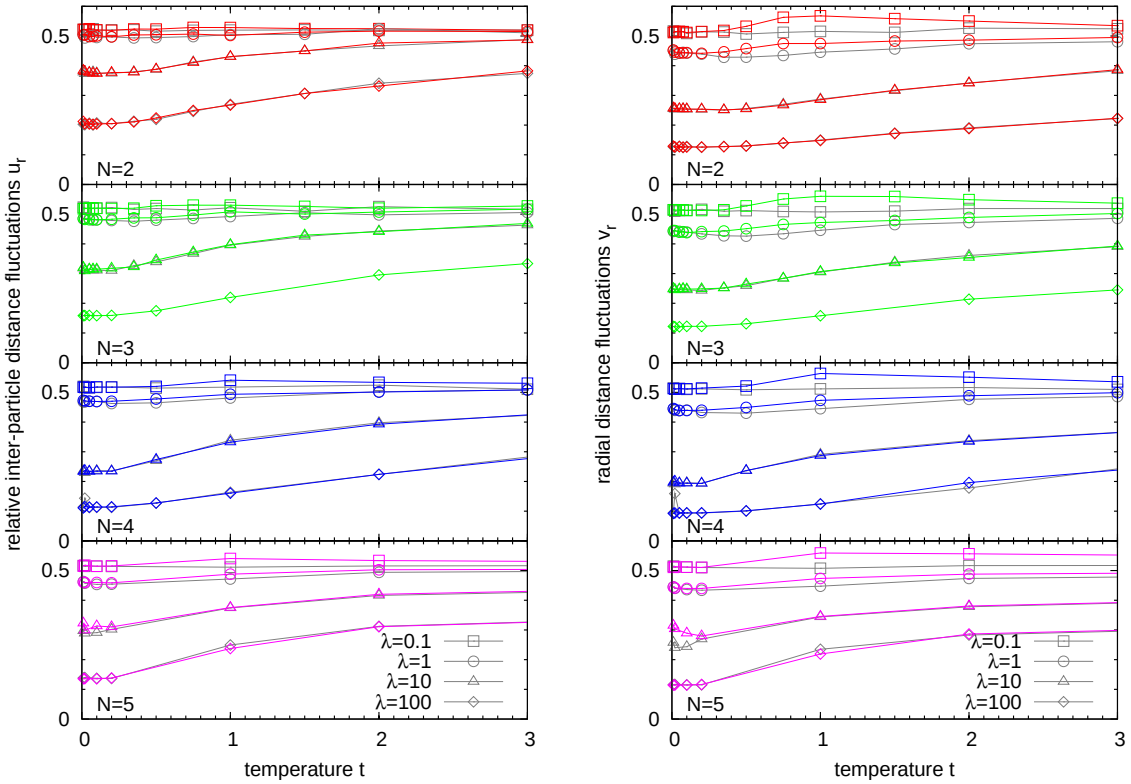

(a) Relative inter-particle distance fluctuations.

(b) Radial distance fluctuations.

Figure 6.17.: *Temperature dependence of relative inter-particle distance fluctuations u_r (left figure) and the radial distance fluctuations v_r (right figure). The colored lines and gray lines correspond the bosonic and boltzmannonic calculations, respectively. A drop of u_r indicates increasing particle localization. If u_r falls below a value of ~ 0.2, the system can be considered to crystallize.*

6.3.4. Relative distance fluctuation

Another property directly linked to the state of matter is the relative inter-particle distance fluctuation u_r, i.e.,

$$u_r = \frac{2}{N(N-1)} \sum_{i \leq j}^{N} \sqrt{\frac{\langle r_{ij}^2 \rangle}{\langle r_{ij} \rangle^2} - 1}, \tag{6.3}$$

where r_{ij} is the distance between the ith and jth particle. u_r measures the fluctuations of the inter-particle distance relative to its corresponding average. A similar quantity, the radial distance fluctuation, can be defined by choosing the trap center as reference point. The temperature dependence of both quantities is shown in figure 6.17 for different coupling parameters λ.

The degree of freedom for the movement of a particle is specific for the state of matter. A phase transition (like e.g., solid→fluid) can, thus, be made visible with a sudden jump in u_r. Such a jump is less sudden and more continuous in mesoscopic systems since a “hard” phase

transition does not exist here. However, one can issue a threshold value for the solid–fluid transition below which the system is assumed to be in a solid like state. Within harmonic lattice theory[58] the threshold can be determined to ~ 0.15 for classical systems and to ~ 0.249 for bosonic systems (see [59] and references therein). Strictly speaking, these values only apply to simulations for macroscopic systems with a specific lattice structure. A value of ~ 0.2 seems appropriate for the system in question considering the density distribution (fig. 6.14).

Ideal and nearly ideal systems do not show any sign of a phase transition, u_r remains essentially constant within the simulated temperature range. Its value of 0.5 characterizes the absence (resp. insignificance) of inter-particle interactions. Bosonic systems achieve even higher values for their v_r due to particle exchange on top of thermal fluctuations. The cause is an abrupt and effectively arbitrary change of the particle's radial distance when it is dislocated to the position of another particle. This effect vanishes at low temperatures since all particles then sit in the trap center on the average. Particle exchange alters the inter-particle distance only marginally, i.e., primarily to particles not participating in the permutation cycle, so u_r shows traces of the effect only for larger particle numbers. In short, an above boltzmannonic value for distance fluctuations can be achieved by a combination of thermal and exchange induced contributions, particularly, when measured to a fixed reference point.

Correlated systems obviously show lesser distance fluctuations due to particle localization. The degree of localization primarily depends on the strength of the particle repulsion, but also on the particle number, as already discussed in the previous section. For example only the 3-, 4-, and 5-particle system's relative distance fluctuations clearly drop below the threshold value of 0.2 in the $\lambda = 100$ case at low temperatures indicating a solid like state according to above point of reference. In all cases, however, u_r typically stays constant below $t \lesssim 0.2$ where changes in the energy are also no longer observable. Attached to this plateau regime is the ascent to the gaseous phase—with a steeper slope for larger particle numbers.

6.3.5. Superfluidity

Figures 6.19(a) and 6.19(b) show the dependence of γ_s on the temperature and relative interaction strength, respectively. Generally speaking, the annotations issued for the 2-particle case also apply for greater particle numbers. Differences largely result from the deviating system size and characteristic temperature.

As the 2-particle case demonstrated with its peculiar two-step behavior, two different contributions to γ_s can be distinguished and must be considered separately.

Thermal contribution $t > t_B$. The thermal contribution depends only on the extension of the particles in comparison to the whole area of the system. It can be observed for higher values of λ only where it is undisguised by the ground state contribution. In this regime the volume of the system increases with each particle added while the particles themselves become more localized. Visual judgment of the density distribution alone (last line of figure 6.14) already allows to estimate the value of γ_s to be larger in smaller systems, which is confirmed by figure 6.19(a).

Ground state contribution $t < t_B$. The ground state contribution always pushes γ_s to unity

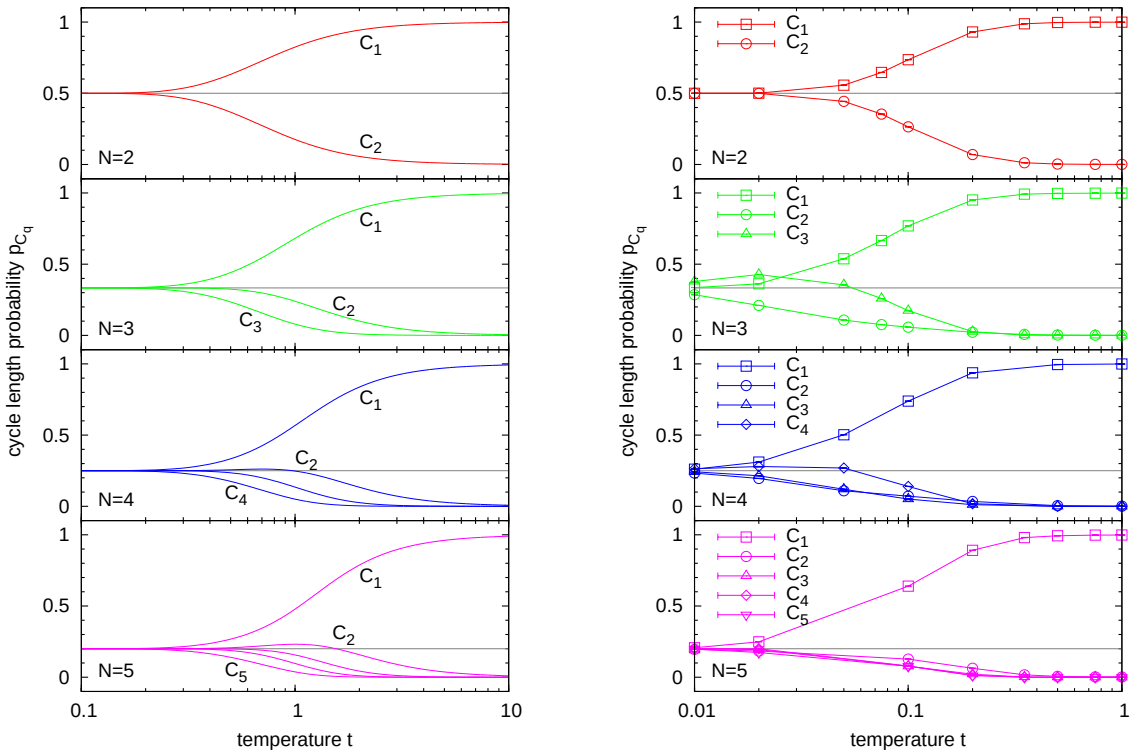

(a) Ideal case (Analytical results).

(b) $\lambda = 10$ (PIMC results).

Figure 6.18.: *Temperature dependence of the cycle length distribution. The left and right panel show the ideal case and the situation for $\lambda = 10$, respectively. Vertically stacked plots are sorted by particle number in ascending order ($N = 2 \ldots 5$). Note that the temperature scale of the right figure is decreased by the factor 10 compared to the left.*

at lower temperatures. The transition to this behavior occurs at the temperature t_B which is determined by the drop of the 1-cycle probability p_{C_1}. It shows that t_B is virtually identical for all particle numbers in the case of $\lambda = 10$ (fig 6.18(b)) and depends on the particle number otherwise. In the nearly ideal case it shifts to higher values with increasing particle number (fig 6.18(a)) and to lower temperatures otherwise. This reversal is reflected in graphs for γ_s—larger particle numbers result in higher values for γ_s in nearly ideal systems, in contrast to the systems with stronger interactions (fig. 6.19(a)). Due to the peculiar shape of the curves for γ_s, the exact value for λ_rev, where the reversal occurs, slightly varies with the temperature (see fig. 6.19(b)). It does not coincide with the energy reversal point.

Figure 6.19(a) ($\lambda = 100$) does not show a two-step behavior for particle numbers other than 2 anymore. The only contribution to γ_s seen for more than 2 particles results from the finite size of the system. However, one should expect to find a transition temperature t_B when making calculations for even lower temperature values than shown, but this regimes grows rapidly more difficult to access for PIMC simulations.

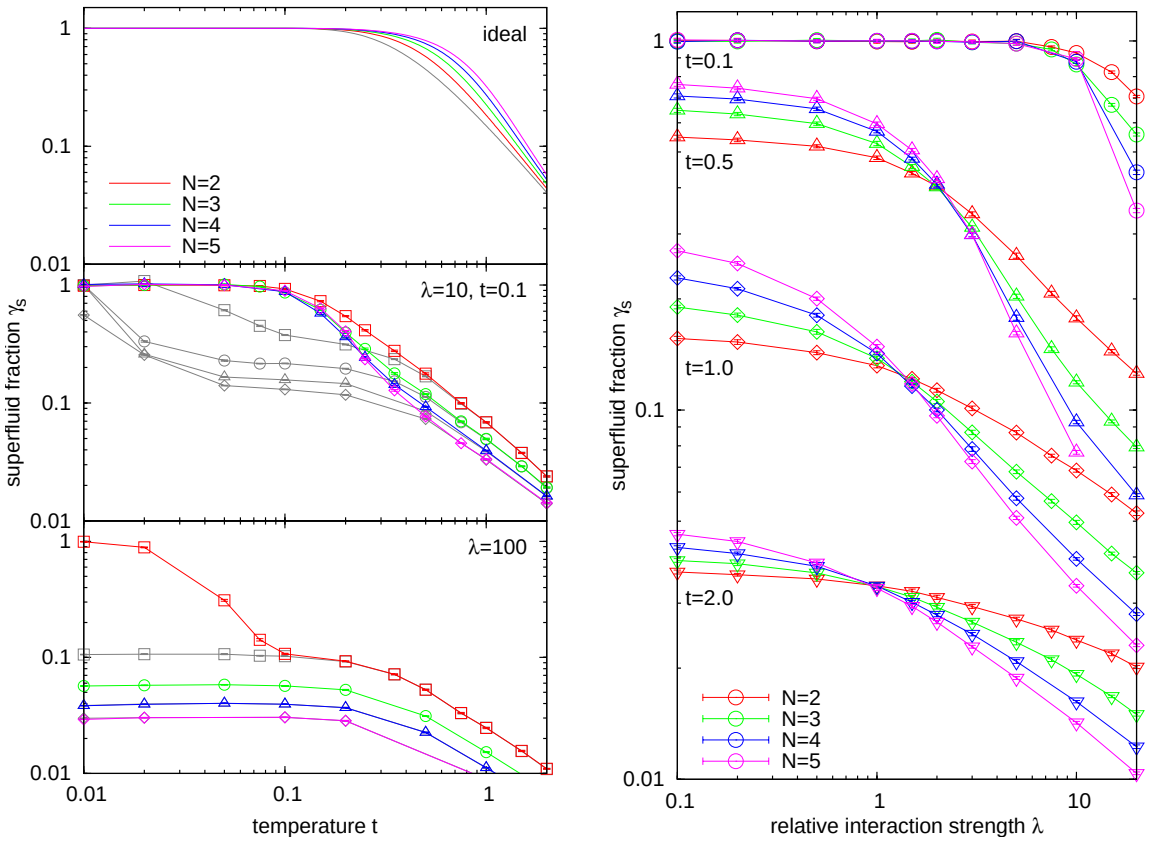

(a) General overview.

(b) Detailed view.

Figure 6.19.: *Superfluid fraction γ_s in 2D trapped system with $N = 2 \ldots 5$ particles. The dependence on the temperature is shown in the left-hand panel. Starting from top, the figures correspond to the ideal, $\lambda = 10$ and $\lambda = 100$ situations, respectively. The colored lines indicate values obtained from bosonic calculations. The corresponding boltzmannonic values are denoted by gray lines. In the ideal case the single gray line applies to an arbitrary number of Boltzmannons. The dependence of γ_s on the relative interaction strength λ is shown in the right-hand panel.*

6.3.6. Condensate Fraction

Last but not least, the results for the condensate fraction shall not remain unmentioned. However, the calculations presented in figure 6.20 for the 5-particle system relies on the estimation formula introduced in section 5.3 for ideal systems. As mentioned there, its validity is unconfirmed for interacting systems. Because of the restrictions to the accuracy of this method (the error of ± 1-particle translates to $\pm 1/N$ in the condensate fraction), the results need to be taken with a pinch of salt. Nevertheless, the general trend that the condensation is suppressed with increasing coupling parameter λ seems believable. A condensate depletion at absolute zero, like in the macroscopic system, is not observed.

Unfortunately, the 5-particle system is still too small to determine a good estimate for the transition temperature T_c. These limitations should be overcome in simulations for larger clusters.

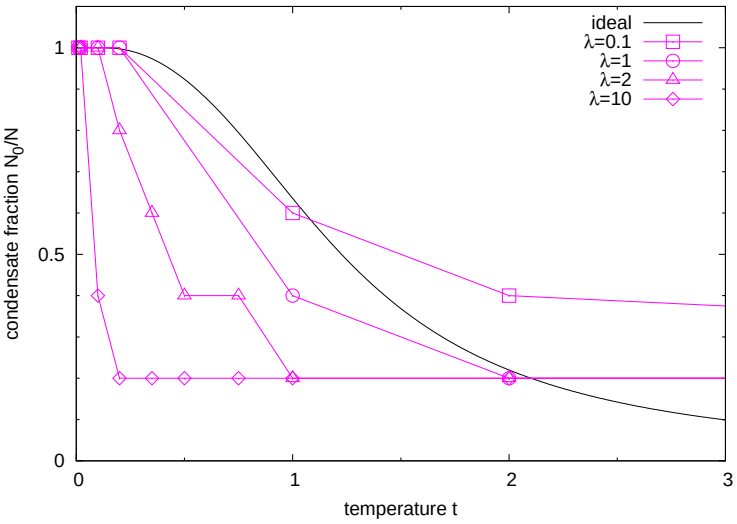

Figure 6.20: *Condensate fraction for 5 particles for varying values of λ. Symbols indicate the estimated values calculated from the cycle configuration with a threshold value of $x = 0.6$ (see sec. 5.3). The error bars of ± 0.2 for each value are not drawn for clarity's sake. Symbols which belong to the same λ are connected with lines in order to guide the eye. The exact values for the ideal system are indicated with the solid black line.*

6.4. Discussion

6.4.1. Superfluidity

Probably the most intruding conclusion drawn from the previous investigations is that the concept of what is known as "superfluidity" in macroscopic systems consists of various different contributions in finite systems. This section intends to summarize their causes and effects.

First of all, reflect the definition of superfluidity in confined mesoscopic systems. The whole investigation is based on the measurement of the deviation from the quantum mechanical moment of inertia from its classical expectation value. Strictly speaking, this quantity solely measures the NCRI whose connection to superfluidity in finite systems has yet to be proven. In macroscopic systems, phase coherence of the wave function over long distances (ODLRO, see above) is a necessary precondition to superfluidity. In particular, Shi recently showed that NCRI can be derived as a consequence of ODLRO in interacting Bose systems [28]. Naturally, the concept of ODLRO is not applicable in systems whose size is comparable with the inter-particle spacing. Thus, other causes for NCRI might exist in mesoscopic systems.

The investigation of γ_s in the preceding chapter allows to differentiate between two competing major contributions

Ground state contribution. Since the energy spectrum of a finite quantum system is discrete, i.e., the excitation of a condensed particle requires a finite energy in order to overcome the energy gap, the ground state always gives rise to NCRI. In particular, ideal systems and even boltzmannonic systems show NCRI.

Thermal contribution. According to the area formula, the NCRI relates to the ratio of the covered area of particle trajectories to the cross-section of the system. Quantum particles always have a finite extension, so this produces some kind of offset contribution with a λ depending maximum value at absolute zero. This contribution is not a ground state effect and shall be referred to as *thermal NCRI*.

A connection of the second contribution to superfluidity certainly is problematic at the least, since ODLRO cannot be assumed if particles are not condensed in the ground state at the same time. On the other hand, superfluidity in ideal systems or without bosonic particle exchange seems plausible as long as these effects remain a pathology of mesoscopic systems. In conclusion, only the first of the two listed effects should relate to superfluidity.

Thus, a method in order to distinguish between both contributions is needed when using NCRI as a measure for superfluidity. Bosonic particle exchange fortunately provides the necessary lever. As demonstrated, the plots for γ_s show a peculiar two-step behavior at certain coupling parameters λ. The step occurs at the λ depending temperature t_B, which marks the transition point to Bose statistics. The boost of γ_s below t_B relates to the predominant ground state occupation stimulated by particle exchange. Contributions to γ_s above t_B are solely a consequence of the thermal NCRI. However, this does not imply that contributions below t_B must be solely a ground state effect. But if not, one has to find a way in order to eliminate the interfering thermal part. A simple subtraction of its assumed value will not do, as this would effectively negate the likely possibility that the system is completely superfluid at low temperatures. So far, this remains an open question.

Viewed upside down, the cause for the peculiar NCRI in mesoscopic systems is obviously constituted by its finite size. The finiteness itself is twofold as it implies a finite volume and a finite particle number. One may associate the observed NCRI contributions to either of them.

Finite particle number. The always finite ground state occupation poses the most important effect of a finite particle number. As a consequence, any mesoscopic system reaches the point, where the ground state occupation is comparable to Bose-Einstein condensation—a state of matter which can only be achieved by some bosonic systems in the macroscopic limit. The result for the small clusters in question is the observed (ground state) NCRI in boltzmannonic systems. In this sense, the only difference between bosonic and boltzmannonic systems is that particle exchange allows for a condensation into the ground state at higher temperatures. The picture of permutation cycles as single particles at lowered temperatures serves as an illustration.

Finite volume. The thermal NCRI is a direct consequence of the finite volume (see above). Increasing the effective volume, e.g., by increasing λ or adding particles to the system, suppresses this contribution. Another consequence of the finite volume is the discrete energy spectrum, which supplies the basis for superfluidity in non-interacting systems.

In all cases, the thermodynamic limit leaves only the ground state contribution. However, only a macroscopically occupied ground state can give rise to superfluidity, so this effect is a characteristic of certain bosonic systems which show Bose-Einstein condensation.

6.4.2. Supersolidity

Supersolidity is a state of matter which is both macroscopically ordered (solid) and superfluid. The existence of such a phase in solid helium is a hotly discussed topic fueled by Kim and Chan's recent claim of experimental evidence. Section 2.2.4 gives an overview about the current status of research in this area.

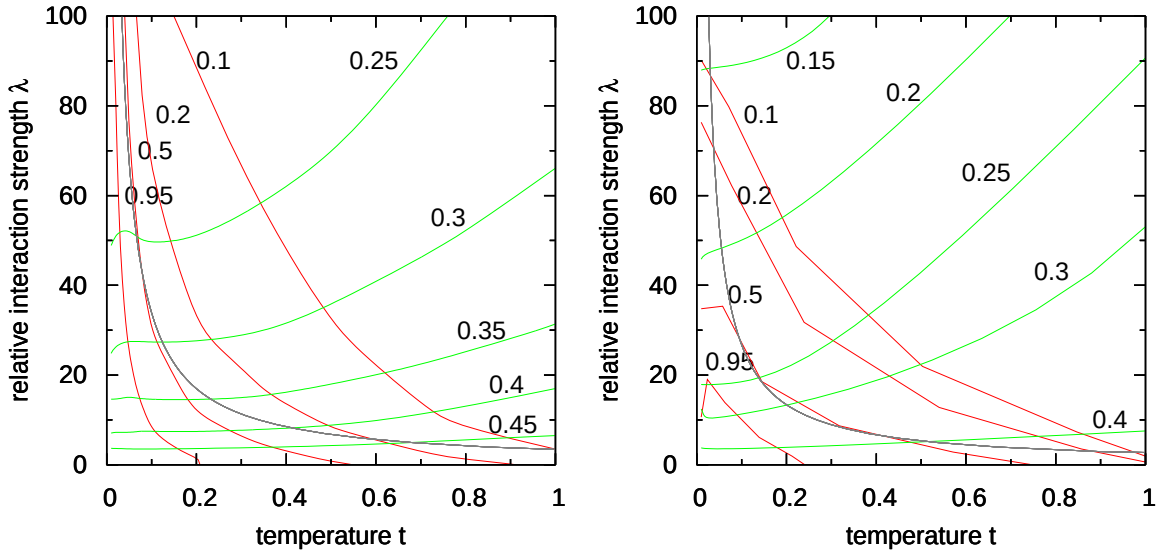

(a) $N = 2$. (b) $N = 5$.

Figure 6.21.: *Topological diagrams showing the correlation between superfluid fraction γ_s and relative inter-particle distance fluctuations u_r for 2 (left) and 5 (right) particles. Red lines indicate isolines of equal γ_s, the labels on the left-hand side denote the specific values. The isolines of equal u_r are shown in green, their corresponding values are denoted in the right-hand tags. The solid gray line separates the bosonic regime in the lower left from the boltzmannonic regime in the upper right. The values of γ_s in the latter result from the thermal NCRI (see text).*

The analogon to solids in the mesoscopic world of small clusters is the crystal like bound state found for large values of λ at low temperatures. A quantitative measure for the bounding strength is the relative inter-particle distance fluctuation as introduced in section 6.3.4. A simultaneous investigation of the superfluid response allows to identify possible parameter regimes in which supersolid behavior can be expected. Figure 6.21 presents the results obtained for the 2- and 5-particle system.

Superfluidity and localization show opposite trends with increasing coupling parameter λ. Superfluidity is at its strongest in nearly ideal systems where the particles do not crystallize. The situation is reversed in the strongly correlated regime. Contrastingly, both quantities change with temperature in a uniform manner—at least for not too small λs, superfluidity and localization both increase when the system is cooled. The existence of superfluid crystals can, thus, be expected.

However, the discussion so far implied the equality of NCRI and superfluidity. Taking the considerations from the previous section into account, one has to differentiate between both effects. The solid gray line in figure 6.21(b) indicates the λ dependence of the transition temperature t_B. The area to the left and below the line shows values for γ_s, which are influenced by bosonic particle exchange. Restriction of superfluidity to this region drastically decreases the possible parameter ranges for which superfluid crystals can be expected.

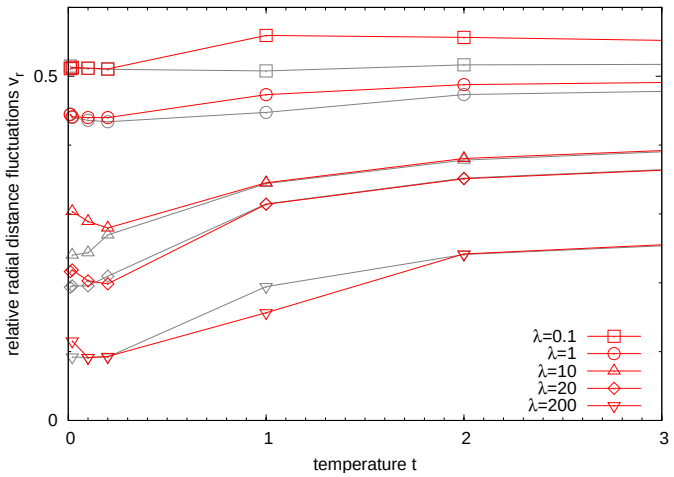

Figure 6.22: *Evidence for reentrant melting in bosonic systems. Shown is the radial distance fluctuations for 5 particles. Unlike the boltzmannonic calculations, the distance fluctuations for bosons show an increase at low temperatures. As a consequence, a bosonic system may first crystallize and then melt again when cooled down from high temperatures.*

6.4.3. Reentrant melting

The investigation of the relative distance fluctuations hint the possible existence of a completely new effect, which is shown in figure 6.22 in detail. As discussed in section 6.3, a system crystallizes at low temperatures if the coupling is strong enough. The distance fluctuation typically levels off at a constant value, which corresponds to the localization strength for the chosen coupling parameter. The simulations for boltzmannonic systems clearly show this behavior. However, simulations for bosonic systems indicate a peculiar increase towards lower temperatures which must be a result of particle exchange, of course. Asbeforementioned, particle exchange can only produce a difference if the radial distance is altered during an exchange. At low temperatures, however, one expects identical radial distances for every particle which would *not* lead to an increase by particle exchange itself. This is the reason why the deviation of bosonic and boltzmannonic calculations vanishes at low temperatures in the ideal case. Hence, the observed effect for correlated systems must correspond to larger particle fluctuations due to some additional effect of Bose statistics. Up to date, such exchange induced low-temperature melting has not been reported.

It should be noted that the simulations for these regions need yet to be carefully checked. The observed effect might be a statistical artifact since exchange effects at very low temperatures become very rare, particularly in combination with the large number of time slices needed.

7. Conclusion

7.1. Summary

Superfluidity is defined as the suppression of friction in spatially homogeneous systems for a linear motion slower than the velocity of sound. The phenomenon is constrained to a fraction of the fluid only, the *superfluid fraction*. Within the two-fluid model of superfluidity, the remaining normalfluid component is considered to be composed of collective excitations from the ground state of the system, namely quasiparticles, with a linear dispersion relation. Superfluidity is, thus, inseparably connected to inter-particle interactions and to the presence of a Bose-Einstein condensate (sec. 2.2.1).

However, this conclusion is only valid for systems without an energy gap between the ground state and the first excited state. In this case, a finite energy is needed which surpasses the energy gap in order to excite a particle from the ground state. Otherwise, the excitation is impossible which leads to suppression of friction for sufficiently slow motions. If a condensate is present, such a system shows a superfluid response without the need of inter-particle interactions[1].

Particularly, finiteness enables non-interacting trapped systems to show a superfluidity since the single-particle energy levels are quantized. Such systems are both 100 % condensed and 100 % superfluid at absolute zero (sec. 5.3)—a peculiarity unseen in macroscopic systems, as inter-particle interaction results in a depletion of the condensate (sec. 2.2.3). Superfluidity vanishes according to the correspondence principle, since the energy gaps are required to close in the thermodynamic limit.

A quantitative measure for the superfluid fraction is provided by the *Hess-Fairbank* effect, also referred to as *non classical rotational inertia (NCRI)*: The superfluid fraction completely ignores a slow rotation of the confining potential, which leads to a deviation of the moment of inertia I_{qm} from its classical expectation value I_{class}. For the discrete time path integral representation of quantum systems, the NCRI can be computed with the so-called *area-formula* (sec. 3.3.2). This formula relates NCRI to the ratio of the projected area enclosed by particle trajectories to the cross-section of the whole system, both taken perpendicular to the rotational axis.

Although strictly valid in the macroscopic limit, the equality of NCRI and superfluidity in mesoscopic systems is not yet proven. Obviously, superfluidity in such systems still leads to NCRI, but one cannot exclude other origins. The area-formula illustrates this in a straightforward manner: The (effective) area of the whole system is obviously finite as well as the spatial extension of quantum particles. This gives a non-zero value for the NCRI regardless whether the system is in its ground state or not. Thermal and ground state contributions result in a peculiar two-step behavior of the NCRI observed in interacting systems (sec. 6.2).

[1] The energy gap itself may be a consequence of inter-particle interaction as, e.g., in superconductors. However, this does not negate the existence of other origins.

The effects of temperature, interaction strength, particle number, and bosonic exchange should be considered separately for both contributions

Ground state contribution. If all particles are condensed, the contribution to the NCRI reaches unity. The value obviously decays with rising temperature due to thermal excitations. The temperature t_0 below which significant values are obtained is affected by other parameters.

- A stronger coupling parameter shifts t_0 to lower values.
- Inclusion of Bose statistics shifts t_0 to higher values in comparison to the boltzmannonic case[2].
- The direction of the shift due to a change of the particle number depends on the coupling parameter. In (nearly) ideal systems the shift is positive, whereas it is negative for strongly correlated systems.

Thermal contribution. Due to its relation to the area ratio, this contribution is affected by a change of the effective system size and the extension of the particles, respectively. Larger systems or smaller particle extensions result in a lesser contribution. In any case, their ratio yields a finite value smaller than 1 at absolute zero.

- The extension of quantum particles decreases with increasing temperature.
- A stronger interaction strength increases the size of the system.
- The effect of the particle number depends on the interaction strength. In the (nearly) ideal case the size of the system decreases with increasing particle number, and for strongly interacting systems vice versa.

Bosonic particle exchange is linked to the condensation of particles and, therefore, gives rise to a ground state contribution only. The temperature t_B below which bosonic particle exchange becomes important coincides with the temperature t_0 indicating the transition from thermal to predominant ground state contributions (sec. 6.2.4 and 6.3.5). However, since exchange is not essentially needed in finite systems for particles to collect the ground state, also boltzmannonic calculations show a two-step behavior.

Even in strongly interacting systems, the values obtained from the NCRI for the superfluid fraction are not negligibly small. The particles form a crystal like structure in this regime, which constitutes the analogon to the "supersolid" in the macroscopic world. However, considering only the ground state contribution of the NCRI as superfluidity the possible parameter regime where such a superfluid crystal is found shrinks drastically (sec. 6.4.2).

For the sake of completeness, here is a short remark about other quantities than the superfluid fraction: As these quantities are not directly sensible to particle exchange, they are affected by Bose statistics in nearly ideal systems only. This is due to the negligibly small (negative) exchange energy compared to the (positive) Coulomb energy in strongly

[2] It does not matter *how* the ground state is reached. In particular, also boltzmannons (distinguishable quantum particles obeying Boltzmann statistics) give rise to the NCRI, since they may occupy identical single-particle states. The inclusion of Bose statistics encourages condensation into the ground state, so the temperature below which significant contributions to the NCRI are obtained is shifted to higher values.

correlated systems. Since both energies have opposite signs, addition of particles into the system has an opposing effect on a quantity in nearly ideal and strongly correlated systems.

7.2. Central results

- Superfluidity traces back to the impossibility of excitations from the ground state. Either a linear dispersion relation or an energy gap between single-particle ground state and first excited state provide a mechanism for this.
- A mesoscopic ideal Bose gas in a harmonic trap shows superfluidity.
- Bose statistics promote superfluidity in mesoscopic systems, but are not its cause.
- The NCRI has a thermal and a ground state contribution in mesoscopic systems which leads to a two-step behavior in its temperature dependence.
- Superfluidity is possible in a crystal like state.

7.3. Outlook

As a closing note, some shortcomings and possible extensions of this work are presented.

- The most intruding question left unanswered by this work is the influence of shell formation, which occurs in correlated systems with more than 5 particles. In particular, one can speculate on a boost of the superfluid fraction for clusters without perfect symmetry. In the macroscopic limit, such systems correspond to incommensurate solids, meaning it is to have zero-point vacancies, or interstitial atoms, or both as an integral part of the ground state. In general opinion, this is a necessary condition for "supersolids" [27, 28].
- The results for the NCRI must be investigated more closely. In particular, an alternative estimator for the superfluid fraction in mesoscopic systems is needed. A possible approach could use the momentum distribution, but the calculation is more complex as it depends on off-diagonal elements of the density matrix. Additionally, one might try to reproduce the results for the NCRI using different confinements and interaction potentials, respectively.
- A central numerical issue of PIMC simulations is the low acceptance probability for permutation changes of strongly correlated systems at low temperatures. A possible solution is the *worm algorithm* extension proposed by Boninsegni *et al.* [36], which introduces a set of new moves providing a mechanism in order to handle open trajectories, called *worms*. Boninsegni *et al.* claim vastly improved acceptance ratios for particle exchanges.

A. Derivation of the effective Bogoliubov Hamiltonian

The Hamiltonian of a free interacting system in second quantization reads

$$\hat{H} = \sum_{\mathbf{k}} \frac{\hbar^2 k^2}{2m} \hat{a}^\dagger_{\mathbf{k}} \hat{a}_{\mathbf{k}} + \frac{1}{2V} \sum_{\mathbf{k},\mathbf{p},\mathbf{q}} W_{\mathbf{q}} \hat{a}^\dagger_{\mathbf{p}+\mathbf{q}} \hat{a}^\dagger_{\mathbf{k}-\mathbf{q}} \hat{a}_{\mathbf{p}} \hat{a}_{\mathbf{k}}, \tag{A.1}$$

where

$$W_{\mathbf{q}} = \int \mathrm{d}^3\mathbf{r}\, e^{-i\mathbf{q}\cdot r} W(\mathbf{r}) \tag{A.2}$$

denotes the Fourier transformed pair potential $W(\mathbf{r}) = W(\mathbf{r}_2 - \mathbf{r}_1)$.

Consider the following assumptions

1. the system has a Bose-Einstein condensated phase and
2. the gas is dilute and only weakly interacting.

Then, two major approximations can be placed upon the Hamiltonian:

1. The dominant contribution to the pair potential results from interactions with at least one condensated particle. Particularly, one can expand the 2-particle interaction in a series with respect to the number of participating condensate particles, i.e.,

$$\begin{aligned} \hat{W} = &\text{ terms with zero } \hat{a}_{\mathbf{k}} \text{ (one possibility)} \\ &+ \text{ terms with one } \hat{a}_{\mathbf{k}} \text{ (not possible)} \\ &+ \text{ terms with two } \hat{a}_{\mathbf{k}} \text{ (6 possibilities)} \\ &+ \mathcal{O}(\hat{a}^3_{\mathbf{k}}). \end{aligned} \tag{A.3}$$

   Here, $\hat{a}_{\mathbf{k}}$ denotes an annihilation (or creation) operator for a non-condensate particle with $k \neq 0$.

2. Addition or subtraction of a single particle to the condensate does not change the physics of the system. This implies that the effect of the condensate annihilation and creation operators $\hat{a}_0, \hat{a}^\dagger_0$ corresponds to a simple multiplication of $\sqrt{N_0}$ without changing the state, i.e.,

$$\hat{a}_0 |\ldots, N_0, \ldots\rangle = \sqrt{N_0} |\ldots, N_0 - 1, \ldots\rangle \approx \sqrt{N_0} |\ldots, N_0, \ldots\rangle, \tag{A.4}$$

$$\hat{a}^\dagger_0 |\ldots, N_0, \ldots\rangle = \sqrt{N_0 + 1} |\ldots, N_0 + 1, \ldots\rangle \approx \sqrt{N_0} |\ldots, N_0, \ldots\rangle. \tag{A.5}$$

The first approximation simplifies $\hat{W}$ to

$$\hat{W} = \frac{1}{2V} W_0 \hat{a}_0^\dagger \hat{a}_0^\dagger \hat{a}_0 \hat{a}_0 + \frac{1}{V} {\sum_\kappa}' \left(W_0 + W_\kappa\right) \hat{a}_0^\dagger \hat{a}_0 \hat{a}_\kappa^\dagger \hat{a}_\kappa + \frac{1}{2V} {\sum_\kappa}' W_\kappa \left(\hat{a}_0^\dagger \hat{a}_0^\dagger \hat{a}_\kappa \hat{a}_{-\kappa} + \hat{a}_\kappa^\dagger \hat{a}_{-\kappa}^\dagger \hat{a}_0 \hat{a}_0 \right) \quad \text{(A.6)}$$

and the second further reduces it to

$$\hat{W} = \frac{N_0^2}{2V} W_0 + \frac{N_0}{V} {\sum_{\mathbf{k}}}' \left(W_0 + W_{\mathbf{k}}\right) \hat{a}_{\mathbf{k}}^\dagger \hat{a}_{\mathbf{k}} + \frac{N_0}{2V} {\sum_{\mathbf{k}}}' W_{\mathbf{k}} \left(\hat{a}_{\mathbf{k}}^\dagger \hat{a}_{-\mathbf{k}}^\dagger + \hat{a}_{\mathbf{k}} \hat{a}_{-\mathbf{k}} \right). \quad \text{(A.7)}$$

Since the occupation of the condensate is still unknown, one can replace N_0 with

$$N_0 = N - N' = N - {\sum_{\mathbf{k}}}' \hat{a}_{\mathbf{k}}^\dagger \hat{a}_{\mathbf{k}}. \quad \text{(A.8)}$$

Insertion of this expression again yields contributions of the order $\mathcal{O}\,\hat{a}_{\mathbf{k}}^4$, which can be neglected. The final result for the approximated Hamiltonian reads

$$\hat{H} = {\sum_{\mathbf{k}}}' \frac{\hbar^2 k^2}{2m} \hat{a}_{\mathbf{k}}^\dagger \hat{a}_{\mathbf{k}} + \frac{N^2}{2V} W_0 + \frac{N}{V} {\sum_{\mathbf{k}}}' W_{\mathbf{k}} \hat{a}_{\mathbf{k}}^\dagger \hat{a}_{\mathbf{k}} + \frac{N}{2V} {\sum_{\mathbf{k}}}' W_{\mathbf{k}} \left(\hat{a}_{\mathbf{k}}^\dagger \hat{a}_{-\mathbf{k}}^\dagger + \hat{a}_{\mathbf{k}} \hat{a}_{-\mathbf{k}} \right). \quad \text{(A.9)}$$

This Hamiltonian can be diagonalized using the Bogoliubov transformation.

B. Density matrix for a single particle in the 1D harmonic trap

As Feynman[37] shows, the density operator obeys the differential equation (see also eq. (3.1))

$$-\frac{\partial\hat{\rho}}{\partial\beta}=\hat{H}\hat{\rho}, \tag{B.1}$$

with the initial condition $\rho(0)=1$ or $\rho(\mathbf{r},\mathbf{r}';0)=\delta(\mathbf{r}-\mathbf{r}')$ in position representation, respectively. Application to the Hamiltonian of a single 1D-particle in a harmonic trap (using the reduced form, see eq. (4.7)) yields

$$-\frac{\partial\rho}{\partial f}=-\frac{\partial^2\rho}{\partial x^2}+x^2\rho, \tag{B.2}$$

where $f=1/t$ is the inverse reduced temperature (eq. (4.5)) and x the reduced length (eq. (4.3)). The initial condition in reduced units reads $\rho(\mathbf{x},\mathbf{x}';0)=\delta(x-x')/l_0$.

The equation can be solved with the ansatz

$$\rho=e^{-[a(f)x^2+b(f)x+c(f)]}, \tag{B.3}$$

leading to the following conditional equations for the coefficients

$$a'=1-4a^2,\qquad b'=-4ab,\qquad c'=2a-b^2. \tag{B.4}$$

The equations are integrated to give

$$a=\frac{1}{2}\coth f,\qquad b=\frac{A}{\sinh f},\qquad c=\frac{1}{2}\ln(\sinh f)+\frac{A^2}{2}\coth f-\ln B, \tag{B.5}$$

where A and B are constants. Insertion into eq. (B.3) yields

$$\rho(x,x';f)=\frac{B}{\sqrt{\sinh f}}\exp\left\{-\left(\frac{x^2}{2}\coth f+\frac{Ax}{\sinh f}+\frac{A^2}{2}\coth f\right)\right\}. \tag{B.6}$$

In the high temperature limit $f\to 0$, the particle should act like a free particle, as its probable kinetic energy is so high. The density matrix will then be given by eq. (3.15), i.e.,

$$\rho\to\frac{B}{\sqrt{f}}\exp\left\{-\frac{x^2+2Ax+A^2}{2f}\right\}\approx\frac{1}{l_0\sqrt{2\pi f}}\exp\left\{-\frac{1}{2f}(x-x')^2\right\}, \tag{B.7}$$

which determines the constants to $A=-x'$ and $B=1/l_0\sqrt{2\pi}$. The final expression for the density matrix of a particle in a harmonic trap reads

$$\rho(x,x';f)=\frac{1}{l_0\sqrt{2\pi\sinh f}}\exp\left\{-\frac{1}{2\sinh f}\left[(x-x')^2\cosh f-2xx'\right]\right\}. \tag{B.8}$$

Generalization to the d-dimensional case is simply achieved as each dimension contributes the same factor, i.e.,

$$\rho(\mathbf{x},\mathbf{x}';f) = \left(2\pi l_0^2 \sinh f\right)^{-\frac{d}{2}} \exp\left\{-\frac{1}{2\sinh f}\left[(\mathbf{x}-\mathbf{x}')^2\cosh f - 2\mathbf{x}\cdot\mathbf{x}'\right]\right\}. \tag{B.9}$$

If the harmonic potential is asymmetric, appropriate geometric means for l_0, $\sinh f$ and $\coth f$ must be inserted.

Integration over the diagonal elements of the density matrix, i.e.,

$$\rho(\mathbf{x},\mathbf{x};f) = \left(2\pi l_0^2 \sinh f\right)^{-\frac{d}{2}} \exp\left\{-\mathbf{x}^2 \tanh f\right\}, \tag{B.10}$$

results in the partition function

$$Z_1(\beta) = \left(2\sinh(\hbar\omega\beta/2)\right)^{-d}. \tag{B.11}$$

C. Transition temperature t_B to Bose statistics

The temperature t_B shall be defined as the temperature below which bosonic and boltzmannonic calculations start to differ. Since the transition does not occur abruptly, one has to use some estimation for its value. A good indicator is the probability for the identity permutation p_{C_1}, as its value deviates from unity if bosonic particle exchange becomes important. The straightforward method is to issue a threshold value p_crit and define

$$p_{C_1}(t_\mathrm{B}) = p_\mathrm{crit}. \tag{C.1}$$

A value of $p_\mathrm{crit} = 0.95 \ldots 0.99$ seems appropriate by trial and error.

The exact functional dependence for p_{C_1} is only known for ideal systems (eq. (5.10)). However, the plots of p_{C_1} for various coupling parameters λ suggest (fig. C.1(a)) that there exists a shift parameter $a(\lambda)$ with

$$p_{C_1}^{\lambda}(t) = p_{C_1}^{\mathrm{ideal}}(t/a(\lambda)). \tag{C.2}$$

Interestingly, the shift parameter $a(\lambda)$ seemingly shows a linear dependence on λ (see fig. C.1(b)). This can be used to estimate t_B for large interaction strengths, where PIMC simulations do not yield reliable results for particle exchange anymore.

Using the shift parameter, one needs to determine t_B only once, which is done preferably for the ideal case. Since $a(\lambda)$ is independent from p_crit, adjustments to p_crit can be investigated more easily.

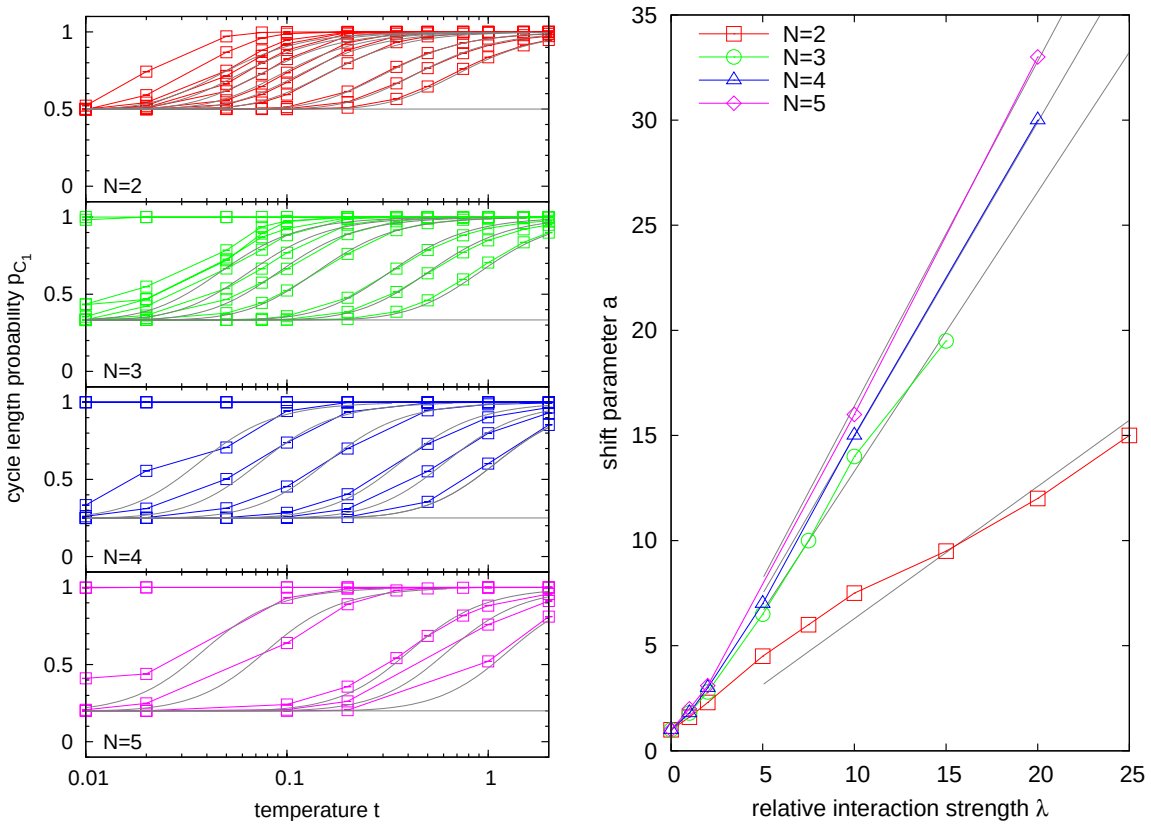

(a) temperature shift of the identity permutation

(b) shift parameter

Figure C.1.: *The left-hand panel shows the functional dependence of p_{C_1} for various coupling parameters λ. The particle number increases from 2 in the top to 5 in the bottom figure. In each case, the coupling increases with each graph from right to left. A single graph can be fitted in good approximation by a shifted ideal function $p_{C_1}^{\mathrm{ideal}}(t/a(\lambda))$, where $a(\lambda)$ is the fitting parameter. Solid gray lines indicate the fits. The right-hand panel displays the dependence of the obtained values for $a(\lambda)$ on the coupling parameter λ. It is $a = 1$ for the ideal case and $a \propto \lambda$ for large λs.*

D. Visualization of densities

Two methods are commonly used in order to visualize path configurations from PIMC simulation.

Snapshot Shows the path configuration by connecting particle positions on consecutive time slices in a x-y plot. Different colors may help to distinguish between separate particles. If the snapshot shows a configuration with permuted end points, the corresponding particle trajectories mend into single longer paths.

World-line view Unravels the snapshot view by showing the position of a specific coordinate (e.g., x or y) separately for each time slice.

Such visualizations can be used to give the reader a general idea over the typical particle configuration obtained with a PIMC simulation for the specifically chosen parameter set. However, both methods cannot claim to have any statistical relevance since they present only a snapshot from a single configuration. In particular, contributions to the density distribution due to thermal fluctuations are obviously excluded. This drawback can be remedied by simultaneously plotting multiple path configurations on top of each other. The rotational symmetry of the system in question unfortunately blurs the density into annular shapes even if the particles actually form strongly correlated crystal like structures.

A method which aims to provide a statistically reliable density distribution in order to gain information about the state of matter needs to exclude the arbitrary rotations. This can be done by choosing a body-fixed frame as reference frame. This means that each snapshot has to be rotated by some angle before joining them to a single plot. Thereby, it is assumed that the particles form a molecule like body with known equilibrium positions for each particle. The center-of-masses from every path are each associated with a specific position in the molecule. The average from their angular difference gives the transformation angle of the whole snapshot. As an illustration, the 2-particle snapshot is rotated in such a way that the connecting line between the particles lies parallel to the x-axis of the plot.

This procedure corresponds to the so-called *Eckart frame transformation*[60] primarily used in molecular chemistry, which finds the greatest possible separation of rotational and vibrational modes (a complete separation is impossible) [56]. In this analogy, the here applied transformation singles the rotational motion out, leaving only density fluctuations corresponding to vibrational motion.

The method works well as long as the system maintains the molecule like state which is the case if the temperature is not too high and the system is far from ideal. In principle, ideal cases are also unproblematic if the system is in its ground state, where the particles sit in the trap center and the wave function is invariant under rotations. Thermal excitations, however, lead to particle displacements out of the trap center. On average, the particles are then distanced to each other which is misinterpreted as a molecule formation and results in

a "kink" in the density plots as it can be seen, e.g., in the upper right plots of figure 6.1. Furthermore, due to the specific nature of the transformation, thermal (vibrational) fluctuations and quantum mechanical broadening of the density cannot be distinguished. Fortunately, the first occurs at high and the latter at low temperatures and a more or less stable molecule like phase is typically situated in between. In short, the density plots do not yield any sound quantitative results but can help to identify different phases qualitatively.

Bibliography

[1] S. N. Bose. *Z. Phys.*, 26:178, 1924.

[2] A. Einstein. Quantentheorie des Einatomigen Idealen Gases. *Sitzber. Kgl. Preuss. Akad. Wiss.*, page 261, 1924.

[3] A. Einstein. Quantentheorie des Einatomigen Idealen Gases. Zweite Abhandlung. *Sitzber. Kgl. Preuss. Akad. Wiss.*, pages 3–14, 1925.

[4] Torsten Fließbach. *Statistische Physik*, volume IV of *Lehrbuch zur Theoretischen Physik*. Spektrum Akademischer Verlag, third edition, 1999.

[5] Franco Dalfovo, Stefano Giorgini, Lev P. Pitaevskii, and Sandro Stringari. Theory of Bose-Einstein condensation in trapped gases. *Rev. Mod. Phys.*, 71(3):463–512, 1999.

[6] A. Filinov, M. Bonitz, P. Ludwig, and Yu.E. Lozovik. Path integral Monte Carlo results for Bose condensation of mesoscopic indirect excitons. *phys. stat. sol. (c)*, 3(7):2457–2460, 2006.

[7] David Snoke. Spontaneous Bose coherence of excitons and polaritons. *Science*, 298(5597):1368–1372, 2002.

[8] L. V. Butov. Condensation and pattern formation in cold exciton gases in coupled quantum wells. *J. Phys.: Cond. Mat.*, 16(50):R1577–R1613, 2004.

[9] Anthony J. Leggett. Superfluidity. *Rev. Mod. Phys.*, 71(2):S318–S323, 1999.

[10] C. N. Yang. *Rev. Mod. Phys.*, 34:694, 1962.

[11] Anthony J. Leggett. Bose-Einstein condensation in the alkali gases: Some fundamental concepts. *Rev. Mod. Phys.*, 73(2):307–356, Apr 2001.

[12] Jens O. Andersen. Theory of the weakly interacting Bose gas. *Rev. Mod. Phys.*, 76(2):599–639, 2004.

[13] N. N. Bogoliubov. Theory of superfluidity. *J. Phys. (Moscow)*, 11:23–32, 1947.

[14] T. Holstein and H. Primakoff. Field dependence of the intrinsic domain magnetization of a ferromagnet. *Phys. Rev.*, 58(12):1098–1113, 1940.

[15] Franz Schwabl. *Quantenmechanik für Fortgeschrittene (QM II)*. Springer, Berlin, third edition, 2004.

[16] E. M. Lifschitz and L. P. Pitajewski. *Statistische Physik. Teil 2: Theorie des kondensierten Zustands*, volume IX of *(L. D. Landau, E. M. Lifschitz) Lehrbuch der Theoretischen Physik*. Akademie Verlag, forth edition, 1992.

[17] L. P. Pitaevski. *Zh. Eksperim. i Teor. Fiz.*, 40:646, 1961.

[18] Eugene P. Gross. Hydrodynamics of a superfluid condensate. *J. Math. Phys.*, 4(2):195–207, 1963.

[19] Anthony J. Leggett. Can a solid be "superfluid"? *Phys. Rev. Lett.*, 25(22):1543–1546, 1970.

[20] G. V. Chester. Speculations on Bose-Einstein condensation and quantum crystals. *Phys. Rev. A*, 2(1):256–258, 1970.

[21] A. F. Andreev and I. M. Lifshits. Quantum theory of defects in crystals. *Zh. Eksp. Teor. Fiz.*, 56(6):2057–2068, 1969.

[22] E. Kim and M. H. W. Chan. Probable observation of a supersolid helium phase. *Nature*, 427:225–227, 2004.

[23] E. Kim and M. H. W. Chan. Observation of non-classical rotational inertia in solid ^{4}He confined in porous gold. 138(3-4):859–864, 2005.

[24] E. Kim and M. H. W. Chan. Observation of superflow in solid helium. *Science*, 305(5692):1941–1944, 2004.

[25] J. G. Dash and J. S. Wettlaufer. Classical rotational inertia of solid ^{4}He. *Phys. Rev. Lett.*, 94(23):235301, 2005.

[26] S. A. Khairallah and D. M. Ceperley. Superfluidity of dense ^{4}He in Vycor. *Phys. Rev. Lett.*, 95(18):185301, 2005.

[27] Nikolay Prokof'ev and Boris Svistunov. Supersolid state of matter. *Phys. Rev. Lett.*, 94(15):155302, 2005.

[28] Yu Shi. Superfluidity or supersolidity as a consequence of off-diagonal long-range order. *Phys. Rev. E*, 72(1):014533, 2005.

[29] Mark W. Meisel. Supersolid ^{4}He: an overview of past searches and future possibilities. *Physica B: Condensed Matter*, 178:121–128, 1992.

[30] Stefan Wessel and Matthias Troyer. Supersolid hard-core bosons on the triangular lattice. *Phys. Rev. Lett.*, 95(12):127205, 2005.

[31] Dariush Heidarian and Kedar Damle. Persistent supersolid phase of hard-core bosons on the triangular lattice. *Phys. Rev. Lett.*, 95(12):127206, 2005.

[32] R. G. Melko, A. Paramekanti, A. A. Burkov, A. Vishwanath, D. N. Sheng, and L. Balents. Supersolid order from disorder: Hard-core bosons on the triangular lattice. *Phys. Rev. Lett.*, 95(12):127207, 2005.

[33] Massimo Boninsegni and Nikolay Prokof'ev. Supersolid phase of hard-core bosons on a triangular lattice. *Phys. Rev. Lett.*, 95(23):237204, 2005.

[34] Evgeni Burovski, Evgeni Kozik, Anatoly Kuklov, Nikolay Prokof'ev, and Boris Svistunov. Superfluid interfaces in quantum solids. *Phys. Rev. Lett.*, 94(16):165301, 2005.

[35] Massimo Boninsegni, Nikolay Prokof'ev, and Boris Svistunov. Superglass phase of ^{4}He. *Phys. Rev. Lett.*, 96(10):105301, 2006.

[36] Massimo Boninsegni, Nikolay Prokof'ev, and Boris Svistunov. Worm algorithm for continuous-space path integral Monte Carlo simulations. *Phys. Rev. Lett.*, 96(7):070601, 2006.

[37] Richard P. Feynman. *Statistical Mechanics – A Set of Lectures.* Frontiers in Physics. Perseus Books, 1972.

[38] D. M. Ceperley. Path integrals in the theory of condensed helium. *Rev. Mod. Phys.*, 67(2):279–355, 1995.

[39] H. F. Trotter. On the product of semi-groups of operators. *Proc. Am. Math. Soc.*, 10(4):545–551, 1959.

[40] Barry Simon. *Functional Integration and Quantum Physics.* AMS Chelsea Publishing, second edition, 2005.

[41] Alexei Filinov and Michael Bonitz. *Introduction to Computational Methods in Many Body Physics*, chapter Classical and Quantum Monte Carlo, pages 235–350. Rinton Press Inc, 2006.

[42] Nicholas Metropolis, Arianna W. Rosenbluth, Marshall N. Rosenbluth, Augusta H. Teller, and Edward Teller. Equation of state calculations by fast computing machines. *J. Chem. Phys.*, 21(6):1087–1092, 1953.

[43] M. P. Allen and D. J. Tildesley. *Computer Simulation of Liquids.* Oxford University Press, USA, 1988.

[44] Michael Bonitz and Dirk Semkat, editors. *Introduction to Computational Methods in Many Body Physics.* Rinton Press Inc, 2006.

[45] M. F. Herman, E. J. Bruskin, and B. J. Berne. On path integral Monte Carlo simulations. *J. Chem. Phys.*, 76(10):5150–5155, 1982.

[46] C. Weiss and M. Wilkens. Particle number counting statistics in ideal Bose gases. *Opt. Expr.*, 1(10):272–283, 1997.

[47] A. Filinov, J. Böning, and M. Bonitz. Path integral Monte Carlo simulations of charged particles in traps. *ArXiv: cond-mat/0611558*, 2007.

[48] Hagen Kleinert. *Path Integrals in Quantum Mechanics, Statistics, Polymer Physics, and Financial Markets.* World Scientific Publishing Company, 3rd edition, 2004.

[49] A. V. Filinov, M. Bonitz, and Yu. E. Lozovik. Wigner crystallization in mesoscopic 2D electron systems. *Phys. Rev. Lett.*, 86(17):3851–3854, 2001.

[50] A. Filinov, M. Bonitz, and Yu.E. Lozovik. Excitonic clusters in coupled quantum dots. *J. Phys. A: Math. Gen.*, 36:5899–5904, 2003.

[51] M. Bonitz, V. S. Filinov, V. E. Fortov, P. R. Levashov, and H. Fehske. Crystallization in two-component Coulomb systems. *Phys. Rev. Lett.*, 95(23):235006, 2005.

[52] M. Bonitz, V. S. Filinov, V. E. Fortov, P. R. Levashov, and H. Fehske. Crystallization of holes in semiconductors. *J. Phys. A: Math. Gen.*, 39:4717, 2006.

[53] P. Ludwig, A. Filinov, M. Bonitz, and H. Stolz. Quantum Stark confined stongly correlated indirect excitons in quantum wells. *phys. stat. sol. (b)*, 243(10):2363–2366, 2006.

[54] K. Balzer, C. Nölle, M. Bonitz, and A. Filinov. Energy spectrum of strongly correlated particles in quantum dots. *J. Phys: Conf. Series*, 35:209, 2006.

[55] K. Balzer, C. Nölle, M. Bonitz, and A. Filinov. Energy spectrum of strongly correlated electrons and indirect excitons in quantum dots. *phys. stat. sol. (c)*, 3(7):2402–2405, 2006.

[56] Philip R. Bunker and Per Jensen. *Molecular Symmetry and Spectroscopy*. NRC Research Press, second edition, 1998.

[57] P. A. Maksym. Eckardt frame theory of interacting electrons in quantum dots. *Phys. Rev. E*, 53(16):10871–10886, 1996.

[58] D. A. Baiko, D. G. Yakovlev, H. E. De Witt, and W. L. Slattery. Coulomb crystals in the harmonic lattice approximation. 61(2):1912–1919, 2000.

[59] G. Chabrier. Quantum effects in dense coulumbic matter: Application to the cooling of white dwarfs. *Astrophys. J.*, 414:695–700, 1993.

[60] Carl Eckart. Some studies concerning rotating axes and polyatomic molecules. *Phys. Rev.*, 47(7):552–558, 1935.

Acknowledgements

This thesis has been carried out at the Institut für Theoretische Physik der Christian-Albrechts Universität zu Kiel. Professor Michael Bonitz has been by supervisor, and I am very grateful for his continuous support and encouragement throughout all my work. I want to thank Alexei Filinov for providing me with the newest versions of his computer program, as without this work had not been possible.

I am deeply thankful to all members of Professor Bonitz' group for the lively discussions and my warm welcome to the familiar working ambience. I would like to point out Andrea Fromm, Karsten Balzer, Christian Henning, and Patrick Ludwig in particular, for their proof-reading and suggestions

Special thanks are devoted to my dearest friend, Claudia Haase, who enriched my life outside the university and kept me fed and alive during the final stages of this work. Her thoroughly proof-reading was also invaluable.

Finally I want to thank my parents with all my heart as it was their patient and enduring support which made my studies possible.

Eidesstattliche Erklärung

Die vorliegende Arbeit ist von mir selbständig und nur unter Zuhilfenahme der angegebenen Quellen und Hilfsmittel angefertigt worden.

(Ort) (Datum) (Unterschrift)